Lanthanide Complexes of Bifunctional Chelates as pH and Ca^{2+} Sensitive Contrast Agents for MR Imaging. Design, Synthesis and Characterization

Lanthanoidkomplexe von funktionalisierten Chelaten als pH- und Ca^{2+}- abhängige Kontrastmittel für die Magnetresonanz-Bildgebung. Design, Synthese und Charakterisierung

D I S S E R T A T I O N

der Fakultät für Chemie und Pharmazie

der Eberhard-Karls-Universität Tübingen

zur Erlangung des Grades eines Doktors

der Naturwissenschaften

2006

vorgelegt von

Ilgar Mammadov

Tag der mündliche Prüfung: 11. September 2006

Dekan: Prof. Dr. Stefan Laufer

1. Berichterstatter   Prof. Dr. H.A. Mayer

2. Berichterstatter   Prof. Dr. M. E. Maier

I

To my wife Sheyda and
our cute daughters

Abbreviations

Abbreviation	Name
AcCN	acetonitrile
Ar	aromatic
Anal	analysis
ATN-4T	manganese porphyrin
ACSF	artificial cerebrospinal fluids
APP	amino polyphosphonate
APC	amino polycarboxylate
BBB	blood brain barrier
BOLD	blood-oxygen-level-dependent
Boc	butoxycarbonyl
br	broad
CBz	chlorobenzoformate
Calcd	calculated
CEST	chemical exchange saturation transfer
CLIO	cross- linked iron oxide
d	doublet (NMR)
dd	doublet of doublets (NMR)
DMC	dichloromethane
DMF	dimethylformamide

Abbreviation	Name
DMSO	dimethylsulfoxide
DTPA	diethylenetriaminepentaacetic acid
DTPA-BMA	diethylentriaminepentaacetic acide bis-methylamide
DOPE	dioleoyl phosphatidyl ethanolamine
DOTA	1,4,7,10-tetraazacyclododecane-1,4,7,10-tetraacetic acid
DOTAM-Gly	DOTA- tetraglycineamide
DPDP	dipyridoxyl diphosphate
DPPE/PA	dipalmitoyl phosphatidyl ethanolamine/palmitic acid
DO3A	1,4,7,10-tetraazacyclododecane-1,4,7-triaacetic acid
DO3AMP	DO3A-methyl phosphonic acid
DO3AEP	DO3A-ethyl phosphonic acid
EA	elemental analysis
EDTA	ethylenediaminetetraacetic acid
EGTA	ethylene glycol bis(2-aminoethyl ether)-N,N,N'N'-tetraacetic acid
EI	electron impact
ESI-MS	electrospray ionisation mass spectrometry
Et	ethyl
FAB	fast atom bombarding
FT	Fourier transformation

Abbreviation	Name
GE	gradient echo sequence (MRI)
HSA	human serum albumin
Hz	Hertz
i-Pr	Isopropyl
Ln	lanthanide
LFER	linear free energy relationships
m	multiplet (NMR)
M	any metal
M	molarity
Me	methyl group
m/z	mass/charge ratio
MRI	magnetic resonance imaging
fMRI	functional magnetic resonance imaging
$^{n}J_{ij}$	coupling constant of nuclei i,j *via* n bonds
N	normality
NMR	nuclear magnetic resonance
OA	oleic acid
q	quartet (NMR)
p	para
Ph	phenyl group
RIME	receptor-induced magnetization enhancement
r.t.	room temperature

Abbreviation	Name
S	singlet (NMR)
SPIO	superparamagnetic iron oxide
SE	spin echo sequence (MRI)
USPIO	ultra small SPIO
tert	tertiary
t-But	tertiary butyl group
TAFI	thrombin-activatabl fibrinolysis inhibitor
TFA	trifluoroacetic acid
THF	tetrahydrofuran
TPPS4	meso-tetra(4-sulfonatophenyl)porphine
TMACl	tetramethylamonium chloride

Table of Contents

Table of Contents

1. INTRODUCTION

1.1. Basic principles of NMR spectroscopy

NMR spectroscopy is the study of molecular structures through measurement of the interaction of a radio frequency electromagnetic radiation with a collection of nuclei immersed in a strong magnetic field.[1] The nuclei of all elements carry a charge. When the spins of the protons and neutrons comprising these nuclei are not paired, the overall spin of the charged nucleus generates a magnetic dipole along the spin axis. The intrinsic magnitude of this dipole is a fundamental nuclear property called the nuclear magnetic moment **μ**. The symmetry of the charge distribution in the nucleus is a function of its internal structure and if this is spherical (i.e. analogous to the symmetry of a 1s hydrogen orbital), it is said to have a corresponding spin angular momentum number of I = 1/2, of which examples are ^{1}H, ^{13}C, ^{15}N, ^{19}F, ^{31}P etc. In quantum mechanical terms, the nuclear magnetic moment of a nucleus with I = 1/2 can align with an externally applied magnetic field of the strength **B$_0$** in only 2I+1 ways, either reinforcing or opposing **B$_0$**. The energetically preferred orientation has the magnetic moment aligned parallel with the applied field (spin +1/2) in contrast to the higher energy anti-parallel orientation (spin -1/2). The rotational axis of the spinning nucleus cannot be oriented exactly parallel (or anti-parallel) with the direction of the applied field **B$_0$** but must preces about this field with an angular velocity given by the expression:

$$\omega_o = \gamma \, \mathbf{B_0} \qquad\qquad\qquad (1)$$

(ω_o - Larmor frequency in Hz)

The constant γ is called the magnetogyric ratio and relates the magnetic moment **μ** and the spin number I for any specific nucleus:

$$\gamma = 2\pi\mathbf{\mu}/hI \qquad\qquad (2)$$

(h is Planck's constant)

For a single nucleus with $I = 1/2$ and positive g, only one transition is possible ($\Delta I = 1$, a single quantum transition) between the two energy levels. NMR is all about how to interpret such transitions in terms of chemical structure. If angular velocity is related to the frequency by $\omega_o = 2\pi\nu$, then

$$\nu = \gamma \mathbf{B_0}/2\pi \qquad\qquad (3)$$

It follows that the proton NMR transitions ($\Delta I = 1$) have the following energy:

$$h \nu = \Delta E = h \gamma \mathbf{B_0}/2\pi \qquad\qquad (4)$$

For a proton $\gamma = 26.75 \times 10^7$ rad T^{-1} s^{-1} and $\mathbf{B_0} \sim$ 2T, $\Delta E = 6 \times 10^{-26}$ J, which is so small that a Boltzmann distribution has to be considered. The relative populations of the higher (n_2) and lower (n_1) energy levels at room temperature are given by the Boltzmann law:

$$n_2/n_1 = e^{-\Delta E/kT} \sim 0.99999. \qquad\qquad (5)$$

For NMR, this means that the probability of observing a transition from n_1 to n_2 is only slightly greater than that for a downward transition, i.e. the overall probability of observing absorption of energy is quite small. This relationship also explains why a larger $\mathbf{B_0}$ favors sensitivity in NMR measurements, increasing the difference between the two Boltzmann levels, and why NMR becomes more sensitive at lower temperatures.

1.2. Relaxation processes

When the sample is inserted into a magnetic field $\mathbf{B_0}$, the Boltzmann distribution of spins occurs between the energy levels. In order to move to a higher energy level, energy in the form of electromagnetic radiation needs to be supplied. Electromagnetic radiation in the radiofrequency (RF) range is of the correct energy to initiate this excitation. RF pulses can be applied to generate a magnetic field $\mathbf{B_1}$ perpendicular to $\mathbf{B_0}$. This causes the spins to flip away from the z-axis and gain x- and y-components (Figure 1). The precessing about the z-axis in the xy-plane generates a detectable alternating RF field. At the end of the applied RF pulse the nuclear spins return to their ground state by interacting with the surrounding environment through a process called spin-lattice relaxation T_1. As the spins realign with $\mathbf{B_0}$, the current produced by rotation in the xy-plane diminishes. The time necessary for disappearance of this current can be measured and is termed the spin-spin relaxation time T_2.
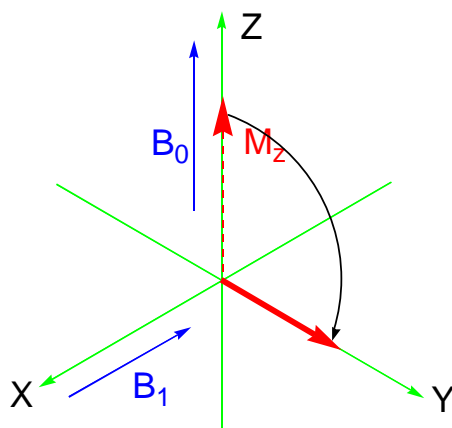
Figure 1.   Behavior of the net magnetization vector $\mathbf{M_z}$ upon exposure to an RF pulse.

T_1 relaxation occurs due to magnetic field fluctuations at the Larmor frequency brought about by the random motions of molecules in the surrounding medium

(lattice). These molecules in motion each have magnetic moments, and the movement of these moments leads to a magnetic 'noise' that encompasses a broad frequency range including the Larmor frequency. Magnetic noise at the Larmor frequency will stimulate transitions to the lower energy state.

T_2 relaxation occurs via fluctuations of a magnetic field caused by the random motion of molecules resonating at the same frequency. Fluctuation in the individual proton spins leads to a loss of phase coherence in the *xy*-plane with no net loss of energy from the system. Spin-spin relaxation is additionally affected by dephasing arising from bulk inhomogenities in $\mathbf{B_0}$.

1.3. Magnetic resonance imaging (MRI)

MRI is a diagnostic scanning technique based on principles of NMR. It measures the signal from the hydrogen nuclei of water, which is modified by the chemical environment. NMR spectroscopy measures the characteristics of any hydrogen nuclei depending on their position in the molecule. Instead of obtaining information about chemical shifts and coupling constants, MRI gives spatial distribution of the intensity of the water proton signal in the volume of the body. This signal intensity depends essentially on three factors: the density of proton spins in a given volume, the longitudinal and transverse relaxation times T_1 and T_2 of these spins.[2,3] Using different RF pulse sequences, image intensity can be weighted with respect to T_1 or T_2.

Spin-lattice relaxation time T_1 and spin-spin relaxation time T_2 may be shortened considerably in the presence of paramagnetic species. Therefore the targeted application of paramagnetic compounds can be used to increase contrast, working as contrast agents (CA). CA's increase the signal intensity of the tissue containing them by increasing the longitudinal and/or transverse relaxation rates ($1/T_1$ or $1/T_2$) using their unpaired electrons to facilitate spin transfer. The diamagnetic ($1/T_{1,2d}$) and paramagnetic ($1/T_{1,2p}$) contributions to the relaxation rates of such solutions are additive:

$$1/ T_{1,2obs.} = 1/ T_{1,2d} + 1/ T_{1,2p} \tag{6}$$

The paramagnetic contribution to the relaxation rate is linearly proportional to the concentration of the paramagnetic species:

$$1/ T_{1,2obs.} = 1/ T_{1,2d} + r_{1,2} [M] \tag{7}$$

where M = paramagnetic substances, $r_{1,2}$ = proton relaxivity ($s^{-1}mM^{-1}$).

For a predetermined image acquisition time, a shorter relaxation time results in a stronger signal because a larger population of the sample relaxes in that given time. This allows increased concentration-dependent contrast, and hence finer spectral resolution. The addition of a contrast agent results in an increased relaxation rate of the surrounding nuclei that appear as a bright spot of increased intensity in T_1-weighted images or as a region of decreased brightness in T_2-weighted images. MRI contrast agents are thus classified as positive or negative, T_1 or T_2, contrast agents. T_1 agents are usually preferred as a positive contrast enhancement is often more easily detected than a negative one. An ideal MRI contrast agent would have as many unpaired electrons as possible. It may be simply a substance[4] (i.e. molecular oxygen), a stable radical[5] (i.e. nitroxide radical) or a metal ion[6] (i.e. transition metal ions). Paramagnetic metal ions do show a suitable effect, which depends on the number of unpaired electrons in the ion. Paramagnetic ions of various transition metals like Fe^{3+}, Mn^{2+} and rare earth metals of the lanthanide series like Gd^{3+}, Dy^{3+} etc. as revealed in Table 1, have received great attention as magnetopharmaceuticals.[7,8] There are more transition metals and lanthanide metals with unpaired spins, but for the metal to be effective as a relaxation agent the electronic spin-relaxation time must match the Larmor frequency of the protons. This condition is met best for Mn^{2+}, Fe^{3+} and Gd^{3+}.[9,10]

Table 1.   Electronic configuration of some paramagnetic metals

Atomic number	Ion	Electronic configuration	3d	4f	Bohr magneton
25	Mn^{2+}	$[Ar]3d^5 4s^0$	↑↑↑↑↑		5.9
26	Fe^{3+}	$[Ar]3d^5 4s^0$	↑↑↑↑↑		5.9
63	Eu^{3+}	$[Xe]4f^6 6s^0$		↑↑↑↑↑ ↑ __	6.9
64	Gd^{3+}	$[Xe]4f^7 6s^0$		↑↑↑↑↑ ↑↑	7.9
66	Dy^{3+}	$[Xe]4f^9 6s^0$		↑↓↑↓↑↑ ↑↑↑	5.9

The prominent feature of gadolinium(III) is that seven unpaired electrons generate a symmetric S-state with a very slow electronic spin relaxation rate.[11] Thus Gd^{3+} exhibits the strongest effect of all elements on the longitudinal relaxation time T_1.

It is fortuitous that water exchanges quite readily on Gd^{3+} aqua complexes. The rate of exchange between aqua ligands on octadentate-chelated Gd^{3+} is approximately $3 \times 10^6 s^{-1}$, which allows thousands of water molecules to transiently coordinate to a single ion on the MRI time scale. Thus, the effect of the metal fragment on relaxation times is widespread, and only low concentrations (0.1-0.3 m*M*/kg) are necessary to be effective.[12-18] At the proper concentration, Gd^{3+} contrast agents enhance T_1 relaxation preferentially, thereby causing increase in signal on T_1-weighted images. Since T_1 weighted protocols in MRI have rapid pulse sequences, Gd^{3+} chelates are the favored agents. Moreover, they do not significantly affect the bulk magnetic susceptibility of the tissue compartment in which they are localized, thereby resulting in minimal macroscopic field inhomogenities and image artifacts. Dysprosium is another interesting paramagnetic lanthanide that exhibits

predominant r_2 susceptibility effects (1.8 times that of Gd^{3+}) and relatively low T_1 relaxivity (1/40 of Gd^{3+}) but it is more toxic than gadolinium.[19] The transition metal and paramagnetic lanthanide ions suitable as MR contrast agents are all potentially toxic at or near doses required for NMR relaxation changes. A major difficulty in the development of any of the paramagnetic metals as CA has been to diminish this toxicity to clinically acceptable levels. Gadolinium remains in the body several days after intravenous administration. This toxicity can only be reduced by coordinating the metal to ligands that are too obstinate to be displaced by water. One or two coordination sites must be open for water molecules, to allow inner sphere spin transitions, or transitions between the metal nuclei and a ligand to which they are directly bound. Owing to its large size, gadolinium tends to favor high coordination numbers in aqueous media. Currently, all Gd^{3+}- based chelates approved for use in MRI are eight to nine-coordinate complexes. This allows the design of various chelators according to the final target. Moreover, the choice of a proper ligand is very important to ensure that gadolinium does not dissociate from the complex in the body in the presence of phosphate, citrate, transferrin and other endogenous chelating substances. The dissociation of a complex generally leads to a higher degree of toxicity stemming from the free metal ion or free chelating ligand.[20]

1.4. Effects of contrast agents on water proton relaxation

CA's affect water magnetization by two primary ways: direct relaxivity and indirect susceptibility effects. Susceptibility effects dominate in large superparamagnetic particles and can be much stronger than relaxivity effects in certain situations. They may be useful even without complete quantization. Susceptibility induced relaxations are due to long-term interactions. For the most of the small gadolinium based CA's direct relaxivity is dominated. The origin of paramagnetic relaxation enhancement generated by paramagnetic lanthanide complexes can be divided into three components: inner sphere water

Introduction

(directly coordinated to the metal), secondary sphere water (molecules are on the hydrophilic side of the complex) and outer sphere water (bulk water) (Figure 2).
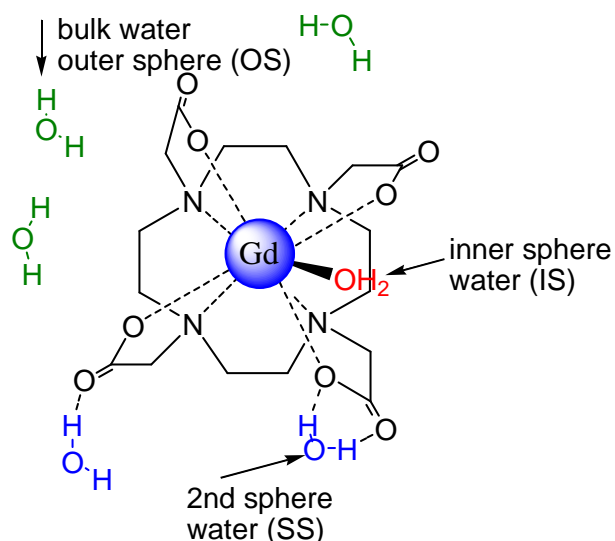
Figure 2. Schematic depicting the interactions of water molecules with gadolinium(III)-based contrast agent.

The inner sphere contribution is due to the interaction between the Gd^{3+} electron spins and the water protons in the first coordination sphere of the metal transmitted to the bulk via chemical exchange of the inner sphere protons. Bulk solvent molecules diffusing around the paramagnetic centre also experience the paramagnetic effect. The relaxation mechanism arising from this random translational diffusion is defined as outer sphere relaxation.[21,22] For the paramagnetic chelates both inner-sphere and outer-sphere components are comparable in magnitude and the final effect is additive, whereas for macromolecular complexes, the inner-sphere contributions tend to dominate the relaxation.

The relaxation of current clinically approved agents is due to approximately 60% inner sphere and 40% second and outer sphere effects.[23] The overall contribution to the relaxivity can be divided into the following terms:

$$r_1 = r_1^{IS} + r_1^{SS} + r_1^{OS} \tag{8}$$

where IS, SS and OS are inner sphere, second sphere and outer sphere water molecules. Inner sphere effects can be modified whereas outer sphere effects cannot easily be affected. The inner sphere term can be broken down further as in equation (9), where c is the molal concentration of the contrast agent, q is the number of bound water molecules per paramagnetic ion, τ_m is the mean lifetime of the water molecules in the inner sphere environment, and $1/T_{1m}$ is the longitudinal proton relaxation rate. The term $1/T_{1m}$ is composed of a dipole-dipole term (DD) and a scalar term (SC) (10).

$$\frac{1}{T_1^{IS}} = \frac{cq}{55.5}\left(\frac{1}{(T_{1m} + \tau_m)}\right) \tag{9}$$

$$\frac{1}{T_{1m}} = \frac{1}{T_1^{DD}} + \frac{1}{T_1^{SC}} \tag{10}$$

$$\frac{1}{T_1^{DD}} = \frac{2}{15}\left(\frac{\gamma_I^2 g^2 \mu_B^2}{r_{GdH}^6}\right) S(S+1)\left(7\frac{\tau_{c2}}{1+\omega_S^2\tau_{c2}^2} + 3\frac{\tau_{c1}}{1+\omega_I^2\tau_{c1}^2}\right) \tag{11}$$

As the scalar term becomes negligible at magnetic field strengths above 10 MHz and since most clinical experimental MR images are acquired at field strengths higher than 10 MHz, the scalar term is not an important factor in proton relaxation, thus $1/T_{1m}$ is essentially determined by the $1/T_1^{DD}$ term (11). The dipole-dipole term is modulated by reorientation of the nuclear spin vectors

with respect to the electron spin vector, changes in orientation of electron spin, and the rate of the water exchange. The theory of T_1 contrast agents demonstrates that numerous parameters affect relaxivity. The parameters q, r_{GdH}, τ_m, τ_r, and T_{1e} can be adjusted by altering the chemical environment around the paramagnetic ion.[24] By increasing the value of q, the relaxivity of the agent will increase. However increasing q above two will most likely result in increased toxicity due to decreased stability of the complex. A decrease in r_{GdH} will lead to an increase in relaxivity. Decreasing the term τ_m will allow more water molecules to be affected by the gadolinium(III) ion resulting in an increase in relaxivity. If the value of τ_m is decreased too much, the relaxivity of a complex will begin to decrease because the lifetime of the water molecules bound to the gadolinium(III) ion will not be long enough to influence the relaxation of the protons of the water molecule. By optimizing the value of τ_r or T_{1e}, the relaxivity of the contrast agent will be increased. There is an interdependence of the terms τ_m, τ_r, and T_{1e}. For most of the small molecule gadolinium (III) complexes, τ_r is the limiting of the three variables. As the value of τ_r becomes optimized the variables τ_m and T_{1e} begin to influence the relaxivity of the contrast agents. The residence lifetime of the protons τ_m modulates the efficiency of the chemical exchange from the inner sphere of water molecules to the bulk. This process can occur in two ways, exchange of the protons independently of the exchange of the entire water on which it resides, or the exchange of water molecule itself.[25]

1.5. Types of contrast agents

As it was shown before, according to major effects they produce on images, contrast agents may be broadly divided into positive contrast agents or T_1 agents (appearing bright on MRI) or negative contrast agents or T_2 agents, appearing dark on MRI. The question of which type of contrast enhancement to choose for a particular application depends on the specific organ or disease suspected and the pulse sequence used.

1.5.1. Non - lanthanide based contrast agents

Iron

When exposed to a magnetic field, the resultant permanent magnetic moment of the iron particles is very large. Magnetic particulates of various iron oxides are now being used as exogenous agents for enhancing $1/T_2$ preferentially at imaging fields.[26] The most common form of iron oxide used is magnetite, which is a mixture of Fe_2O_3 and FeO. Iron oxide particles (diameter = 5-200 nm) are said to possess superparamagnetic properties if the "magnetic" ions are mutually aligned.[27] For solutions or suspensions of sufficiently large paramagnetic or ferromagnetic particles (greater than or equal to 25 nm diameter), the paramagnetic contributions to the relaxation rates satisfy $1/T_2$ much better than $1/T_1$ at typical imaging fields.

Depending on the overall size of the crystal, the iron oxides are broadly classified into two categories. Those with diameter more than 50 nm are called superparamagnetic iron oxide (SPIO) particles. As with its use as an oral contrast agent, SPIO causes marked shortening of the T_2 relaxation time

resulting in a loss of signal in the liver and spleen with all commonly applied pulse sequences.[28,29] Organically coated iron oxide crystallites with diameters of 5-50 nm ('nanoparticles') are called ultra-small SPIO (USPIO) and are potential magnetic contrast enhancing agents for the reticule endothelial system. USPIO with crystal sizes less than 10 nm have been reported to have excellent T_1-enhancement properties.[30-33] Iron particle based agents generally lead to a much larger increase in $1/T_2$ and are best visualized on T_2 weighted scans.[34]

Manganese(II) chelates

The manganese ion (Mn^{2+}) is an excellent T_1 contrast agent for MRI. Manganese chloride is commercially available as Lumen-Hance (Bracco) for such applications. The paramagnetic manganese ions are able to substitute partially for calcium, which rapidly fluxes in and out of synaptic terminals regulate neurotransmitter release.[35] Topical administration of $MnCl_2$ solution via intravitreal injection to neurons in mice leads to enhancement of contrast along the respective pathways, thereby permitting visualization of neuronal connections.[36] Mn^{2+} mesoporphyrin, a lipophilic compound, was investigated as a potential hepatobiliary contrast agent.[37] Aime and coworkers have developed an oxygen-tension responsive contrast agent based on the redox switch of Mn(II/III)-Porphyrin complexes which have had success in the visualization of tumors because these complexes tend to localize in tumors.[38] Manganese dipyridoxyl diphosphate (MnDPDP) was shown to be useful in establishing the diagnosis of acinar cell carcinoma, a rare pancreatic exocrine neoplasm.[39] MnDPDP, which specifically labels liver tumors over healthy liver tissue, helps to determine if surgery on hepatic tumors is a viable option.[40-42] The manganese porphyrin (ATN-4T) accumulates in subcutaneous tumors in rabbits while rapidly clearing from surrounding tissues to yield images with enhanced tumor intensity.[42] HOP-8P, a manganese porphyrin complex demonstrated sustained tumor enhancement of squamous cell carcinoma in mice.[46]

1.5.2. Lanthanide metal chelates

According to the chemical structure lanthanide containing CAs are divided in two groups: acyclic and macrocyclic agents. Usually they are based on two most widely used chelators for the complexation of Gd^{3+}, diethylenetriaminepentaacetate (DTPA) and 1,4,7,10-tetraazacyclododecane-1,4,7,10-tetraacetate (DOTA).[47,48] Chelates with a higher stability constant have been developed and used successfully.[49-52]

Gd-DTPA and its derivatives

Diethylenetriaminepentaacetic acid (DTPA) is a readily available octadentate ligand. As shown in Chart 1, the Gd-DTPA family constitutes a large and widely used group of MRI contrast agents.[53] DTPA chelates are easily derivatized. Various complexes have been designed and evaluated using thermodynamic stability, rates of excretion, toxicity, lipophilicity, biodistribution, and percent change in MR signal intensity as critera keeping Gd-DTPA as the gold standard. The complexes are anionic, and therefore, quite water-soluble (usually to about 0.5–1.0 M). The formation constant of Gd-DTPA (log K) is 10. The ionic chelates are also hyperosmolar with respect to body fluids and some of their side effects may be attributed to this property. This causes the intravascular fluids to osmotically absorb water and blood at the vessels in which it resides.
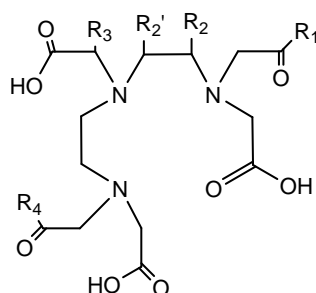
No	Molecule	R_1	R_2 and R_2'	R_3	R_4
a	DTPA	-OH	-H	-OH	-H
b	DTPA-BMA	$-NHCH_3$	-H	$-NHCH_3$	-H
c	DTPA-BMEA	$-NH(CH_2)_2-OCH_3$	-H	$-NH(CH_2)_2OCH_3$	-H
d	BOPTA	-OH	-H	-OH	$CH_2-O-CH_2-C_6H_5$
e	EOB-DTPA	-OH	$R_2=$-H $R_2'=-CH_2-C_6H_4-O-Et$	-OH	-H
f	MS-325L	-OH	$R_2=CH_2PO_3HC_6H_9(Bz)_2$ $R_2'=$-H	-OH	-H

Chart 1. Some important diethylenetriaminepentaacetate (DTPA) analogs: **a**) DTPA; **b**) bismethylamide of DTPA (DTPA-BMA); **c**) bismethoxy- ethylamine derivative of DTPA (DTPA-BMEA); **d**) benzyloxymethyl substituted DTPA (BOPTA); **e**) ethoxybenzyl substituted DTPA (EOB-DTPA); **f**) MS-325.

As the complexes are distributed through the circulatory system, this effect becomes negligible. The median lethal doses (LD50) of these complexes in rats are 10 m*M*/kg body weight. Typical counterions to these complexes include sodium and *N*-methylglucaminium. There is little difference between these ions in terms of toxicity (LD_{50}) or solubility, but *N*-methylglucaminium is usually

preferred, as it can be safely administered even in patient with hypernatremia. Gd-DTPA (Gadopentetate Dimeglumine Magnevist™, Berlex Laboratories, Wayne, NJ) was the first intravenous ionic MR contrast agent to be approved by the FDA in mid-1988 for human use.[54,55] Gd-DTPA is distributed in the intravascular and extracellular fluid spaces, does not cross an intact blood brain barrier (BBB), and is excreted rapidly (within 2-3 h of administration) by glomerular filtration. After injection, half-life of Gd-DTPA in blood is ~20 minutes. Being a structurally simple complex, it is not site-specific, and is most commonly used as a contrast agent for systemic MRI; e.g., to search for tumors with compromised BBB or the metastasis lesions of tumors.

Since Gd^{3+} and Ca^{2+} have approximately the same ionic radius, and Ca^{2+} is prominent in physiological settings, there is danger of metal substitution, which would release free Gd^{3+} into the system. In fact, this does happen to some extent, which explains the detectable residual Gd^{3+} after 14 days. However, replacement of a carboxylate binding moiety with an amide group increases the ligand binding affinity by a factor of ~10/amide group, and this is the advantage of Gd-DTPA-BMA, the bismethylamide of Gd-DTPA or gadodiamide (Omniscan™, Sanofi-Winthrop Pharmaceuticals, NY) as shown in Chart 1b. Gadodiamide is a nonionic complex with two-fifths of the osmolality of Gd-DTPA.[56] This agent distributes non-specifically throughout the plasma and leaks rapidly from blood into the interstitial space with a distribution half-life of about 5 min.[57] In Gd-DTPA-bis(methoxyethylamide) or Gadoversetamide, the two carboxylate binding moieties of DTPA are replaced with methoxyethyl substituted amide groups (Chart 1c). OptiMARK® (Gd-DTPA-BMEA; Mallinckrodt Inc., St. Louis, MO) is a sterile, nonpyrogenic aqueous solution of gadoversetamide, a nonionic gadolinium chelate, developed for use as an intravenous MR contrast agent.[58]

The hydrophobic benzyloxymethyl substituent of Gd-BOPTA Chart 1d or Gadobenate Dimeglumine (MultiHance™) renders it more susceptible to hepatocellular uptake and excretion into the bile ducts, gall bladder, and intestines than the parent complex, Gd-DTPA. However, it is not so hydrophobic as to be completely absorbed into fatty tissue. Therefore, it is useful as an

extracellular fluid agent, such as Magnevist (Gd-DTPA) or ProHance (Gadoteridol) or as a liver-specific agent to target the liver and bile ducts, such as Teslascan (mangafodipir) or iron oxides (e.g., Endorem). Gd-BOPTA is a positive MR contrast agent for intravenous application that couples specific, long lasting enhancement of magnetic resonance signal intensity in the liver parenchyma with the plasma kinetics of agents targeted to the extracellular fluid space.[59-61] In comparison to other gadolinium-chelates it has a nearly 2-fold increased relaxivity due to weak protein binding with plasmatic macromolecules. It also has potential to become a useful contrast agent for MRA as demonstrated in the volunteers. A related compound, gadolinium-ethoxybenzyl-diethylenetriamine pentaacetic acid as shown in Chart 1e, (Gd-EOB-DTPA) is absorbed to an extent of approximately 5% by the liver and has been used as an intrabiliary contrast agent for depicting biliary structures.[62,63]

The large hydrophobic diphenylcyclohexyl moiety in MS-325 (Chart 1f) (Gadophostriamine Trisodium) or Angiomark™, a gadolinium based MRI blood pool agent,[64] allows it to bind strongly to serum proteins (especially albumin). As depicted in Cart 1f. The hydrophilic phosphodiester group in MS-325, placed in between the hydrophobic group and the chelate allowed for high reversible albumin binding affinity. MS-325 is highly protein bound (80%-96% in human plasma) after injection, which decreases the concentration of free drug in serum, resulting in its retention in blood for a longer time (~1 h) than most other Gd^{3+} contrast agents (~30 – 180 sec). The longer stay of the complex in blood allows one to obtain more acquisitions, and thus higher resolution images with better vascular signal enhancement than otherwise possible. MS-325 exhibits a relaxivity approximately 6-10 times that of Gd-DTPA. MS-325 is the prototype blood pool agent for use in the imaging of blood vessels and blood flow in patients with cardiovascular disease, including peripheral vascular disease.

The DO3A family

Owing to a lower entropy loss in chelation, macrocyclic compounds release less free Gd^{3+} into their physiological surroundings than do their linear acyclic counterparts. 1,4,7,10-tetraazacyclododecane-1,4,7-tricarboxylic acid (DO3A) (Chart 2g), is itself not an ideal chelating agent for Gd^{3+} contrast agents, but it serves as a starting point for the synthesis of numerous derivatives since a 12-atom ring appears to be ideal for MRI contrast agents.[65] The Gd chelate of DOTA, marketed as Dotarem™ (Chart 2h), is an extracellular (systemic) MRI contrast agent.[66,67] Gd-DOTA is as safe a contrast agent as Gd-DTPA and has similar diagnostic efficacy. It targets no specific anatomical site or physiological function. The major distinct advantage of Gd-DOTA over Gd-DTPA lies in its lower relative viscosity so that it diffuse faster and pass through the injection needle more quickly for a given applied pressure, thereby minimizing patient discomfort because a burning sensation due to osmolality is felt otherwise.[68]
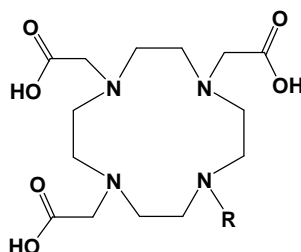
No	Molecule	R
g	DO3A	-H
h	DOTA	$-CH_2COOH$
i	HP-DO3A	$-CH_2CH(OH)CH_3$
j	DO3A-butrol	$-CH(CH_2OH)-CH(OH)-CH_2OH$

Chart 2. 1,4,7,10-tetraazacyclododecane-1,4,7-triacetate (DO3A) and its derivatives: **g**) DO3A; **h**) DOTA; **i**) HP-DO3A; **j**) DO3A-butrol.

The applications of Gd-HPDO3A (Chart 2i) are generally parallel to those of Gd-DOTA, but are more often for visualization of the brain, spinal cord and

cerebrospinal fluid than for tumor detection. Its derivative, the Gd^{3+} complex of 10-(2,3-dihydroxy-1-hydroxymethylpropyl)-1,4,7,10tetraazacyclododecane1,4,7-triacetic acid (Chart 4j) Gd-DO3A-butrol or gadobutrol, or Gadovist™) is a neutral Gd-chelate for use as an extracellular contrast agent in similar clinical settings as the parent moiety.[69] An i.v.-LD$_{50}$ of 23 mM/kg in mice combined with a comparatively high T_1-relaxivity (5.6 l/mM per s at 0.47 T and 6.1 l/mM per s at 2 T) in plasma promises a high margin of safety. Gadoteridol (ProHance®, Squib Diagnostics, Princeton, NJ) is another low osmolar, nonionic contrast agent.[70,71] In human intracranial metastatic disease, administration of 0.3 mM/kg Gadoteridol (Gd-HPDO3A) (Chart 2i) has permitted detection of additional lesions not visualized at 0.1 mmol/kg.

Smart contrast agents

To image extra or intracellular activities, researchers are tailoring the agents so that they are 'turned on' only in the presence of a threshold concentration of a specific molecule.[72] The relaxivities of these designer magnetopharmaceuticals are dependent on certain biochemical variables. These smart 'bioactivated agents' sense their biochemical environment either through enzyme-induced relaxivity changes or changes in the levels of a biomarker metabolite. The concept is to utilize injectable compounds of high tissue specificity with the ability to provide information of the physico-chemical environment, when activated in response to a change in some biochemical event. The choice of the biochemical target, the chelates and the physiological/pathological situation are critical deterministic parameters in the design, development and applications of such agents in imaging the biological functions.

Enzyme sensitive contrast agents

Synthesis of 1-(2-(β-galactopyranosyloxy)propyl)-4,7,10-tris (carboxy methyl)-1,4,7,10-tetraazacycododecane) gadolinium (Gd-DO3A-gal) which consists of a DOTA type ligand that occupies either of the nine binding sites on gadolinium and replacing one of the acid group by a galactopyranose residue positioned to block the remaining coordination site on the gadolinium ion from water, was reported to selectively enhance MRI signal from cells or tissues containing β-galactosidase enzyme.[73-74] These are cage-like molecules (a gadolinium ion inside a chemical scaffold or molecular basket) wherein the access of nearby protons of water to gadolinium in chelated CA is physically blocked with an enzyme substrate (galactopyranose residue at the open co-ordination site of gadolinium) amounting to 'latching the basket'. Upon the production of the targeted enzyme, which can clip the molecular cage open and dissolve the shield on the gadolinium, the activity of CA will be fully turned on.

These agents have two states of activity, weak and strong. The effect is just half as the galactose group coordinates to the Gd^{3+} lowering the final relaxivity, and is turned on in the presence of specific enzymes or other biologically important molecules that cleaves the galactopyranose group. Specifically tailored marker enzyme, β-galactosidase react with specific substrates to open the cage by dissolving galactopyranose (amounting to 'lifting the lid') and thereby activating the CA. Thus, in the presence of the right enzyme the barrier dissolves and due to free interaction of water with gadolinium, MRI signal doubles in strength. This physiologically sensitive MRI CA opens up a wealth of new avenues of study, even including the *in vivo* imaging of gene expression. Meade's group has demonstrated that such agents light up special biological action and it is even possible to monitor gene transfer and to trace the cellular expression of specific genes[75]. Anelli and coworkers have synthesized a DTPA derivative which can detect carbonic anhydrase.[76] The gadolinium complex contains a sulfonamide group in place of one of the carboxylic acid arms of the DTPA, helping it to

selectively target the enzyme carbonic anhydrase. Upon binding to the enzyme, the relaxivity increases significantly due to an increase of the rotational correlation time (τ_r) caused by binding to the large enzyme. Nivorozhkin and coworkers prepared an agent that is sensitive to the presence of human carboxypeptidase B (a thrombin-activatable fibrinolysis inhibitor (TAFI)), which has been implicated in thrombotic disease.[77] TAFI cleaves a trilysine masking group attached to the agent exposing an aromatic functional group. This aromatic group has a high binding affinity for human serum albumin (HSA). The contrast agent binds HSA leading to an increase in τ_r resulting in an increase in relaxivity. This event is known as a receptor-induced magnetization enhancement (RIME). The trilysine chain makes this agent a pro-RIME agent because the trilysine chain inhibits interaction with HSA. Bogdanov and coworkers prepared a peroxidase activatable agent.[78] This agent consists of a gadolinium(III) chelate linked to benzene-1,2-diol that acts as a monomer. In the presence of peroxide, the monomers are oligomerized yielding a threefold increase in relaxivity due to an increase in τ_r.

Perez and coworkers have utilized the difference in relaxivity between solitary CLIO particles and those in close proximity to other cross-linked iron oxide (CLIO) particles to detect DNA cleaving agents.[79] Two strands of complementary DNA are each conjugated to a CLIO particle. When the complementary strands bind, the CLIO particles from each strand come into close proximity to each other. Upon cleavage of the double strand by a DNA-cleaving agent, the two CLIO particles become separated leading to a detectable change in relaxivity. Utilizing a similar mechanism, Zhao and coworkers have developed a protease sensitive MRI contrast agent.[80] With this agent, the strong interaction between biotin and avidin is exploited. A molecule of biotin is conjugated to each side of a peptide that is cleaved by proteases. CLIO particles coated with avidin are exposed to the bi-biotinylated peptides. In the presence of protease specific for the peptide, the CLIO particles will not aggregate; however, in the absence of protease, aggregation of the CLIO particles will occur resulting in an increase in relaxivity. Up today this agent has only been used in vitro.

pH sensitive CA

Fe(III) meso-tetra(4-sulfonatophenyl)porphine (Fe-TPPS4) has been investigated as a potential pH-sensitive NMR proton image contrast agent. Relaxation rates ($1/T_1$ and $1/T_2$) of water protons were measured as a function of pH and concentration of Fe-TPPS4 in phosphate-buffered isotonic saline. The transverse relaxation rates ($1/T_2$) did not change appreciably at pH > 6.0. The longitudinal relaxation rates ($1/T_1$) increased from pH 7.75 to 5.75.[81]

Aime explored the chemical exchange saturation transfer (CEST) properties of a series of lanthanide(III) complexes (Ln = Eu, Dy, Ho, Er, Tm, Yb) with the macrocyclic DOTAM-Gly ligand, which is the tetraglycineamide derivative of DOTA (1,4,7,10-tetraazacyclododecane-1,4,7,10-tetraacetic acid). These complexes possess two pools of exchangeable protons represented by the coordinated water and the amide protons. Yb-DOTAM-Gly displays the most interesting CEST properties when its amide N-H resonance (16 ppm upfield H_2O signal) is irradiated. Up to 70% suppression of the water signal is obtained at pH 8. As the exchange rate of amide protons is base-catalyzed, Yb-DOTAM-Gly results to be an efficient pH-responsive probe in the 5.5-8.1 pH range.[82]

The low molecular weight gadolinium chelate diethylentriaminepentaacetic acide bis-methylamide (GdDTPA-BMA) encapsulated within pH-sensitive liposomes is introduced as a novel type of pH-sensitive paramagnetic contrast agent. The in vitro relaxometric properties of the liposomal gadolinium chelate were shown to be a function of the pH in the liposomal dispersion and the membrane composition. Only a minor pH-dependency of the T_1 relaxivity (r_1) was observed for liposomal GdDTPA-BMA composed of the unsaturated lipids dioleoyl phosphatidyl ethanolamine (DOPE) and oleic acid (OA). On the other hand, the r_1 of GdDTPA-BMA encapsulated within saturated dipalmitoyl phosphatidyl ethanolamine/palmitic acid (DPPE/PA) liposomes demonstrated a strong pH-dependency. At physiological pH and above, the r_1 of this system was significantly lowered compared to that of non-liposomal gadolinium chelate, which was explained by an exchange limited relaxation process. A

tetrasubstituted derivative of 1,4,7,10-tetraazacyclododecane[83] with amide coordinating groups and extended noncoordinating phosphonate groups forms a complex with Gd^{3+}, which contains one slowly exchanging inner-sphere water molecule. The water proton relaxivity of the complex was found to be highly pH dependent. Protonation of the noncoordinating phosphonate groups appear to catalyze prototropic exchanges of the bound water protons, thereby providing a mechanism for enhanced water contrast below pH 7. Another approach is based on a microenvironmental responsive polyion complex in the form of a mixture of two polymers. The complex exhibits a fifty percent increase in relaxivity upon decreasing pH from 7.0 to 5.0. The mechanism of how the complex works is unknown; however, it is detectable in the presence of tumors in mice but inot in the absence of tumors.[84,85] Hovland and coworkers have developed a pH-sensitive contrast agent which is a DO3A derivative with a tertiary amine-containing side arm.[86] The side arm amine contains two long alkyl chains. When the amine is protonated (pH 3-6) the relaxivity is low. Upon deprotonation (pH 8-10), the agents form colloidal aggregates due to the higher lipophilicity of the deprotonated complex. The aggregation causes an increase in τ_r and a subsequent increase in relaxivity of 142%.

Metal ion sensitive contrast agents

Several metal ions (e.g. Ca^{2+}, Zn^{2+}) are essential or beneficial to life while others, such as lead, cadmium or mercury, are highly detrimental. Many diseases have been associated in a way or another to altered metal ion concentrations in the body. Deficiencies can be as damaging as overloads. Copper deficiency has been associated to anemia while excess copper can lead to Wilson's disease (liver cirrhosis). Anemia may also be caused by a lack of iron and overload of this same metal ion is connected to thalassemia and siderosis.[87] In vivo determination of the metal ion distribution is thus highly desirable and progresses have been made towards the design of MRI contrast

agents sensitive to the concentration of some metal ions such as Ca^{2+}, Mn^{2+}, Fe^{2+} and Zn^{2+}.

An iron-sensitive contrast agent was synthesized by Aime and coworkers functionalizing DO3A with salicylate moieties as shown in Schema 1.[88] Upon addition of iron(III), the gadolinium(III) DTPA-salicylate complexes bind to the iron ions via the salicylate functional groups. This binding yields an increase in t_r and relaxivity.
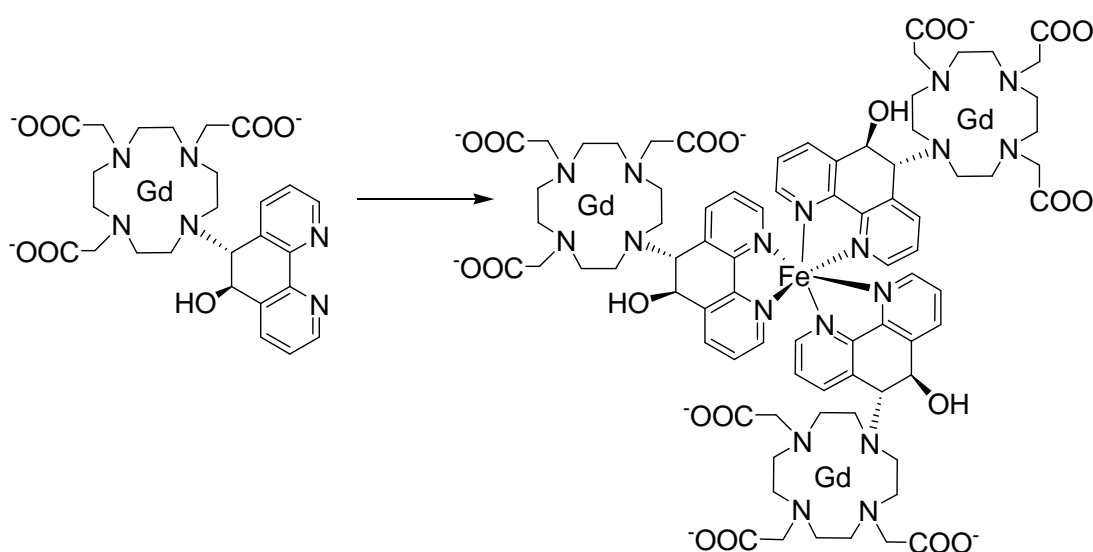
Schema 1. Iron sensitive contrast agent.

Zinc is a key component of many enzymes, transcription factors, and synaptic vesicles. Hanaoka and coworkers have developed a series of contrast agents to detect zinc(II) (Schema 2).[89,90] Their design consists of gadolinium(III) DTPA modified with pyridine ligands and carboxylic acids. In the absence of zinc(II), water is bound to the gadolinium(III) ion. In the presence of zinc(II), the carboxylic acid and pyridine moieties coordinate to zinc(II) thus restricting the access of water to the gadolinium(III) ion. This decrease in q yields a decrease in relaxivity in the presence of zinc(II).
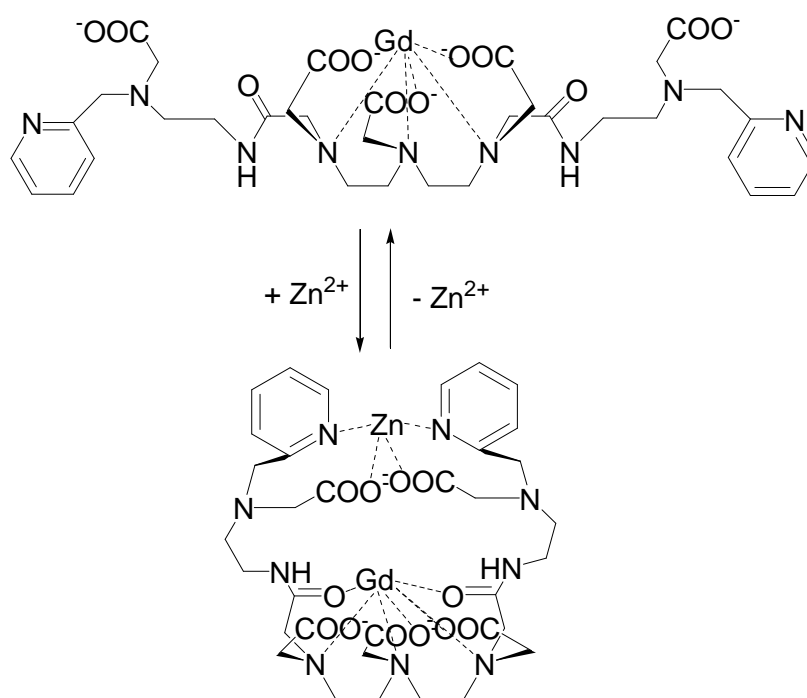
Schema 2.   Zinc sensitive contrast agent.

Li et al (1999) synthesized a calcium-responsive agent, DOPTA-Gd, using calcium-chelating BAPTA fluorophores (Schema 3).[91,92] The relaxivity of the complex is controlled by the presence or absence of the divalent ion Ca^{2+}. In the presence of low concentraions of calcium, the aromatic iminoacetate group may coordinate in some fashion to the gadolinium ion, maintaining low (outer sphere) relaxivity.By structurally modulating inner-sphere access of water to a chelated Gd^{3+} ion, a substantial and reversible change in T_1 could be affected upon the addition of Ca^{2+} and not other divalent ions. After Ca^{2+} is bound to DOPTA-Gd, the molecule undergoes a substantial conformational change that opens up the hydrophilic face of the tetraazacyclododecane macrocycle.
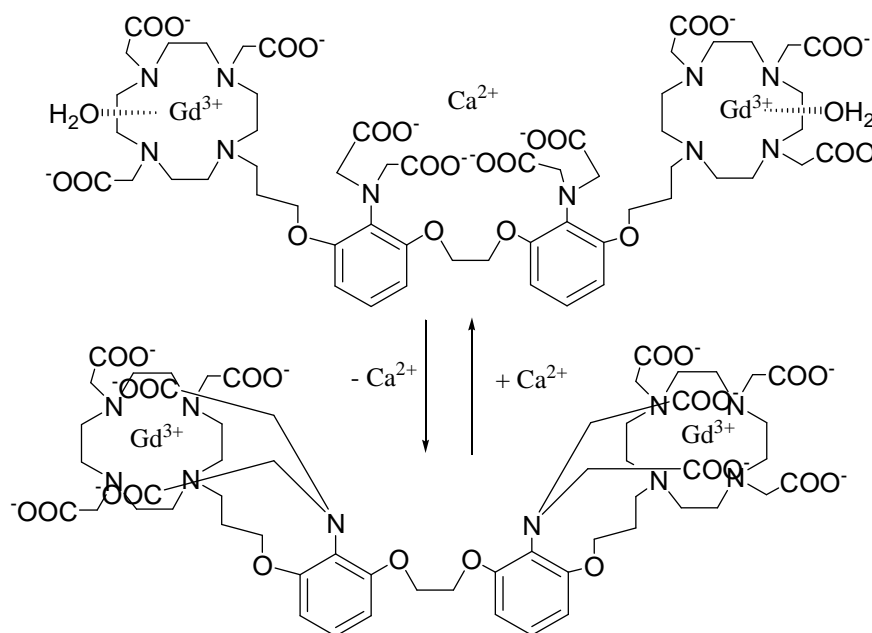
Schema 3.   Calcium sensitive contrast agents.

This change dramatically increases the accessibility of the chelated Gd^{3+} ion to the bulk solvent. As the concentration of calcium approaches micromolar levels, the EGTA binds calcium, possibly releasing the Gd^{3+} coordinated iminoacetates and increases (doubles up) relaxivity by more than doubling the number of inner-sphere water molecules. With the swing of the calcium concentration from low to high to low, these smart CA switches from off to on to off, thereby acting as reversible smart contrast agent. This may have interesting implications for monitoring of brain functions or nerve activities based on calcium dependence or detection of turning on and off of cell signals by secondary messenger like calcium. It has been shown that the paramagnetic properties of lanthanides can be exploited to obtain information on specific parts of a protein surface. Owing to the high affinity of coordinatively unsaturated lanthanide complexes for oxygen donors, carboxylate groups can be used as preferential targets for the interaction. The DO3A ligand is particularly useful in these studies, as it coordinates lanthanides in a heptadentate fashion, leaving two sites available

for exogenous donors. Gd^{3+}-DO3A is thus a valuable semi-selective probe for clusters of negative charges on the protein surface.[93]

1.6. Contrast agents in neuroscience

In the neuroimaging field MRI has evolved as a very useful tool that offers quantitative assessments of tissue characterization in studies of cerebral neoplasm,[94] ischemic events,[95] inflammations and demyelinating diseases,[96] thereby, yielding insights towards both diagnosis and prognosis, as well as for monitoring therapeutic response. If the MRI experiment is done while a mental task is given to a subject, a so-called functional magnetic resonance image (or fMRI) image is generated. The fMRI is based on the increase in cerebral blood flow to the local vasculature accompanied by increase in oxygen level and glucose consumption that follows neural activity in the brain. The blood-oxygen-level-dependent (BOLD) magnetic resonance signal used in functional imaging of the brain reflects the loss of oxygen from hemoglobin, causing its iron to become paramagnetic, which influences the magnetic field experienced by protons in surrounding water molecules.[97-99] The fMRI is currently the most widely used method for brain mapping and studying the neural basis of human cognition.[100-103] On such an image one can see how different tasks activate different parts of the brain relatively specifically. By listening to music, for example, a specialized area in the so-called *auditory cortex* along the sides of the brain shows increased signal.[104] Vision activates a region in the back of the brain (the occipital cortex), localized precisely to regions of the visual field.[105] Touch brings increased signal along the side of the brain, particularly in the side of the brain opposite to the part of the body that is touched[106] and movements activate regions in the front and the top of the brain in cortex specialized for motor control.[107] It has been shown that the BOLD contrast mechanism directly reflects the neural responses elicited by a stimulus and that it is most closely correlated with the local field potentials, implying that activation in a given area

is often likely to reflect the incoming input and the local processing in that area rather than the spiking activity.[108-113] Unfortunately BOLD fMRI is not fully sufficient for the study of neural networks, because of a local blood flow the BOLD hemodynamic signal is the indirect indicator of neural activity, and an associated time lag broadens the response and also causes the problems in spatial colocalization.

1.7. *Aim of the project*

The aim of this project is to develop contrast agents that are 'smart' biochemical functional markers rather than anatomical agents. The markers are supposed to detect neuronal activity in real time and translate it into changes in MR contrast. This would permit a direct visualization of neural activation independent of the state of the vascular system. A series of the markers can be used to follow the changes in the neuronal signals (pH, metal ions concentrations, enzymes).

Currently no suitable extracellular agents are available for examining concentration changes of ions or molecules involved in the neural signaling process. However, some works,[89-92] which were described previously in detail, appear to be useful models for designing agents for these requirements.

Ca^{2+} ions play a central role in the process by which the electrical potential across the membrane of presynaptic nerve terminals regulates the release of neurotransmitter substances into the synaptic cleft. The release occurs when a voltage-dependent Ca^{2+} channel in the presynaptic membrane opens, thus permitting an influx of Ca ions and diffusion of Ca^{2+} in cytoplasm, followed by binding of Ca^{2+} at some cytoplasmic site that triggers the exocytotic release of quanta of neurotransmitter. Although the general role of Ca^{2+} as a presynaptic messenger is well supported, many important specifics of its action remain to be resolved.[111-115]

Introduction

The goal is the development of contrast agents, which are sensitive to local extracellular pH or calcium ions concentration changes during the neuronal activation.
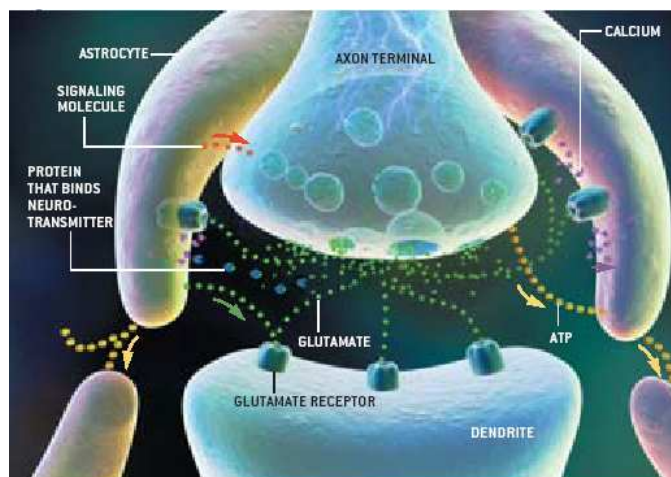
Figure 3. Ca^{2+} ions in the synaptic cleft.

At the beginning novel acyclic bifunctional or macrocyclic ligands should be developed. The compounds should have parts containing gadolinium, to act as a contrast agent, and sensors which are responsive for the contrast changes during the changes in the chemical environment. On this purpose the new macrocyclic chelators with the different types of donor atoms (carboxylates or phosphonates) can be used for the design of the selective classes of specific "smart" pH / calcium-sensitive contrast agents. The monophosphonate containing part of the molecule can act as pH sensor, because of their sensitivity to changes of the pH of the solutions. The aminobis(methylene)phosphonate containing macrocycles should act as calcium sensors with the high affinity toward the calcium. The different length of the phosphonate side chain can be used to adjust the complexing properties of the complexes and fine tune the sensitivity toward the calcium. All agents first should be evaluated by means of *in vitro* MR measurements in simulated

30

physiological conditions and characterized by physico-chemical methods (such as potentiometric titration, NMR spectroscopy and NMRD profiles). Subsequent *in vivo* characterization, in rats, should examine their distribution, half-time and toxicity. Those experiments should provide more information about the behaviors of complexes in order to optimize their final structures.

2. GENERAL PART

2.1. Synthesis of acyclic bifunctional chelates and their lanthanide complexes

2.1.1. Introduction

Aminocarboxylic acids are ideal to chelate metal ions. Particularly stable chelates are formed with metals from the alkaline earth, transition and rare earth metal series. Bifunctional ligands can bind tightly to the metal ion forming a chelate while at the same time bearing a second functionality which confers upon it desirable chemical, physical and/or biological properties. Such physical properties of the chelators differ depending on the purpose of the metal chelate. The metal chelates which act as a contrast media for NMR imaging or general purpose X-ray imaging, require high water solubility, viscosity and osmolality of a formulated drug solution as close as possible to those of *in vivo* conditions. Furthermore functionalized chelates, or bifunctional coordinators, are capable of being covalently attached to bigger molecules such as biopolymers and supports.[116,117] Aminocarboxylic acid chelating agents have been known and studied in the literature for several years.[118] Typical of the aminocarboxylic acids are ethylenediaminetetraacetic acid (EDTA), ethylene glycol bis(2-aminoethyl ether)-N,N,N'N'-tetraacetic acid (EGTA), diethylenetriamine pentaacetic acid (DTPA) as well as 1,2-Bis(2-aminophenoxy)ethane-N,N,N',N'-tetraacetic acid (BAPTA) (Chart 3).
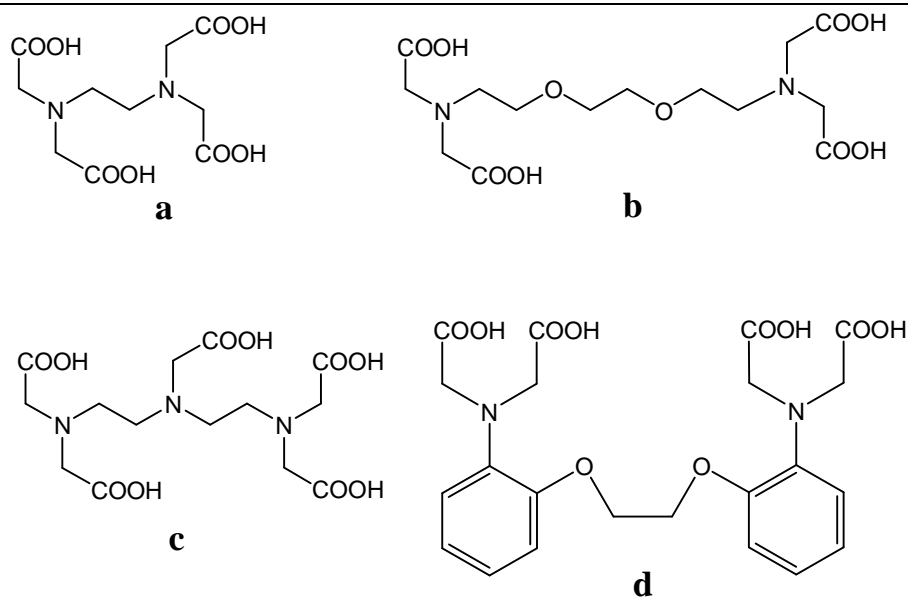
Chart 3. Aminocarboxylate as chelating agents a) EDTA, b) EGTA, c) DTPA, d) BAPTA.

The functionalized aminocarboxylates (a – d) have been applied as a dyes for optical imaging[119]. For example a series of compounds based on the BAPTA were developed as contrast agents for optical trace of metal ions like Ca^{2+}, Mg^{2+} and Zn^{2+}).[120-123]

Although, a series of the metal chelators were developed until now, the design of new chelating agents with new complexing properties is of current interest. The new bifunctional chelating agents described in Chart 4 can be used to chelate or sequester metal ions. The complexes, because of the presence of the moiety -NH_2, can be attached to functionalized polymeric supports, or preferably covalently attached to antibodies or antibody fragments. For example complexes with gadolinium themselves can be used as contrast agents in MRI. The ability of the ligands to chelate calcium can be used for the design of the calcium sensitive dyes and relaxometric probes.
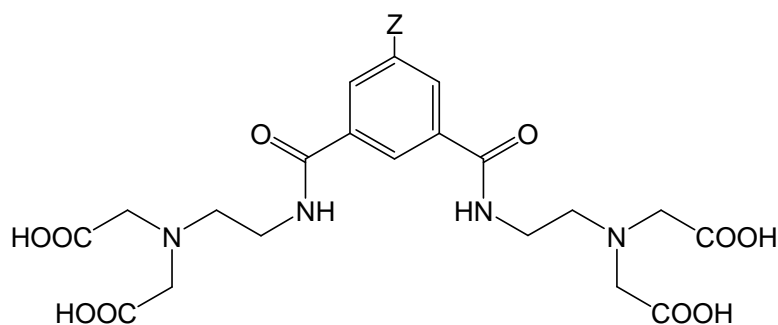
Chart 4. Bifunctional chelating agent. Z= -NO$_2$, -NH$_2$.

2.1.2. Synthesis of the ligands 5, 11 and complexes 6a, b; 12a, b

The nitro and amino derivatives of the ligands **5** and **11** were synthesized by two different ways according to Schemes 4 and 5. The alternative route depicted in Scheme 5 was developed after the non satisfactory reduction of the nitro group in compound **5**, which gave very poor yields in the catalytic hydrogenation with platinum oxide or palladium catalysts.

According to Schema 4, the synthesis of the ligand **5** started from the commercially available nitroisophtalic acid (**1**) which was treated with excess of ethylendiamine to give compound **3**. Compound **3** was alkylated in the presence of K$_2$CO$_3$ with *tert*-buthyl ester of the bromoacetic acid resulting in **4**, which was deprotected by TFA in DCM. Recrystalization from hot methanol gave the final ligand **5** as a yellow powder in 78% yield.
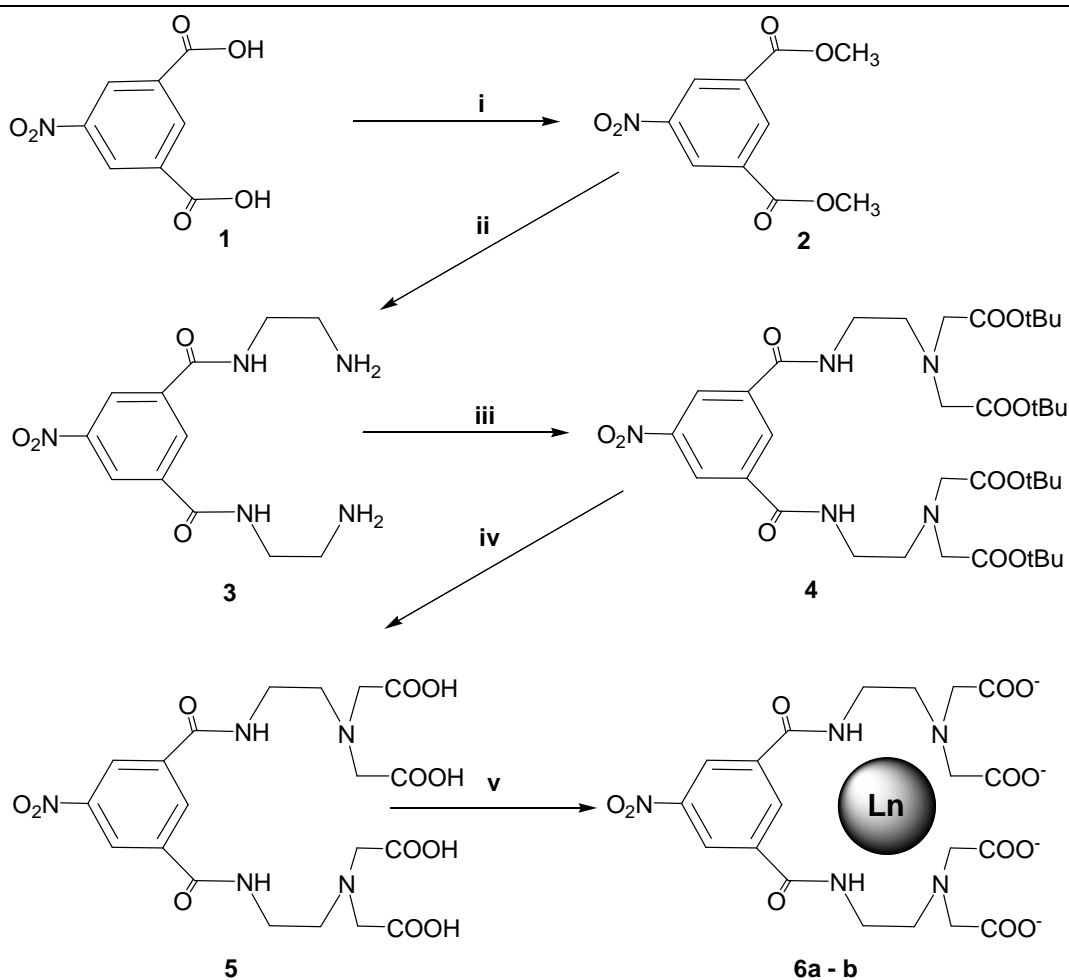
Scheme 4. Synthesis of the acyclic complexes **6a, b;** i) HCl/ MeOH; ii) ethylendiamine, r. t., 12h; iii) t-Butyl bromoacetate, K_2CO_3, CH_3CN; iv) DCM, TFA; v) H_2O, $GdCl_3$ x H_2O (**6a**) H_2O, $EuCl_3$ x $6H_2O$ (**6b**).
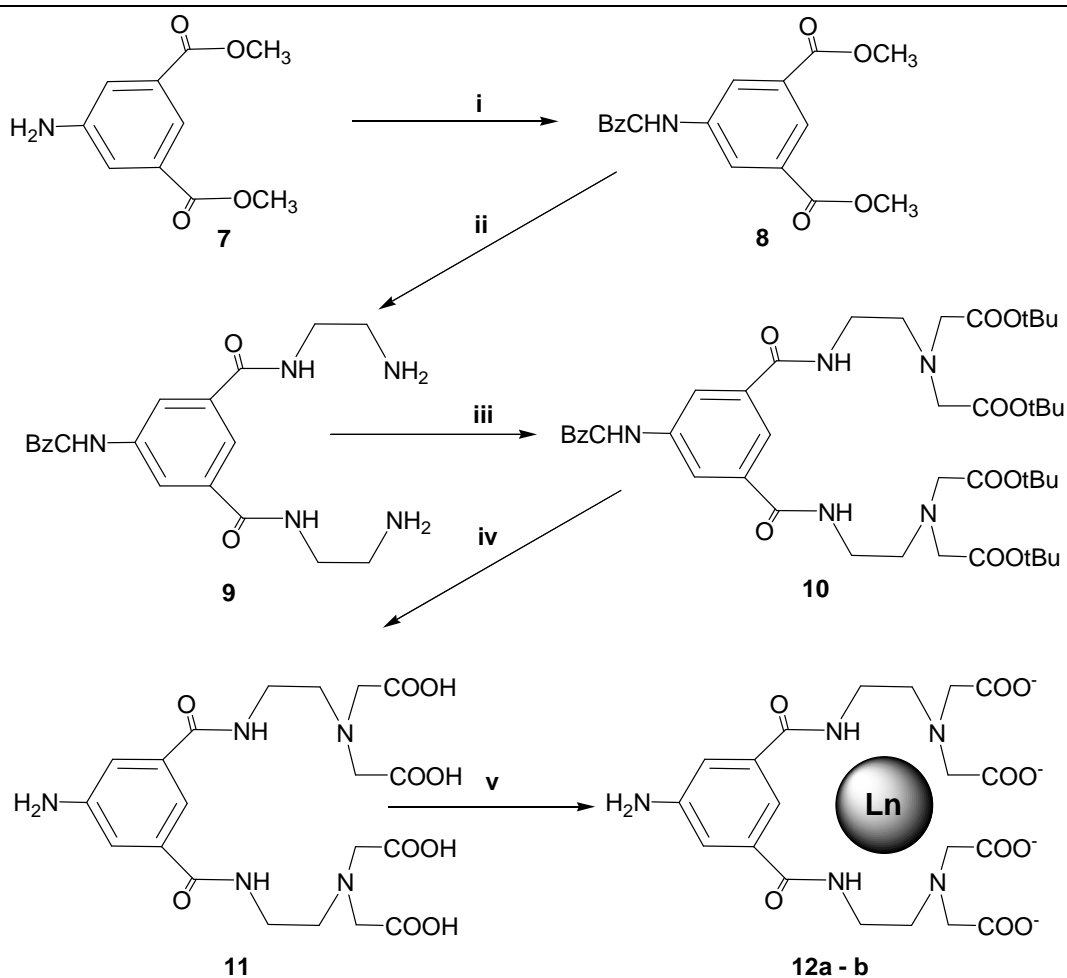
Scheme 5. Synthesis of the acyclic complexes **12a, b;** i) CBz, K_2CO_3 ; ii) ethylendiamine, r. t., 12h; iii) t-Butyl bromoacetate, K_2CO_3, CH_3CN; iv) H_2, Pd\C, DCM, TFA; v) H_2O, $GdCl_3$ x H_2O (**12a**) H_2O, $EuCl_3$ x $6H_2O$ (**12b**).

The amino derivative **11** was synthesized starting from dimethylester of aminoisophtalate **7**. The aminogroup was protected using chlorobenzoformate (CBz). Compound **8** was treated with ethylenediamine and alcylated with *tert*-buthyl ester of bromoacetic acid by a similar way as it was done for compound **5.** Hydrogen reduction in the presence of Pd/C catalyst of **10** and deprotection of the *tert*-butyl groups with TFA in DCM resulted in compound **11,** which was

recrystallized from hot methanol to give the final ligand in the 72% overall yield. The ^{13}C {^{1}H} NMR spectrum of **11** is presented in Figure 4 and contained all the resonances according to the symmetry of the molecule. The substituted aromatic carbon atoms can be distinguished from the unsubstituted ones by the chemical shifts and the decrease of the peaks intensity because of the longer relaxation times of the non-proton-bearing carbons which was also supported by DEPT spectrum of the ligand.
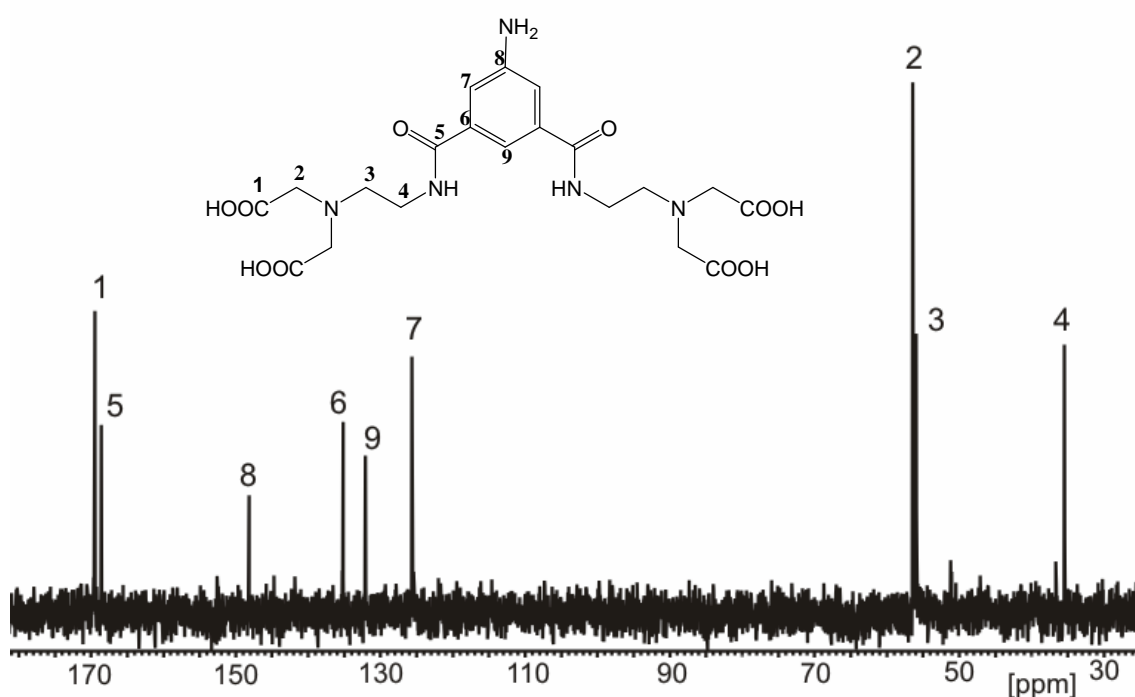
Figure 4. ^{13}C{^{1}H} NMR spectrum of the compound **11.**

Complexation with lanthanides was preformed by stirring the ligands **5** and **11** (1.0 eq) with the corresponding lanthanide chlorides (0.9 – 1.0 eq) in water solutions at r.t. for 12 h at pH 5.0 – 5.5. A low pH of the solutions is preferred to avoid precipitation of the metals in the form of their hydroxides. After filtration through a 0.2 mm syringe filter complexes **6a, b** and **12a, b** were obtained.

The main drawback of the synthesized complexes is their solubility. The compounds are poorly soluble in water and in most of the organic solvents at r.t. This makes it not only difficult to obtain relaxometric data it is also a drawback

for later application as CA. This effect was not obtained by the complexation of ligands **5** and **11** with the other metals (Ca^{2+}, Mg^{2+}, Zn^{2+}, Cu^{2+}).

Relaxivity studies

Relaxivity studies of the complexes were preformed at a 300 MHz vertical imaging magnet, r.t. (~ 21°C) and pH 7.4 (potassium salt of 3-(N-morpholino)-propanesulfonic acid (KMOPS) buffer). Four different concentrations of **6a** were prepared (0.1mM, 0.2mM, 0.35mM and 0.5mM) and the relaxivity was calculated as the slope of the graph in the Figure 5. The relaxivity of compound **6a** was found to be 4.5 $s^{-1}mM^{-1}$. The measurements of the relaxivity were also preformed in the presence of different metal ions in artificial cerebrospinal fluids (ACSF). The results show that there are no changes of the relaxivity observed even after the addition up to 10 eq of calcium chloride. This means that the gadolinium complexes are relatively strong and no demetalation of the complexes in the presence of high amounts of other metals is observed.
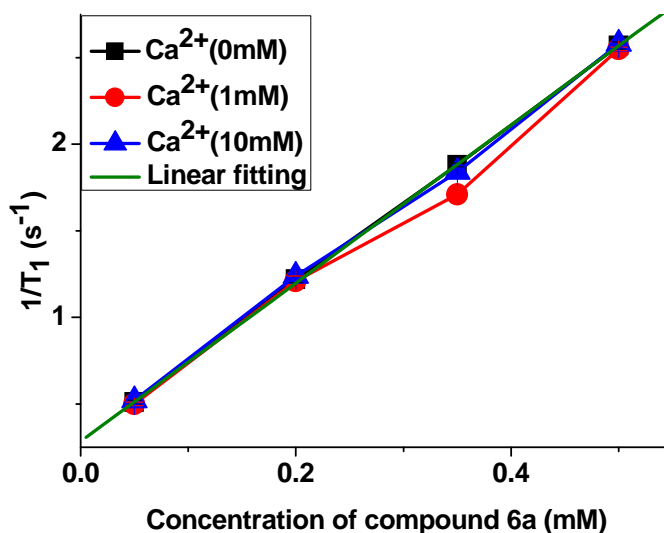
Figure 5. Relaxivity rate versus concentration of complex **6a** (300 MHz and 25 ^{o}C).

Conclusions

In conclusion, two derivatives of acyclic bifunctional chelating agents based on the nitro and amino isophtalic acid were synthesized. T_1 relaxivity rates of the compounds were determined in the presence of up to 10 eq of calcium ions. It was shown that the excess of calcium does not affect on the T_1 relaxation times of the complexes. Precipitation of the complexes was observed during the complexation with lanthanides which is the biggest drawback in the application of the compounds as relaxation agents. That can be an effect of dimerization or polymerization during the complex formation. Similar behavior for the acyclic benzyl containing compounds was mentioned in the works of Raymond.[124] Further modifications of the complexes, such as introduction of hydrophilic poly(ethylene)glycols or solubilizing dendrimers, are needed to make them more attractive as a relaxometric probes for the MR imaging.[125] Complexation of the ligands **5** and **11** with Ca^{2+}, Mg^{2+}, Zn^{2+} and Cu^{2+} does not show any precipitation. The ligand **11** due to the presence of the amino group can be used as building block for the synthesis of the specific MRI contras agents.

2.2. Synthesis and characterization of DO3A based mono(alkylphosphonate) complexes as potential pH sensitive contrast agents

2.2.1. Introduction

pH is one of the important factors for the design and development of innovative exogenous "smart" CAs that are responsive to changes in their microenvironment. Phosphonate containing ligands seem to be a promising building block in the design and synthesis of "smart" contrast agents for MRI, which are sensitive to changes of the pH. Phosphonates form hydrogen bonds with the surrounding water molecules which are sensitive to changes of the acidity of solutions. Consequently phosphonates were introduced into macrocyclic complexes (Chart 5). Two molecules were reported by Aime's group (Chart 5a and b), where phosphonate and carboxylate derivatives of macrocyclic complexes are compared.[126-129] It was suggested that the relaxivity of the phosphonate containing derivatives which increase at low pH, was due to the protonation of the phosphonates. This results in an increase of the number of water molecules in the inner sphere of the complexes. However that can also lead to a drastic decrease of the stability of the complexes. Formation of ternary complexes with carbonates from CO_2 of the air at basic pH has been suggested as a reason for the relaxivity changes in carboxylate complexes. It also was shown, that the presence of two phosphonate moieties decreases the number of water molecules in the inner sphere, but they can increase the second hydration sphere of the complexes.
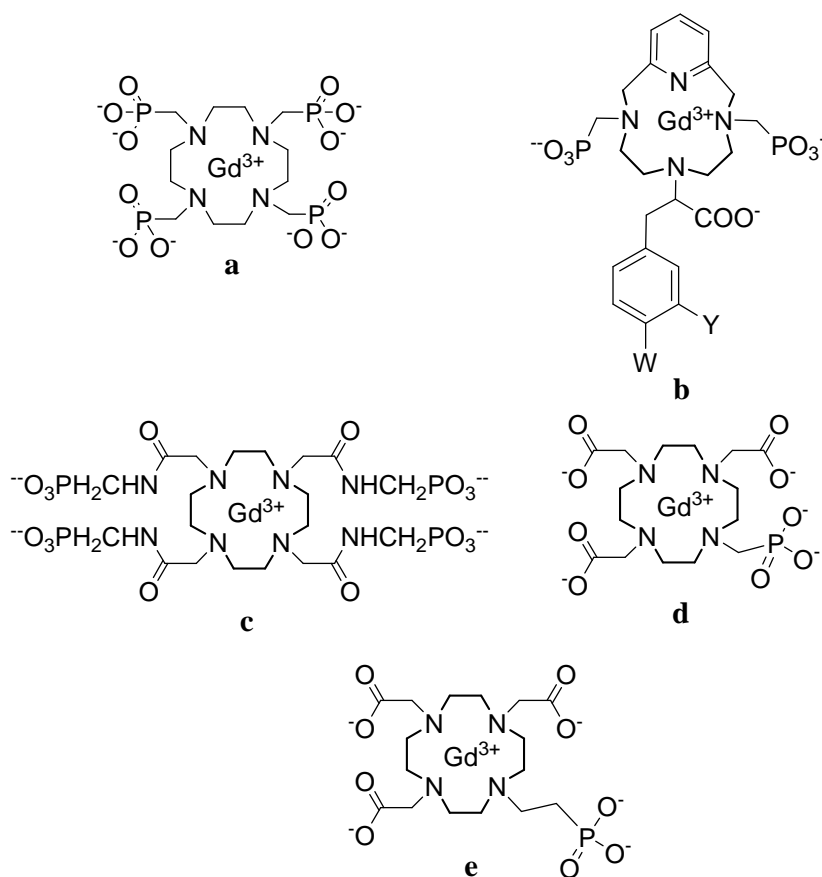
Chart 5.   Phosphonate containing macrocyclic complexes.

As an example it was found that compound a in the Chart 5 has no water molecule in the inner sphere, but its relaxivity is comparable with that of the DOTA derivative with one water coordinated to gadolinium. The phosphonates initiate the formation of second sphere water molecules, which leads to an increase of relaxivity.

Sherry and coworkers described a molecule with amidophosphonate moieties (Chart 5b). First *in vitro* results were presented in 1999 which showed that relaxivity changes by changes of the pH in the physiological range.[130] Recently the possibility for *in vivo* application was demonstrated by the determination of

the pH of tumor tissue. pH maps with improved spatial resolution were obtained compared to the MR spectroscopic methods used before.[131]

The groups from Prag and Brno introduced the methylphosphonate derivatives of DO3A (Chart 5d). A single crystal X-ray analysis was preformed and physico-chemical characteristics were described, which showed that the phosphonate of the pendant arm is complexing to gadolinium.[132,133] The complex exists as a mixture of two isomers SAP (square antiprisma) and TSAP (twisted square antiprisma) which contains one water molecule in the inner sphere. Moreover the residence life time of the water molecule in the inner sphere of the complex depends on pH which is probably due to the domination of one of the isomers at different pH. No visible changes of relaxivity versus pH are observed.

On the bases of these literature data phosphonate containing macrocyclic compounds with protected (**18**) and unprotected (**16**) propylphosphonate moieties were synthesized (Scheme 6). The motivation was to study the dependence of the length of the phosphonate side chain on the complexing properties (by comparison with DO3AMP and DO3AEP in Chart 5 (**d** and **e**)). In addition the investigation of the effect of the charge of the complexes on the relaxivity with the aim to get a significant change of the MRI contrast by changes of the pH was performed.

2.2.2. Synthesis of the ligands and complexes

The ligands **16** and **18** were synthesized according to Scheme 6. Alkylation of the *tert*-butyl ester of DO3A[134] (**14**) with the diethyl ester of bromopropylphosphonic acid in presence of 1.5 eq of potassium carbonate in acetonitrile gave the protected phosphonate ligand **15**. For compound **16** a two step deprotection was performed, first trimethylbromosilan was used to remove
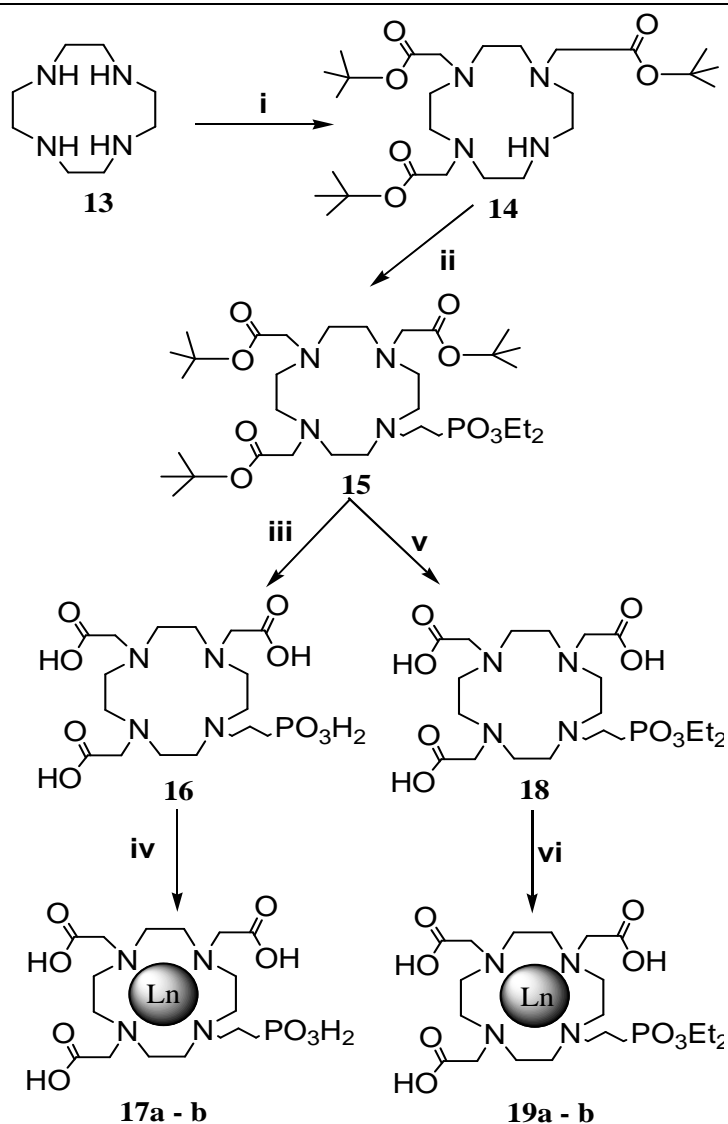
Scheme 6. Synthesis of the macrocyclic phosphonate containing complexes (**17a**, **b; 19a, b**); i) t-Butyl bromoacetate, NaHCO$_3$, CH$_3$CN; ii) Diethyl(3-bromopropyl) phosphonate, K$_2$CO$_3$, CH$_3$CN; iii) (CH$_3$)$_3$SiBr, DCM, TFA; iv, vi) H$_2$O, GdCl$_3$ x H$_2$O (**17a; 19a**), H$_2$O, EuCl$_3$ x 6H$_2$O (**17b; 19b**) v) DCM, TFA.

the ethyl groups of the phosphonates followed by TFA cleavage of the *tert*-butyl groups of the carboxylates. Two times recrystalization from diethyl ether and acetone gave clean **16**. The different types of recrystalization lead to the successful remove of excess TFA. The deprotection was followed by NMR

spectroscopy. Compound **18** was obtained after selectively deprotection of **15** with a TFA / DCM mixture. The same procedure as for compound **16** was followed to remove the rest of the TFA.

The number of resonances and their chemical shifts in the $^{13}C\{^1H\}$ and ^1H NMR spectra agree with the symmetry of the molecules (Figure 6). The most characteristic features are two resonances in the ratio 1:2 in the low field area, related to the absorption of the carboxylates, and doublets of the CH_2-PO_3H_2 moieties (11) in the $^{13}C\{^1H\}$ NMR spectrum of the phosphonates (24.4 ppm, $^1J_{PC}$ = 134.7 Hz)).
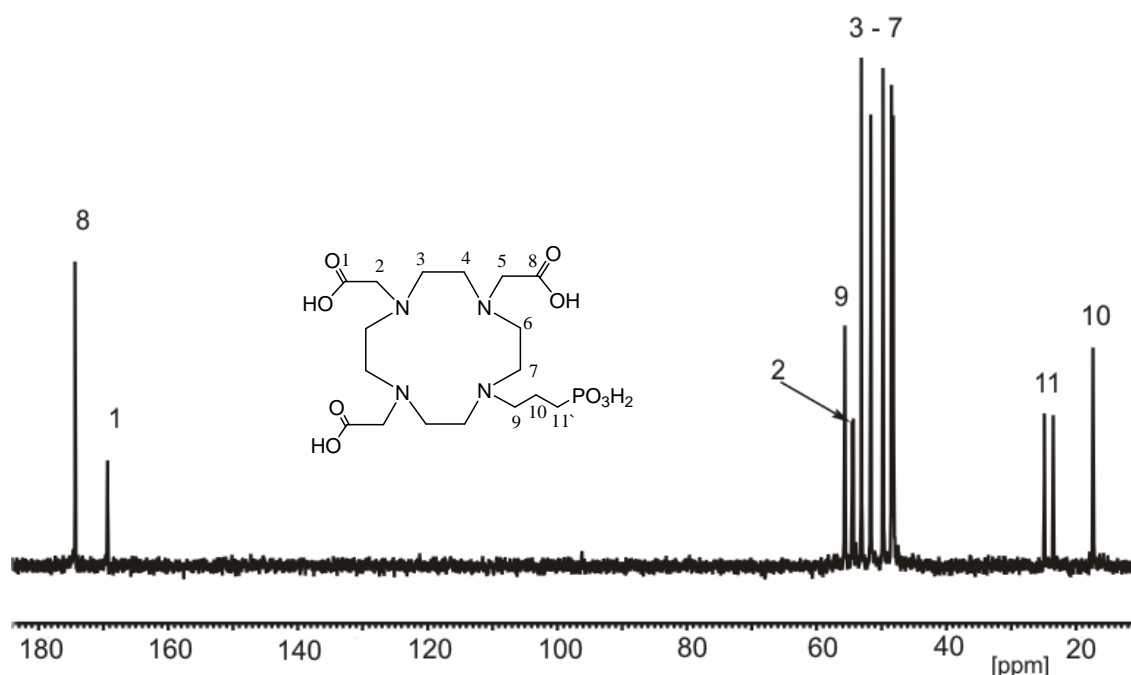
Figure 6. $^{13}C\{^1H\}$ NMR spectra of the compound **16.**

Stock solutions of the metal ions with known concentrations were prepared from the chloride salts of the corresponding metals. The exact concentrations were

determined by complexometric titration with a standard solution of the disodium salt of ethylenediaminetetraacetic acid (EDTA). The complexes were prepared by stirring of the mixtures of the corresponding stock solutions and the ligands **16** and **18**, respectively, in a ligand : metal ratio of 1 : 0.9. Finally the complexes were filtered and lyophilized. The xylenol test was preformed to insure that there are no free metal ions in solution (see experimental part).[135]

In the mass spectra of **17b** and **19b** all peaks related to the mass of the $[M+H]^+$ complexes are present. For the compounds **17a** and **19a** seven gadolinium isotopes are observed in the mass spectra of complexes.

2.2.3. Physico-chemical characteristics of the ligands and complexes

Potentiometric studies of the ligands and complexes

The acidobasic and complexing properties of the newly synthesized ligands **16** and **18** were studied by means of glass electrode potentiometric titrations. In order to follow the effect of the pendant arm on the acidobasic and complexing properties of the new macrocyclic ligands, the DO3A ligand was also included for comparison.

Determination of protonation constants

The protonation constants of the macrocyclic ligands **16** and **18** were studied at 25 °C and 0.1 M ionic strength adjusted adding sodium chloride in order to compare the experimental values with those reported in literature (Scheme 7). The fully deprotonated species of the macrocyclic ligands form stable

complexes with sodium ions (e. g. log K_{Na} = 2.2 – DO3A, 4.03 – DOTA, 4.77 – DO3AMP[136] (Chart 5d)). The same phenomena, but less pronounced can be seen for potassium salts applied as inert electrolyte. They also form complexes but with reduced stability compared to the analogous sodium ones. As a consequence of this fact, the first protonation constant of the ligands is decreased more for electrolytes which form more stable complexes with the cation of the salt. Therefore the protonation of macrocyclic ligands is studied in tetramethylammonium chloride (TMACl) as inert electrolyte to adjust a constant ionic strength of the solution (Table 2).

$$[L^{5-}] + [H^+] \xrightleftharpoons{\log Kp,1} [HL^{4-}] + [H^+] \xrightleftharpoons{\log Kp,2} [H_2L^{3-}] + [H^+] \xrightleftharpoons{\log Kp,3}$$

$$[H_3L^{2-}] + [H^+] \xrightleftharpoons{\log Kp,4} [H_4L^-] + [H^+] \xrightleftharpoons{\log Kp,5} [H_5L]$$
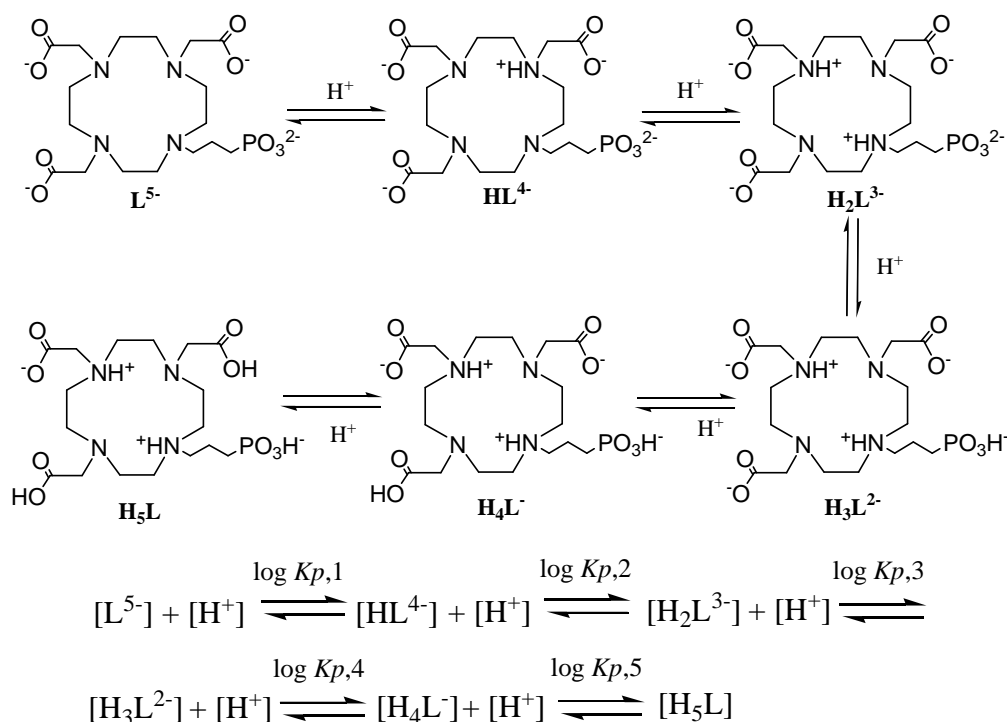
Scheme 7. Protonation of the compound **16**.

Table 2. Logarithmic values[a] of protonation constants of DO3A, DOTA, DO3AMP, **16** and **18**[b]

Ligand	Log $K_{p,1}$	log $K_{p,2}$	log $K_{p,3}$	log $K_{p,4}$	log $K_{p,5}$	Σ log $K_{p,n}$ ($n = 4$)	Reference
DO3A	11.19	9.48	4.21	3.35	----	28.23	This work
DO3A	11.59	9.24	4.43	3.48	---	28.74	147,148
DO3A	11.55	9.15	4.48	---	---	---	147, 148
DO3A	10.51	9.08	4.36	---	---	---	147,148
DO3A	10.72	9.51	4.40	4.00	---	28.63	149
DO3A	12.46 (11.24[c])	9.49	4.26	3.51	1.97	29.72	139
DO3A	11.96[e]	9.66	4.23	3.51		29.36	150
DOTA	11.73	9.40	4.50	4.19	---	29.82	147
DOTA	11.14	9.50	4.61	4.30	---	29.55	147, 148
DOTA	9.37	9.14	4.63	3.91	---	27.05	147, 148
DOTA	11.34	9.90	4.60	4.00	---	29.84	149
DOTA	11.74	9.76	4.68	4.11	2.37	30.29 (27.36[c])	139
DO3AMP[c]	13.83 (10.05[c])	10.35	6.54	4.34	3.09	34.37 (27.83[d])	136
DO3AEP[b]	10.06	10.11	6.71	4.38	3.42	34.68 (27.97[e])	This work
16[b]	11.09	9.94	7.17	4.00	2.82	35.02 (27.85[e])	This work
18[b]	9.37	9.45	4.13	2.94[d]	---	25.89	This work

[a]For log $K_{p,i}$ the standard deviation $\leq$ 0.04 log K unit; [b]$t = 25$ °C, $I = 0.1$ M NaCl (otherwise the medium is stated in parenthesis);

[c]measured at $I = 0.1$ M TMACl, corrected for sodium ion complexation (log $K_{Na} = 2.2$ – H$_3$DO3A, 4.03 – H$_4$DOTA, 4.77 – H$_5$DO3AMP);

[d]estimated value; [e]the value of overall protonation constant calculated without protonation constant of phosphonic pendant arm;

[f]determined by ^{1}H NMR spectroscopy

On contrary, the first high protonation constant of the ligand in tetraalkylammonium salts can not be observed with potentiometric methods and therefore some values which appeared in literature are questionable (Table 2).

The most probable values seem to be those determined by means of NMR spectroscopy or glass-electrode potentiometry where the correction for liquid-junction potential in alkaline pH range was taken into account (Table 2). Thus the recommended protonation constants for DOTA are those published recently[137,138] and therefore the values for DO3A determined in the same manner are acceptable.[139] The sodium complex formation is more pronounced for the DOTP and DO3AMP ligands (Chart 5a and d) in which the phosphonate pendant arm is capable to stronger bind to sodium.[140] In the case of compounds **16**, **17a**, **18** and **19a**, the protonation constants were determined in sodium chloride solutions for several reasons. Firstly, the experimental conditions should be close to conditions *in vivo*, and, secondly, they overcome the problems associated with obtaining the highest protonation constants. In addition, knowing the stability constant of the sodium complexes, allows a correct calculation of the protonation constants. This has been demonstrated in the case of DO3A where the experimental values are in good agreement with literature data (Table 2).[139]

The protonation constants of the ligands **16** and **18** together with the values for some analogous ligands are presented in Table 2.[132,133] The step sequence of ligand protonation was studied for DO3AMP (Chart 5d) by ^{31}P and ^{1}H NMR spectroscopy and it was found that two protons are bound to nitrogen atoms while their location depends on the number of protons of the protonated species. In addition, it was found that there is a strong hydrogen interaction between the oxygen atom of the phosphonic pendant arm and the protonated adjacent nitrogen in the cyclen ring. This bond is probably weakened in the presence of sodium ions. Since the structural changes of the macrocyclic ligands are not so dramatic, it can be supposed that the protonation scheme will be valid for other DO3A-like

derivatives. The indirect proof is the fact that the overall protonation constant log $K_{p,2}$ representing the protonation of two nitrogen atoms in the cyclen ring are similar: 20.67 (DO3A), 20.40 (DO3AMP), 21.03 (**16**). The overall basicity of the ring nitrogens remains while the change of the protonation of the first nitrogen atom is simultaneously compensated by the change of the ability of the second nitrogen atom to be protonated (Figure 7).
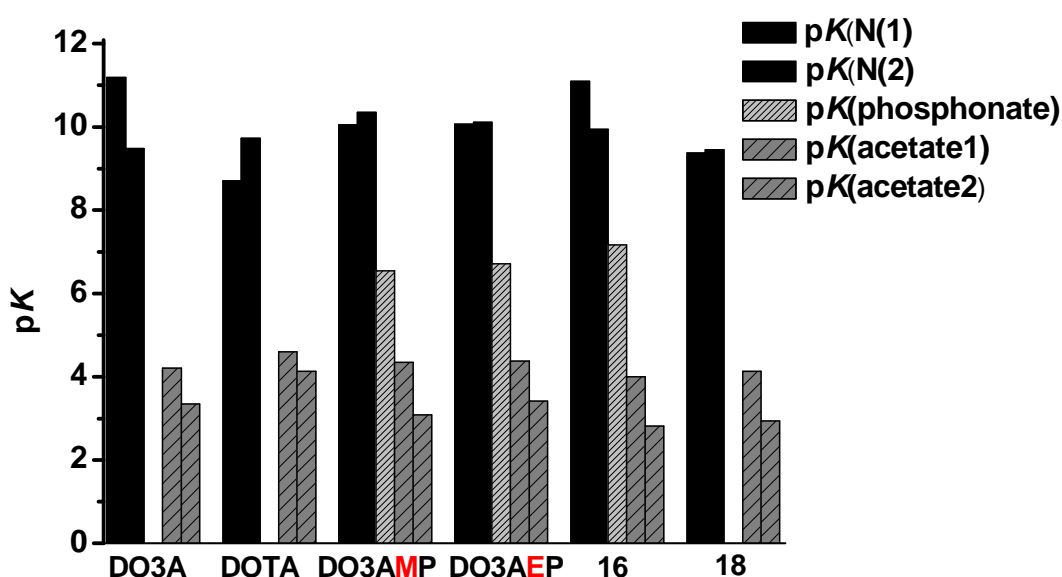
Figure 7.   Bar diagram of the stepwise dissociation (protonation) constants of studied and discussed macrocyclic ligands.

The same phenomena can be observed for the overall protonation constant, representing the protonation of two nitrogen atoms in the cyclen rim and two acetate pendant arms (Figure 8). Comparing the protonation patterns in the bar diagram, the DO3A-like derivatives are more similar to DO3A than to DOTA. In addition, the protonation constant of the phosphonic acid is dependent on the length of the chain of the pendant

arm (Figure 9) and is approaching the protonation constant of methylphosphonic acid (log K_p = 7.54, I = 0.1 M NaCl, t = 25 °C).[141]
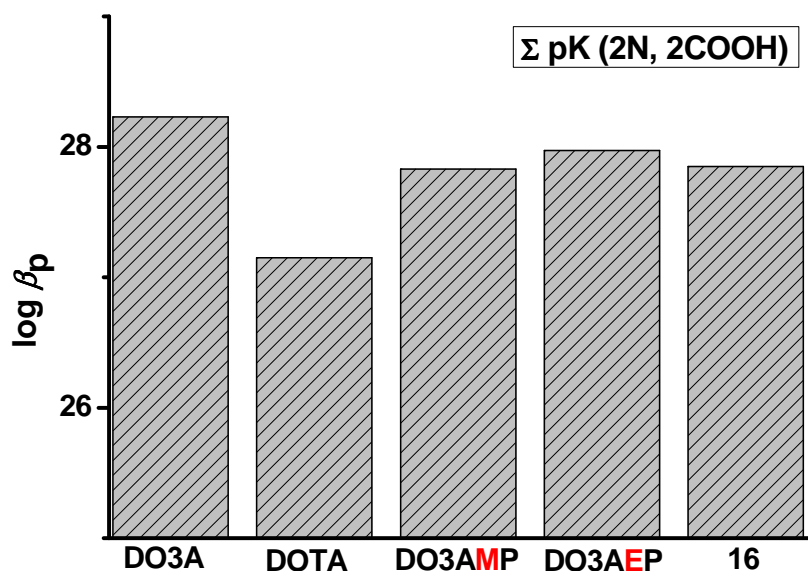
Figure 8.   Bar diagram of the overall protonation constant of studied and discussed macrocyclic ligands.

This effect is probably related to the weakening of the hydrogen bond with prolongation of the chain length and thus the phosphonic functional group becomes less acidic. This is supported also by the fact that the DO3APP ligand has the most compatible pattern of the protonation constants to DO3A. It probably means that the propylphosphonate arm does not take part in the formation of the hydrogen bond. Also it cannot be excluded that the phosphonate group can interact with other acetate arms. In case of the protection of the phosphonate pendant arm in the form of bis(esters), the lower protonation constants of nitrogen atoms of the cyclen ring were determined and they are much closer to the values found for DOTA than for the mixed macrocyclic ligands DO3AMP, DO3AEP, **16**. This sharp decrease of basicity was observed also for other macrocyclic ligands having ester groups[142,143].
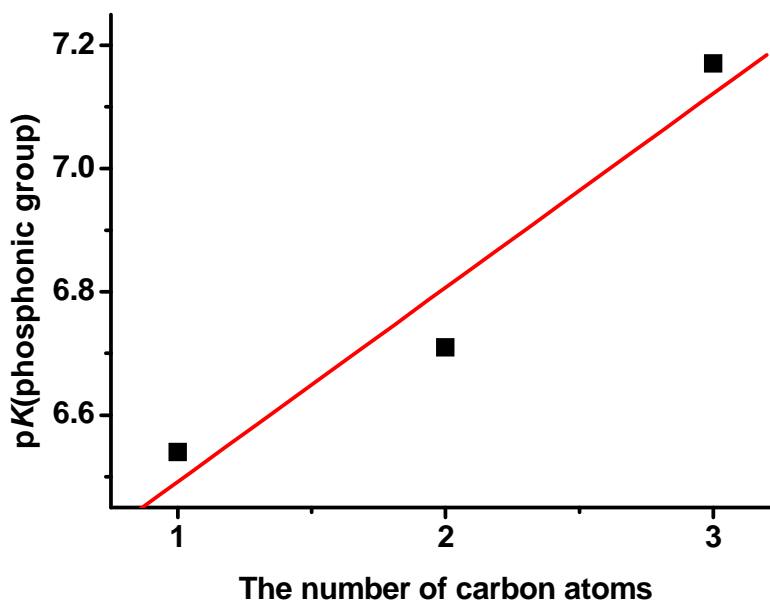
Figure 9.   Plot of dissociation constant of phosphonic pendant functional group bound to macrocyclic ring as function of the number of carbon atoms in the pendant arm chain.

Determination of the stability constants of the calcium(II) complexes

The interaction of calcium(II) ions with the macrocyclic ligands was studied by means of potentiometric titration with a glass ion-selective electrode. The results are given in Table 3. As it can be seen (Figures 10 and 11), the highest stability of all calcium(II) complexes shows DO3AMP which is comparable with that of DOTA. The order of the stability of the calcium complexes is as follows: DO3AMP ≈ DOTA > **16** ≈ DO3A > DO3AEP. This

can be explained by steric reasons. Interestingly they also decrease with the ability of the phosphonate to bind to gadolinium.

The first protonation constant of the CaL complex is related to the protonation of the oxygen atom of the phosphonic pendant arm which is not coordinated to the calcium(II) ion (Chart 6). On contrary, protonation constant of the second oxygen of the phosphonate does not depend on the chain length as it was observed for the first protonation constant. The second and third protonation constants belong to the protonation of the

$$[Ca(H_3L)] - [H^+] \rightleftharpoons [Ca(H_2L)]^- - [H^+] \rightleftharpoons [Ca(HL)]^{2-} - [H^+] \rightleftharpoons [Ca(HL)]^{2-} - [H^+]$$
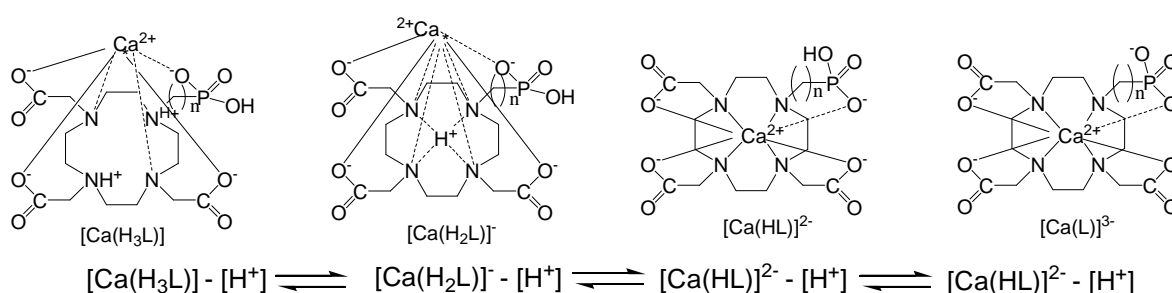
Chart 6. Formation of calcium complexes with DO3A based phosphonate containing ligands.[136]

nitrogen atoms of the cyclen ring (Chart 6). This hypothesis is supported by the fact that the proton affinity increases with the prolongation of the chain length of the phosphonic pendant arm. This is a consequence of the longer distance between the calcium(II) ion and the macrocyclic ring. In addition, the same decrease of the stability constants of the calcium(II) complexes in a sodium chloride medium was observed as for the ligand protonation which is in agreement with literature data.[142,144] The stability of the calcium(II) complexes of ligand **18** where the phosphonic group is blocked by the ethylester functions is slightly decreased.

Table 3.   Logarithmic values of stability constants of complex formation with studied macrocyclic ligands

Reaction[a]	DO3A	DOTA	DO3AMP	DO3AEP	16	18
$Ca + L \rightarrow CaL$	11.96 13.39[f] (12.16[d])	17.22[f] (14.19[d])	17.38[f] (13.27[d])	9.56	11.99	10.13
$Ca + L + H \rightarrow Ca(HL)$	17.47	---	24.87[f] (21.10[d])	17.18	19.68	14.8[e]
$Ca + L + 2H \rightarrow Ca(H_2L)$	22.82	---	29.05[f] (25.28[d])	22.49	25.71	---
$Ca + L + 3H \rightarrow Ca(H_3L)$	---	---	32.16[f] (28.39[d])	27.74	30.97	---
$CaL + H \rightarrow Ca(HL)$	5.51	3.80[f]	7.83	7.62	7.69	4.7[e]
$Ca(HL) + H \rightarrow Ca(H_2L)$	5.35	3.77[f]	4.18[a]	5.31	6.03	---
$CaL + 2H \rightarrow Ca(H_2L)$	10.86 11.36[f]	7.57[f]	12.01	---	---	---
$Ca(H_2L) + H \rightarrow Ca(H_3L)$	3.8[f]	---	3.11	5.25	5.26	---
$Ca + HL \rightarrow Ca(HL)$	6.28	9.28	10.75	7.12	8.59	5.41
$Ca + H_2L \rightarrow Ca(H_2L)$	2.15 2.79	3.29	8.39	2.32	4.67	---
$Ca + H_3L \rightarrow Ca(H_3L)$	2.33	---	7.16	0.86	2.76	---
$CaL + OH \rightarrow CaL(OH)$	---	---	---	---	---	-11.6
$GdL + H \rightarrow Gd(HL)$	---	---	5.42	---	5.2	---
$GdL(H_2O) \rightarrow GdL(OH) + H$	---	---	-12.72	-11.2	-11.4	-11.1
$Ca + GdL \rightarrow Ca(GdL)$	---	---	---	---	2.7	---

[a]The charges are omitted for the sake of clarity; [b]t = 25 °C, I = 0.1 M NaCl (otherwise the medium is mentioned), [c]for logK the standard deviation ≤ 0.04 logK unit (calcium(III) omplexation) or ≤ 0.2 logK unit (gadolinium(III) complexation); [d]ref. 136 – corrected for sodium ion concentration; [e]estimated value; [f]ref. 139
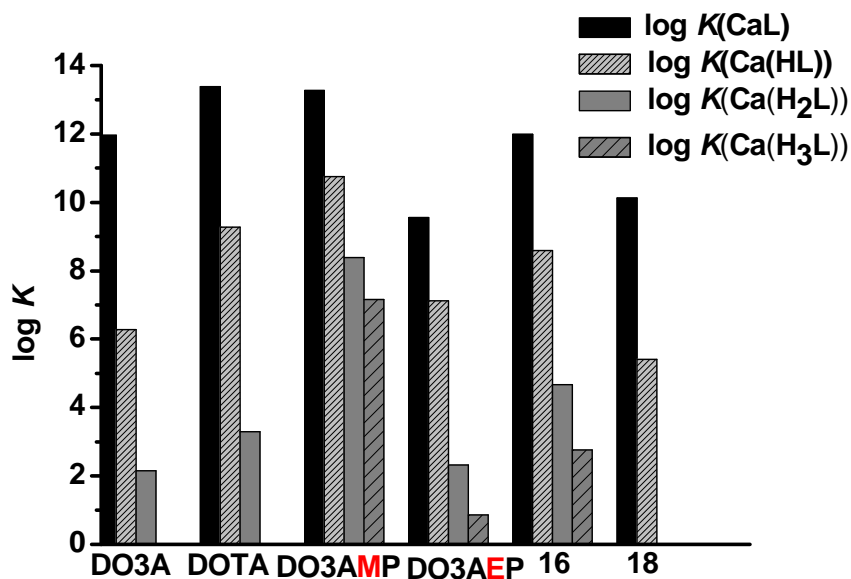
Figure 10.   Bar diagram of the stability constants of calcium(II) complexes of studied and discussed macrocyclic ligands.
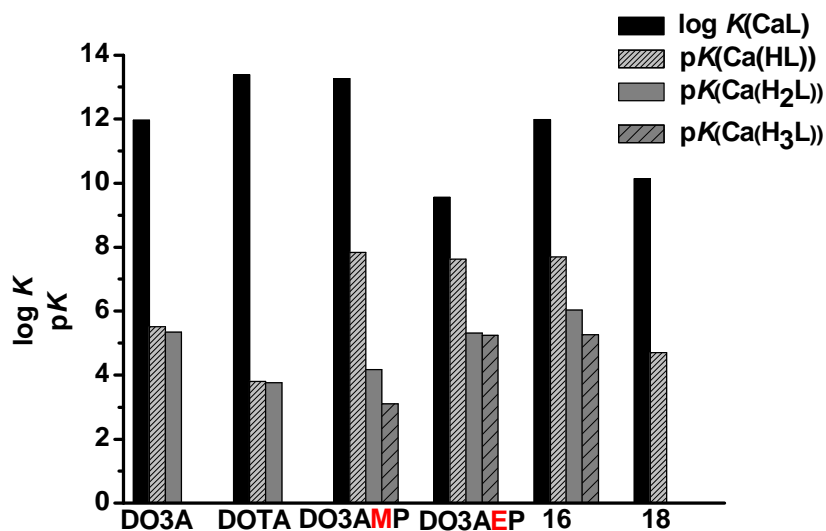

Figure 11.   Bar diagram of the stability and dissociation constants of the calcium(II) complexes studied.

Properties of the gadolinium(III) complexes

The stability constants of gadolinium(III) complexes found in literature vary for different experimental conditions (mostly pH, kind of inert electrolyte, temperature, etc.) and employed experimental techniques[137]. Probably the most critical parameter is the reaction time in acidic pH where the complexation reaction is taking place in about several hundreds of hours. Therefore there are discrepancies in values of the stability constants reported in literature.[137] In order to overcome these difficulties, the equations based on LFER (linear free energy relationships) for the estimation of the stability constant of gadolinium(III) complexes from acidobasic properties were derived as: $\log K_{GdL} = (0.85 \pm 0.02) \times \Sigma\, pK_a$ (Table 4).[140] Using this equation, the stability constants of gadolinium(III) complexes were estimated to: 24.0 (GdDO3A), 25.0 (GdDOTA), 29.2 (GdDO3AMP), 29.8 (**16**), 22.0 (**18**) (Table 4).

Table 4.   Calculated stability constants of gadolinium complexes

Compounds	$\log K_{GdL}{}^{a)}$	$\log K_{GdL}{}^{b)}$	$\log K_{GdL}{}^{c)}$
GdDO3A	24.0	19.2	21.2(20.00)
GdDOTA	25.0	22.4	26.6(23.6)
GdDO3AMP	29.2	21.1	26.8(23.0)
17a	29.8	19.3	---
19a	22.0	16.7	---

a) $\log K_{GdL} = (0.85 \pm 0.02) \times \Sigma\, pK_a$;

b) $\log K_{GdL} = (1.4 \pm 0.1) \times \log K_{CaL} + (2.5 \pm 1.2)$; (calculated for NaCl medium)

c)   values corrected for a sodium chloride medium (calculated for TMACl medium).;

The complexing properties with respect to calcium(II) ion can be used as well to calculate the stability constants: $\log K_{GdL} = (1.4 \pm 0.1) \times \log K_{CaL} + (2.5 \pm 1.2)$. This relationship suggests that any differences in the stability of both complexes are the same. Applying the above mentioned relationships simultaneously with the knowledge of the stability constants of the calcium(II) complexes the following stability constant of Gd(III) complexes were calculated: 19.2 (GdDO3A), 22.4 (GdDOTA), 21.1 (GdDO3AMP), 19.3 (**17a**), 16.7 (**19a**) (Table 4). The logarithmic value of the stability constant for the GdL complex corrected for a sodium chloride medium is 23.7 (GdDO3AMP), 19.8 (GdDO3A), 20.6 (GdDOTA) (Table 4). This was used to verify the calculations. As it can be seen, the experimentally obtained values are in the range of limits found for both estimations but they are closer to the values obtained from CaL-GdL according to LFER. The overestimation obtained from the overall protonation constant can be caused by the fact that all pendant arms are considered as potential binding sites which cannot be a real situation in case of the longer phosphonic arm of **17a**. However, the solved solid-state structure and NMR study of Ln(III) complexes of DO3AMP ligand proved that the lanthanide(III) ions are fully bound by this octadentate ligand.[145,146] The calcium(II) ion can be bound by the gadolinium(III) complex and a rough estimate of the stability constant of the ternary complex [Ca]**17a** is about 2.7 (Table 3). This value is higher than that described for the stability constant of the calcium(II) complex with methylphosphonic acid (DOA3MP) ($\log K \approx 1.6$). This could be either a consequence of Ca(II) binding not only to the phosphonate group but also partially to the acetate arms which contribute to stabilize the chelate. On the other hand in **17a** the phosphonate group provides two hydroxyl functions to bind calcium. All the known values of the equilibrium constants were used to simulate the distribution diagrams of the gadolinium(III) complex as function of solution acidity (Figure 12). The results are in agreement with those obtained from pH dependence of the relaxivity of the GdL complexes.
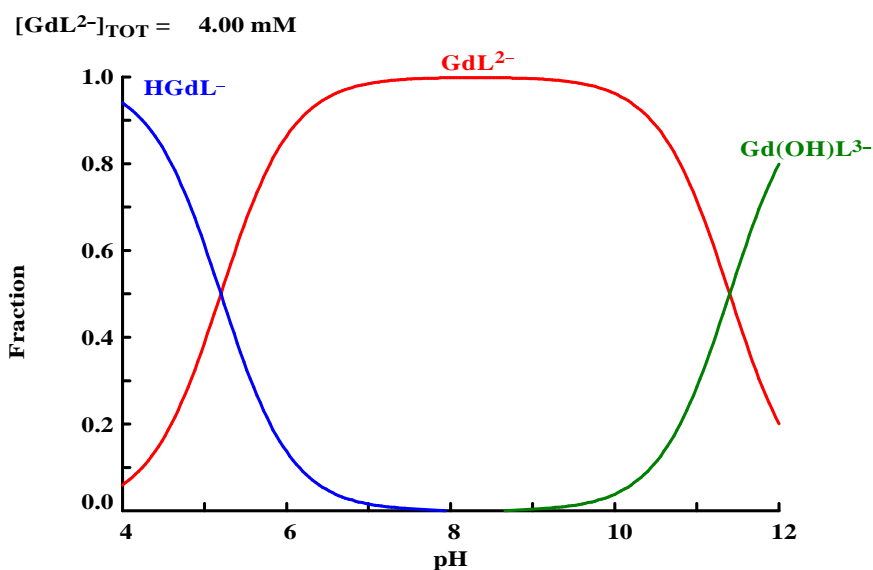
Figure 12. Distribution diagram of the protonated species of complex **17a.**

Thus complex **17a** is suitable for relaxiometric measurements at pH between 4 and 7 while **17a** slowly decomposes at pH < 3. Complex **17a** is capable of binding calcium(II) in mM concentrations in the physiological region at pH = 7.4 (Figure 13). Therefore **17a** can be considered as a promising diagnostic agent for the study of neurochemical processes.
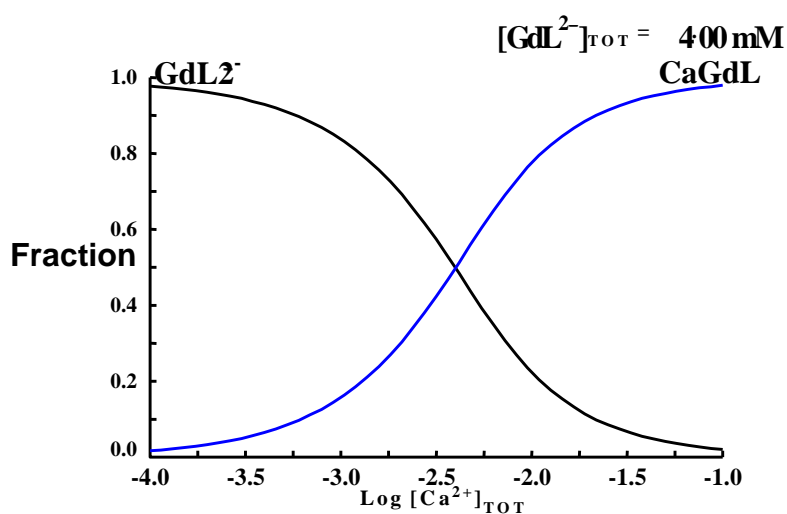
Figure 13. Distribution diagram of calcium(II) ion binding by gadolinium(III) complex **17a** (pH 7.4).

Relaxivity studies of the complexes 17a and 19a

The paramagnetic properties of the gadolinium(III) complexes **17a** and **19a** have been studied by relaxometry at low magnetic fields (20 and 60 MHz, 37 °C, Figure 14) as well as at high magnetic field (300 MHz). The most dramatic change of the relaxivity for both complexes is observed in the pH range between 4 and 7. The relaxivity (20 MHz) of 4.79 mM^{-1}s^{-1} (**17a**) and 3.83 mM^{-1}s^{-1} (**19a**) at neutral pH increase upon acidifying the solution medium to pH 4 up to 5.90 mM^{-1}s^{-1} (**17a**) and 8.57 mM^{-1}s^{-1} (**19a**), respectively. This is equal to 23% of relaxivity changes for compound **17a** and 60% for **19a**. Experimental values determined for the same samples and under similar conditions (pH, temperature) at 60 MHz were similar to those at 20 MHz.
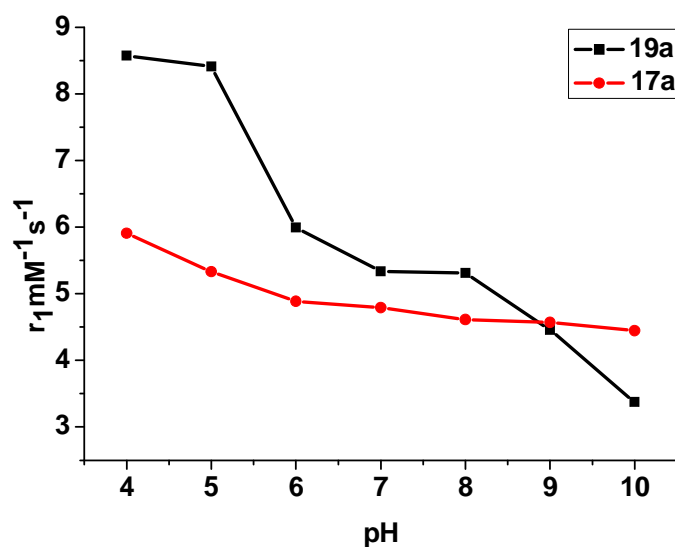
Figure 14. Relaxivity vs. pH for the unprotected (**17a**) and protected (**19a**) phosphonates (20 MHz, 37 °C).

The decrease of the relaxivity at higher pH can be explained either by the formation of ternary complexes with carbonates from the CO_2 from air or by the exchange of water molecules with the OH groups in basic conditions. The pH dependence of the relaxivity at low pH could be due to the presence of uncoordinated phosphonate groups in the complexes **17a** and **19a.** The protonation of these groups can catalyze the exchange of protons between the bound water molecule and the bulk water by providing an efficient hydrogen bond network.[151] To demonstrate that pH changes can be sensed in MR imaging experiments, two phantoms each consisting of four Eppendorf tubes, filled with 2 mM solutions of CA at different pH (4, 5, 6 and 7) were prepared and T_1-weighted images were obtained (Figure 15). The results demonstrate a relative increase of 46% for **17a** and 37% for **19a** in the relaxation rate between pH 4 and 7, giving a promising outlook for the application of compounds **17a** and **19a** as CAs even in high field MRI.
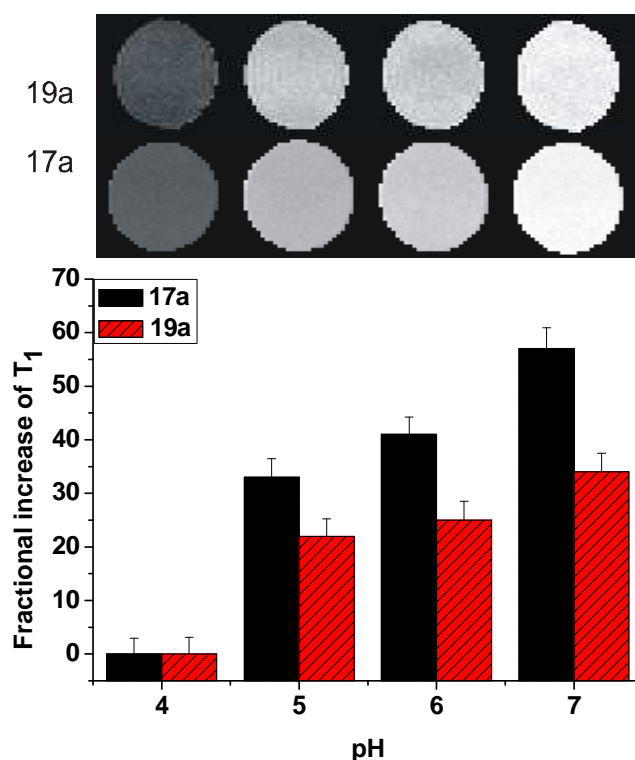
Figure 15. Phantom images of **19a** and **17a** in the pH range 4-7 (top) and the appropriate fractional increase of T_1 (bottom).

^{31}P NMR spectra of the europium complexes were recorded to prove, that no dissociation processes take place at low pH (Figure 16). As it is shown, no changes in the spectra are observed by allowing the sample to stay for several days in solutions with pH 4 to 10. Slow decomplexation was observed in the spectra after one day at pH 3, which is shown as an additional signal in spectrum **c**. The lifetime of the complexes at pH below 2 was found to be around 30 min.
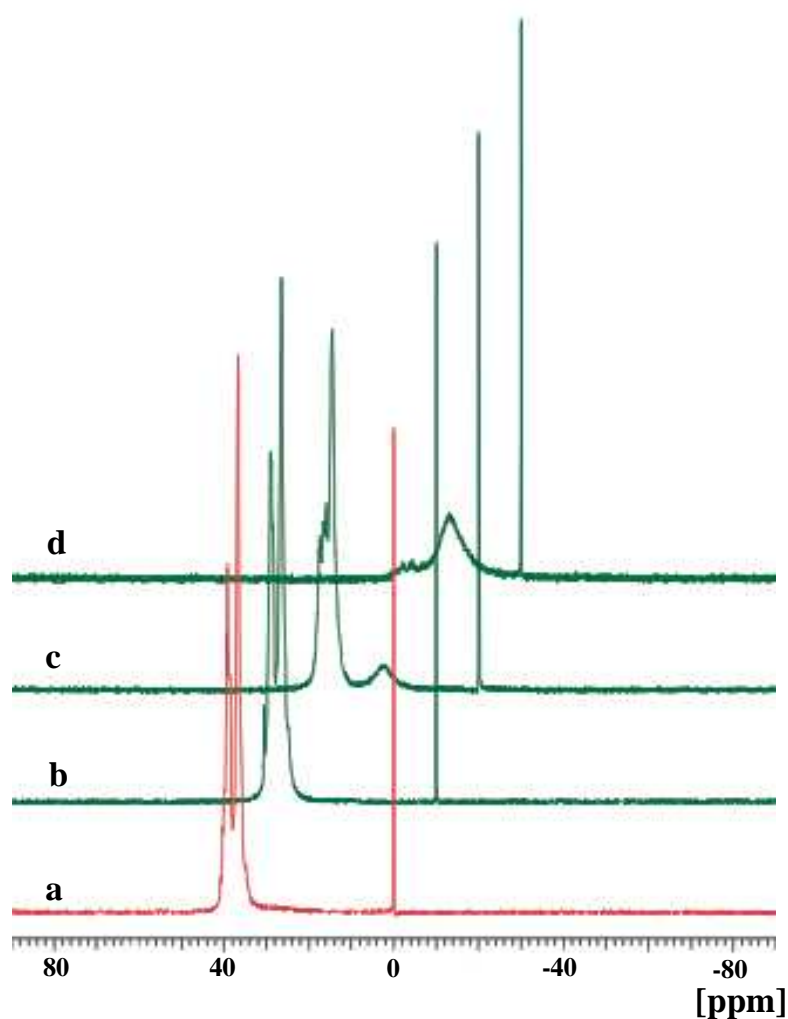
Figure 16. ^{31}P NMR spectra of the Eu DO3APPE (**19b**) complex versus pH: **a)** pH 7, **b)** pH 4, **c)** pH 3 and **d)** pH 2; (H$_3$PO$_4$ used as reference 0 ppm).

This was confirmed by the potentiometric studies of the complexes. According to these results it can be concluded, that the change of the relaxivity in the pH range between 4 and 7 is not due to decomplexation processes and release of the free gadolinium ions into the solution.

The relaxivity behavior of complexes **17a** and **19a** at different temperatures were studied at 20 MHz (Figure 17). The water proton relaxivities of the compounds increase when the temperature is lowered from 40 to 5 °C independent of the pH, which indica tes that at low temperatures there are no limitations by the water residence time.
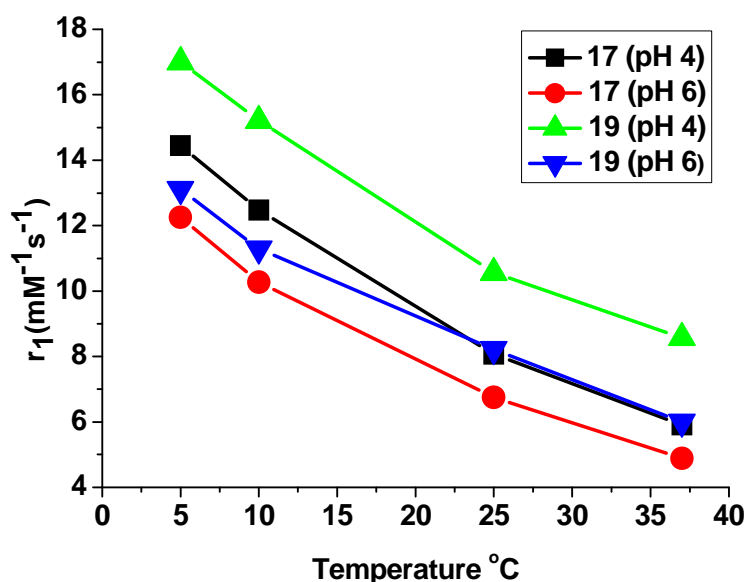
Figure 17. Evolution of the proton relaxivity vs. temperature for the compounds **17a** and **19a** at pH 4 and 6.

The interpretation of the evolution of the relaxivity as a function of magnetic field in the NMRD profiles (Nuclear Magnetic Relaxation Dispersion profiles), with the help of appropriate theoretical models allows to get information about the parameters governing the relaxivity (like τ_M, τ_R, τ_{SO}, τ_v ....)(Table 5).[151] The experimental data were fitted using

61

either the classical innersphere (IS) and outerspehre (OS) model or innersphere (IS), outerspehre (OS) and second sphere (SS) model (Figure 18).

Table 5.   Fixed and found data of NMRD profiles fitting

Compound	**19a** pH 6	**19a** pH 4	**19a** PH 4	**17a** pH 6	**17a** pH 4	**17a** pH 4
model	IS+OS	IS+OS	IS+OS+SS	IS+OS	IS+OS	IS+OS+SS
d (nm)	0.36	0.36	0.4	0.36	0.36	0.4
D $(10^{-9}\,m^2s^{-1})$	3.3	3.3	3.3	3.3	3.3	3.3
r (nm)	0.31	0.31	0.31	0.31	0.31	0.31
τ_R **(ps)**	76	92	75	51	64	51
τ_M **(ns)**	100	100	100	100	100	100
τ_{SO} **(ps)**	74	159	95	69	77	51
τ_V **(ps)**	24	40	24	7	13	7
q	2	2	2	2	2	2
r_{ss}**(nm)**			0.36			0.36
q_{ss}			4			3
τ_{SS} **(ps)**			30			30

The following parameters were fixed:

IS + OS model: distance of closest approach d = 0.36 nm, relative diffusion constant D = 3.3 10^{-9} m^2s^{-1}, distance for the innersphere interaction (r) = 0.31 nm, number of coordinated water molecules (q) fixed to 1 or 2 depending on the complex, the water residence time (τ_M) to a value which does not influence the fitting (100 ns).

IS + OS + SS model: distance of closest approach d = 0.4 nm, relative diffusion constant D = 3.3 10^{-9} m^2s^{-1}, distance for the innersphere interaction r = 0.31 nm, number of coordinated water molecules (q) fixed to 1 or 2 depending on the complex, the water residence time (τ_M) to a value which does influence the fitting (100 ns).

The rotational correlation time (τ_R), the electronic relaxation time at zero field (τ_{SO}), the correlation time responsible of the modulation of the electronic relaxation (τ_V) were adjusted in both models. In addition, when the second sphere model is included, the number of second sphere water molecules (q_{ss}), and the correlation time for the second sphere model ($\tau_{SS}= [\tau_R^{-1} +\tau_{Mss}^{-1}]^{-1}$) are adjusted whereas the distance for the second sphere was set to 0.36 nm (Table 5).
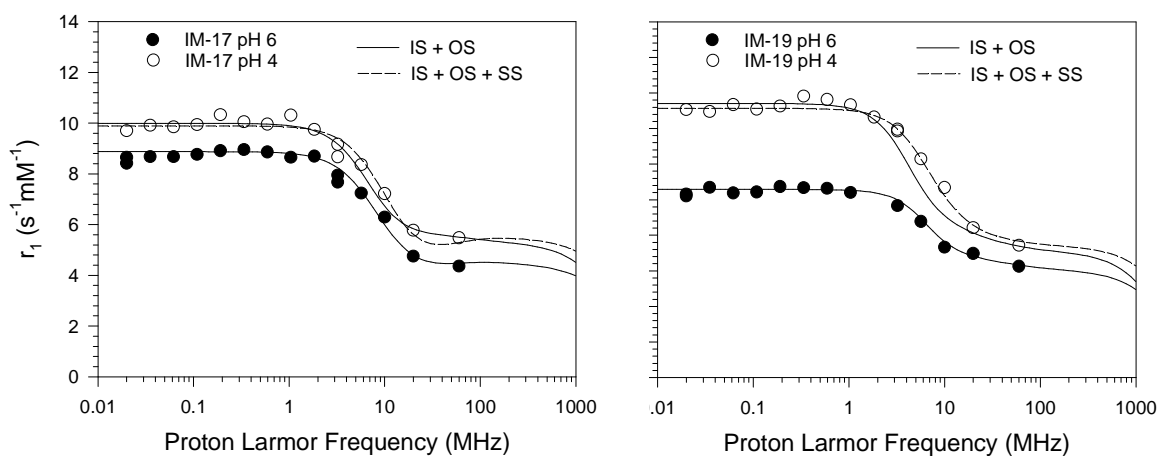
Figure 18. NMRD profiles of the compounds **17a** and **19a.**

For both complexes, at pH 6, the IS+OS fitting is well. At pH 4, better results are obtained with the IS+OS+SS model for the compound **19a** but for complex **17a** both models fit correctly the data.

Nevertheless, it is to be noticed that at pH 4 when only IS + OS is used, the value of τ_R has to be increased or the value of q has to enhance whereas when the SS is included τ_R is similar at both pH. That, probably means, that at low pH secondary sphere water molecules form which contribute to the relaxivity increase considerably.

2.2.4. Conclusions

In conclusions, the synthesis and initial physicochemical studies of two novel contrast agents has been achieved. They are designed to exhibit relaxivity changes in different pH environments, since the pH sensitive, phosphonate group is appended to the macrocyclic ring. Comparison of the acidobasic properties of the ligands (**16** and **18**) and complexes (**17** and **19**) with the literature data shows that pKa of the phosphonates depend on the length of the side chain and the phosphonates *do not* contribute to the thermodynamic stability of the gadolinium and calcium complexes. Relaxometric experiments with complexes **17a** and **19a** have been performed at various magnetic fields (20, 60 and 300 MHz) and pH of solutions (pH 4-10). The most interesting results were obtained at acidic pH where relaxivity of **17a** and **19a** increased by 23% and 60% respectively, when the pH of the medium has changed from neutral to pH 4 (20 MHz). The phantom images at 300 MHz confirm the possibility to sense the contrast changes visually. ^{31}P NMR spectra of the europium complexes were recorded to prove, that no dissociation processes take place at low pH. The complexes are stable in the range of pH 4 to 10, but slow decomplexation was observed in the spectra after one day at pH 3. The lifetime of the complexes at pH below 2 was found to bee around 30 min. This was confirmed by the potentiometric studies of the complexes. According to these results it can be concluded, that the change of the relaxivity in the pH range between 4 and 7 is not due to decomplexation processes and release of the free gadolinium ions into the solution.

The potential application of reported complexes with the relaxivity changes in the range of pH 4-7 might be found in the diagnosis of e.g. late stages of cancer, or the detection of the necrotic core of cancer tissues, where very low pH values could be observed. With the further optimizations of compounds which should show larger relaxivity changes in the relative small physiological pH range, one could find much broader applications.

Such contrast agents might be used not only in early cancer diagnostic but also as functional markers in the tracking of regular physiological pH-dependent processes *in vivo*.

2.3. Synthesis and characterization of DO3A based amino(bismethylene)phosphonate complexes as potential Ca sensitive contrast agents

2.3.1. Introduction

Aminophosphonic acids are becoming increasingly important for biological applications[152-154] as well as in the design of new synthetic ligands as chelating agents for metal ions.[155-159] This fact provides new evidence for the effectiveness of aminophosphonate donor groups in the binding of metal ions, and provides more precise data for the phosphonate analogue of DTPA and EDTA (Cart 15a and c).[160-161] Over the last years series of CAs for MRI with aminophosphonates and bis(phosphonates) as targeting group have been developed[162-164] Aminophosphonates are known to have affinity for calcified tissue and a series of EDTA and DO3A based compounds were investigated as potential bone targeted contrast agents for MRI (Chart 15b and d).[165]
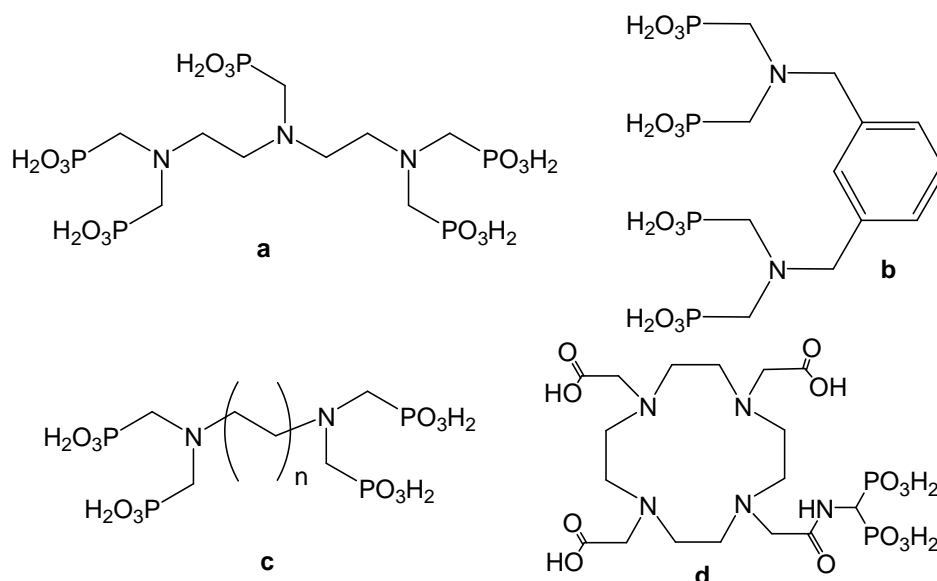
Chart 7.   Aminophosphonates as chelators for gadolinium.

The properties of amino polyphosphonates (APP) were reported by Schwarzenbach and physico-chemical characteristics studied by Martell in comparison with amino polycarboxylates (APC).[166-171]

The thermodynamic characteristics and complex affinity of aminophosphonates towards the alkali and alkali-earth elements was described in a series of publications.[172-176] It was shown that the stepwise replacement of N-acetate by N-methylenephosphonate groups in nitrilotriacetic acid (NTA) results in an increase in the Ca^{2+} and Mg^{2+} stability constants, although the increase over NTA does not follow a linear relationship. There is no large decrease in binding of Ca^{2+} and Mg^{2+} in going from nitrilotrimethyltriphosphonates (NTMTP) to its N-oxide. This suggests that binding of Ca^{2+} and Mg^{2+} in compounds containing the $NCH_2PO_3H_2-$ moiety is principally by the phosphonate group with little or no interaction by the tertiary nitrogen (Chart 8). The formation constant of magnesium chelates with amino polycarboxylate is usually smaller than that of calcium and the same behavior is expected for the similar aminophosphonates.[177]
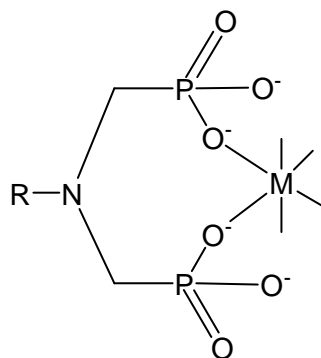
Chart 8. Complex formation of amino(bismethylene)phosphonates with the alkali-earth metals.

The hydration energy of Mg^{2+} is fairly large because of its small ion size, and thus the enthalpy of the formation of Mg^{2+} chelates is much smaller than those of other alkaline earth-metal ions.[178]

Among the several factors the steric crowding effect was discribed to be the important issue to influence the rate at which the gadolinium bound

water exchanges with molecules into the bulk.[179,180] Furthermore the overall charge of the chelate ligand has an impact of water exchange rates and thus of altering the relaxivities of the complexes.[181] Negatively charged substituents on the surface of paramagnetic complexes are able to bind water molecules which contribute to the overall relaxivity of the complexes.[182,183]

According to these data the DO3A based macrocyclic compounds with the variable length of the methylenphosphonate side chain was designed (Chart 9). Due to the higher affinity of Ca^{2+} towards AMP it is expected that Ca^{2+} ions can bind to the phosphonate groups leading to a reduced overall charge of the complexes and/or generate an additional coordination side at the gadolinium. Both effects should provoke the water exchange rates and thus result in a change in relaxivity. In this way the complexes act as Ca^{2+} sensitive contrast agents. The different lengths of the (aminobis)methylenephosphonate side chains allow exploiting the fine-tuning of the sensitivity of the agent towards calcium ion concentration.
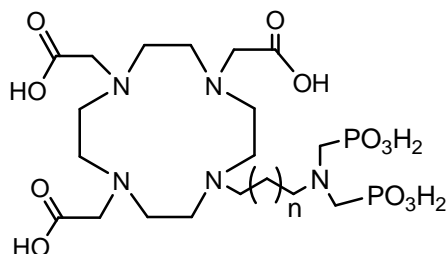
Chart 9. Macrocyclic compounds with variable length of the side chain **25a**, n = 1; **25b**, n = 3: **25c**, n = 4.

2.3.2. Synthesis of the ligands and complexes

The ligands **25a** - **c** were synthesized according to the Scheme 8. Aminoalkyl alcohols were brominated with HBr/acetic acid solution and amino groups were protected using Boc$_2$O at basic conditions to give compounds **21a** - **c**.
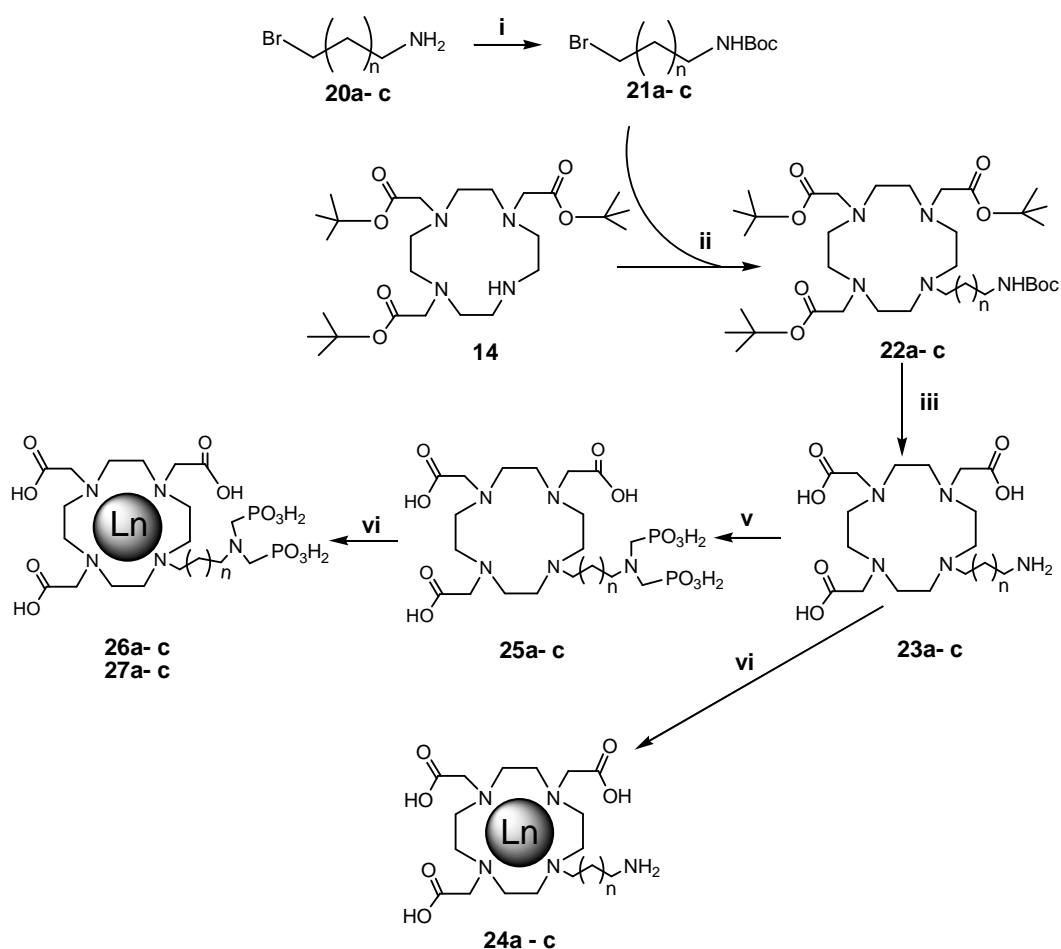
Scheme 8: Synthesis of the macrocyclic compounds **24a – c, 26a – c, 27a – c;.a**: n = 1; **b**: n = 3; **c**: n = 4; i) Boc$_2$O, NaOH, DCM; ii) K$_2$CO$_3$, CH$_3$CN; iii) DCM, TFA; iv) H$_2$O, GdCl$_3$ x H$_2$O (**24a – c**); v) H$_3$PO$_3$,H$_2$CO, H$_2$O;vi) H$_2$O, GdCl$_3$ x H$_2$O (**26a – c**), H$_2$O, EuCl$_3$ x 6H$_2$O (**27a – c).**

The *tert*-butyl ester of DO3A[185](**14**) was alkylated with the corresponding Boc protected bromoalkylamines to give **22a – c**. The carboxyl and amino groups were deprotected in a one step reaction with trifluoroacetic acid in dichloromethane. After recrystallisation from diethyl ether followed by recrystallization with acetone the aminoalkyl substituted DO3A **23a – c** were obtained. Remowing of the TFA was followed by ^{13}C NMR spectroscopy. The methylenephosphonates were attached to the amino side chains by a Mannich reaction using phosphorous acid and formaldehyde at 100°C.[186] After recristallization from water / ethanol or water / isopropanol solutions finally the ligands **25a – c** were obtained as a colorless powders. Several times recrystallization were requiered to remove the excess of phosphoric acid which was followed on ^{31}P NMR spectroscopy. The synthesized ligands were characterised by ^{1}H, ^{13}C, ^{31}P NMR spectroscopy and HR-MS spectrometry. Characteristic resonances are presented in the ^{13}C NMR spectrum of compounds **26c** (Figure 19)**.** Due to the interaction of the carbon 14 with the phosphorous nucleus the resonance is split into a doublet ($^{1}J_{PC}$ = 33.8 Hz).

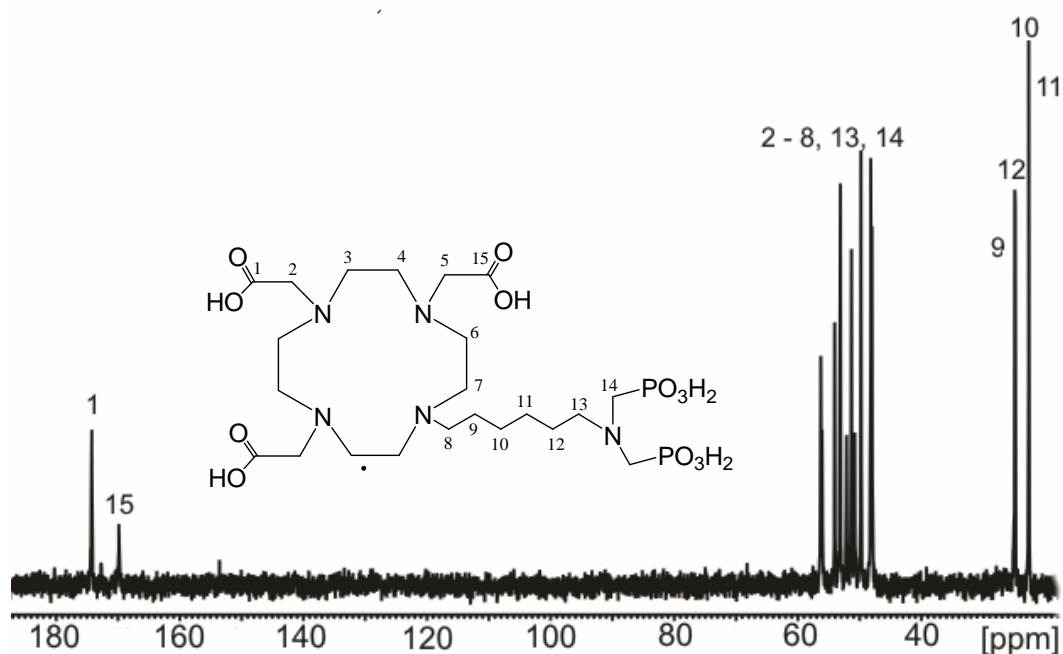**Figure 19**. ^{13}C{^{1}H} NMR spectrum of compound **26c.**

Stock solutions of the metals with known concentrations were prepared from the chloride salts of the corresponding metals. The exact concentrations were determined by the complexometric titration with the standard solution of the disodium salt of EDTA. The complexes **26a – c** and **27a – c** were formed by stirring the mixtures of the corresponding stock solutions and ligands in a ligand : metal ratio 1 : 0.9. Finally the complexes were filtered and lyophilized. The xylenol test was preformed to insure that there are no free metal ions in solution. The formations of the complexes were confirmed by the ESI-MS mass spectrometry in the negative and positive mode. The molecular ion peaks with the characteristic seven isotopes for the gadolinium(III) complexes **26a – c** were present in the spectra. In the mass spectra of compounds **27a – c** all peaks related to the mass of the $[M+H]^+$, $[M+Na]^+$ and $[M+2Na]^+$ complexes are observed.

2.3.3. Physico-chemical characteristics of the ligands and complexes

Potentiometric studies of the ligands

The acidobasic properties of the synthesized ligands **26a – c** were studied by means of glass electrode potentiometric titrations at 25 °C and 0.1 M ionic strength (NaCl). Compounds **26a – c** represent a set, in which each of the phosphonate (PO_3^{2-}) groups is capable of accepting two protons and the nitrogen atom of the aminophosphonates moiety one proton. Fully protonated ligands contain ten dissociable protons [$H_{10}L$]. However, under the applied experimental conditions only seven deprotonation processes could be detected (Scheme 9). The reason for this is the strong acidity of PO_3H_2 groups, which prevents evaluating the

first two *pK* values from the pH-metric titration in water. On the other hand, the strong basicity of the nitrogen protons of the aminophosphonate moieties causes the last *pK* value undetectable as it is too high. The exceptionally high basicity of the nitrogen protons can be explained by the formation of intermolecular hydrogen bonds between the oxygen of the phosphonate groups and hydrogen of the protonated iminogroups.[187]

$$[L^{7-}] + [H^+] \xrightleftharpoons{\log Kp,1} [HL^{6-}] + [H^+] \xrightleftharpoons{\log Kp,2} [H_2L^{5-}] + [H^+] \xrightleftharpoons{\log Kp,3} [H_3L^{4-}] + [H^+] \xrightleftharpoons{\log Kp,4} [H_4L^{3-}] + [H^+] \xrightleftharpoons{\log Kp,5}$$

$$[H_5L^{2-}] + [H^+] \xrightleftharpoons{\log Kp,6} [H_6L^-] + [H^+] \xrightleftharpoons{\log Kp,7} [H_4L^{3-}] + [H^+] \xrightleftharpoons{\log Kp,8} [H_7L]$$
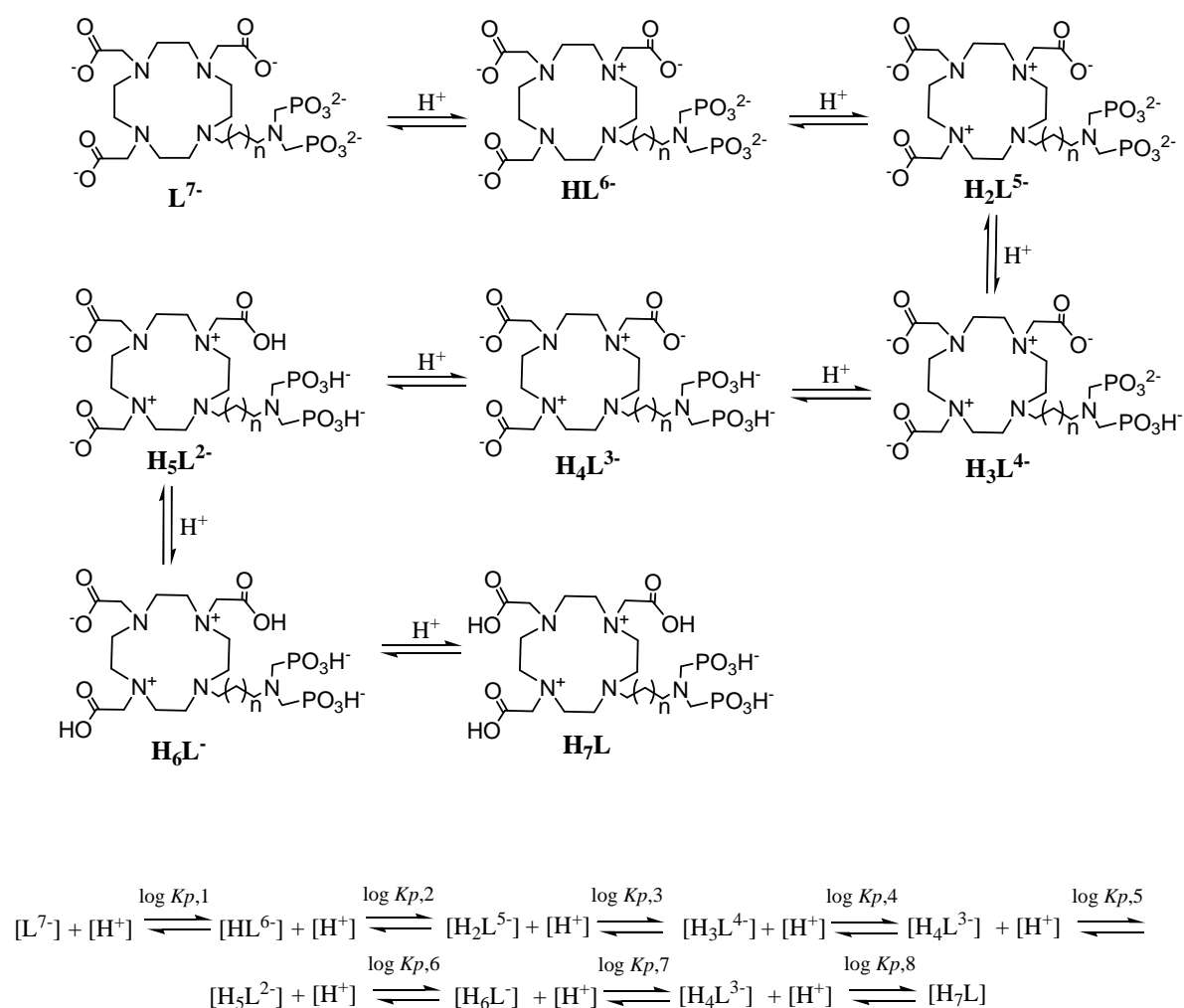
Scheme 9. Protonation of the compounds **26a – c** (only the steps where the protonation constants could be determined are shown).

The pK values characteristic for the dissociation of the two protons from the two $-PO_3H_2$ groups are ~ 1 – 1.5 and thus they are fully deprotonated in the pH range studied and do not take part in metal coordination equilibria. Further deprotonation of the phosphonic groups may cause an overlapping of the *pK* values, which means that the *pK* values of $-PO_3H^-$ are not characteristic for the real acidity of this groups.[188-189] The basicity of the compounds increase with the increase of the length of the phosphonate side arm (Table 5 and Figure 20).

Table 5. The protonation constants of the ligands **26a – c** *(t* = 25 °C, *I* = 0.1 M NaCl)

Ligand	$\log K_{p,1}$	$\log K_{p,2}$	$\log K_{p,3}$	$\log K_{p,4}$	$\log K_{p,5}$	$\log K_{p,6}$	$\log K_{p,7}$
26a	9.61	9.30	6.03	5.01	3.51	1.7[a)]	1.7[a)]
26b	10.14	9.41	6.08	4.82	4.34	---	3.49[a)]
26c	10.16	10.13	7.12	6.32	5.39	4.32	3.71[a)]

[a)]Estimated values
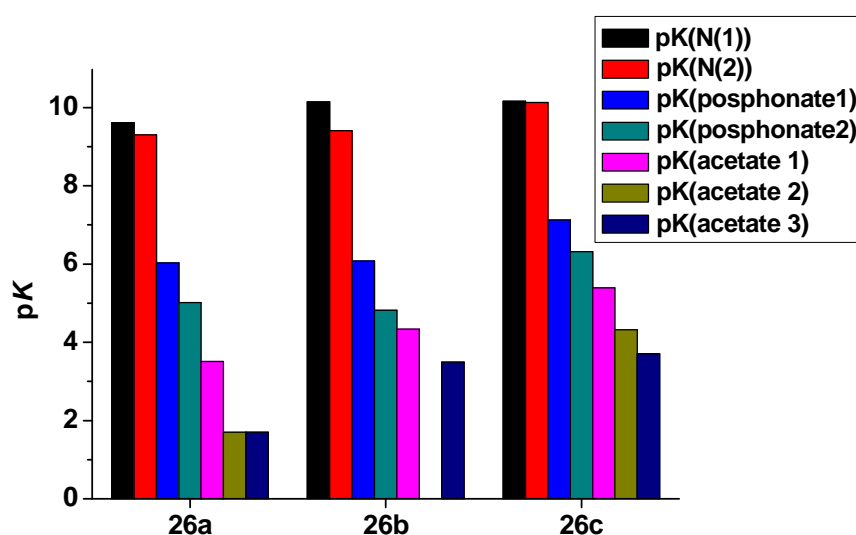
Figure 20. The bar diagram of the stepwise dissociation (protonation) constants of studied and discussed macrocyclic ligands.

That can be explained by weaknesses of the interactions between the cyclen rim and the phosphonate containing side arm. Also it cannot be excluded that the phosphonate groups can interact with other acetate arms or forming dimeric units consisting of hydrogen bonds due to the PO_3H_2 / PO_3H^- interaction between the side arms of two molecules. That will lead to higher protonation constants. This can be seen from the diagram of the overall protonation constants (Figure 21) representing the protonation of two nitrogen atoms in cyclen rim and two acetate pendant arms. The basicity of the ligands **26a – c** increases by prolongation of the side chain. Probably, the prolongation of the side chain facilitates the formation of dimeric units.

Figure 21. Bar diagram of the overall protonation constant of macrocyclic ligands.

Relaxivity measurments

The paramagnetic properties of Gd complexes **26a – c** were studied by relaxometry at high magnetic fields (300 MHz, 21°C) (Figure 22(left)) The

T_1 relaxation time of water was measured for four concentrations of the complexes **26a – c** (0.1, 0.4, 0.7 and 1.0 mM) while varying the c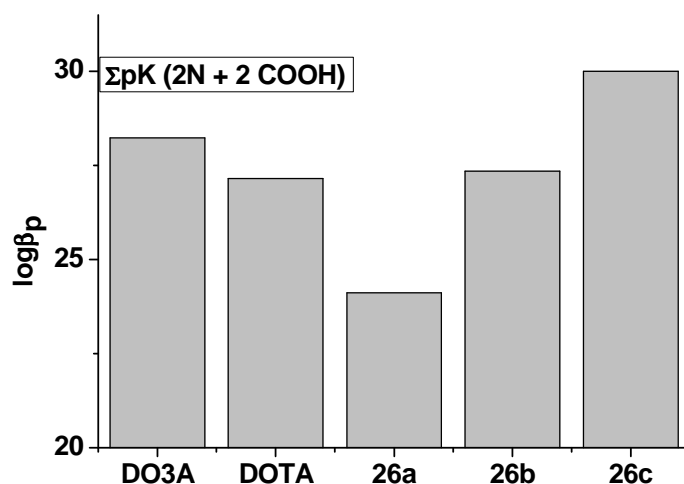oncentrations of Ca^{2+} ions from 0 to 100 mM. Relaxivity was calculated as the slope of the graph of the linear dependence of relaxation rate $1/T_1$ vs concentration of the complexes. No significant changes of the water relaxivity of **26a** were found over the whole span of Ca^{2+} concentration. Interestingly, the water relaxivity of **26b** solutions which remained constant in Ca^{2+} concentrations from 0 to 1.0 mM dropped from 3.49 to 2.56mM^{-1}s^{-1} when the Ca^{2+} concentration was increased to 10 mM. More importantly in **26c** solutions the major effect of the change in relaxivity was shifted to the Ca^{2+} concentration range from 0.01 to 5 mM which is covering the physiologically relevant area (0.5 – 2.5 mM for extracellular conditions). A maximum decrease in r_1 of 36% and of 11% within the physiological range was observed (Figure 22(right)).
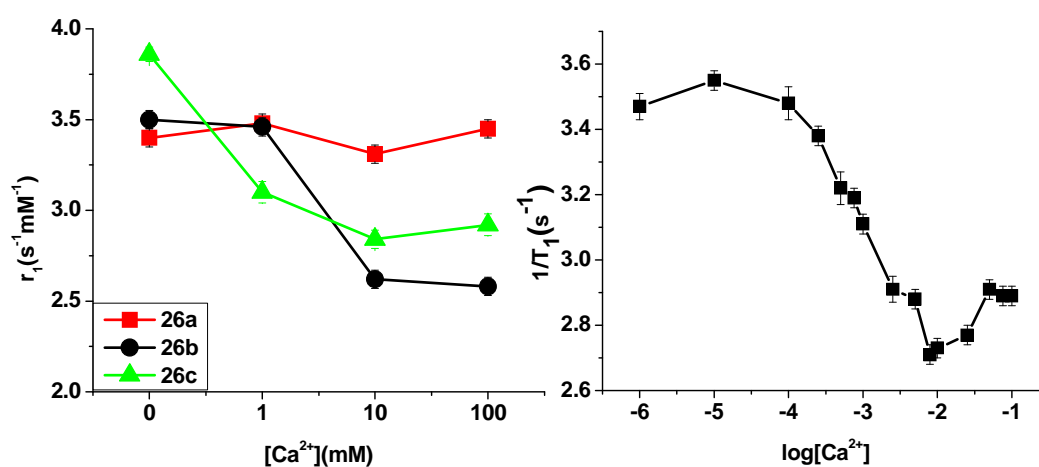
Figure 22. Relaxivity studies of complexes **26a – c** (left) and relaxivity rate vs calcium concentration in physiological range for compound **26c.**

75

To confirm that the changes of relaxivity are because of changes in calcium concentrations, an experiment in the presence of EDTA as a strong calcium chelator was performed. In each Ependorf tube which was used in the experiment with calcium (Figure 22 (left)) 1 eq. of EDTA was added. After complexation with EDTA no calcium should be in solution and relaxivity will be the same for all probes. As expected (Figure 23), after all calcium was taken by EDTA no relaxivity changes were observed any more between the samples. This confirms, that the changes in relaxivity in the first experiments were due to calcium. Furthermore the changes of relaxivity are reversible.
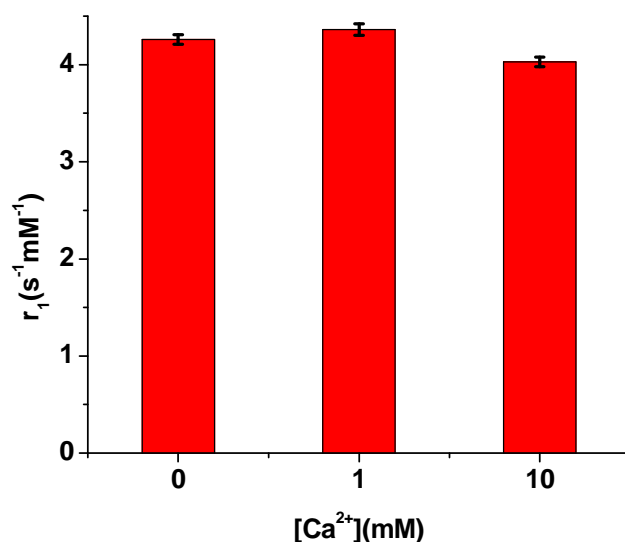
Figure 23.   Relaxivity vs calcium ions concentration measurments in presence of equimolar concentratons of EDTA for compound **26a.**

In order to simulate in *vivo* conditions where a number of other ions compete with Ca^{2+}, relaxivity studies were performed in artificial cerebrospinal fluids (ACSF)[190]. Still the relaxivity decreased by 30% in

CSF, which implies that compound **26c** is a potential candidate to act as a CA for the detection of modulations of extracellular Ca^{2+} concentrations. The next experiment was designed to study the behavior of compound **26c** in the presence of a protein mixture. Therefore the experiments were repeated in the presence of streptochinase proteins mixture at 37°C and results were compared with those in the protein free solutions. The results are presented on the Figure 24 according to which the longitudional relaxation time is by the variation of calcium ion concentrations also in the presence of proteins.
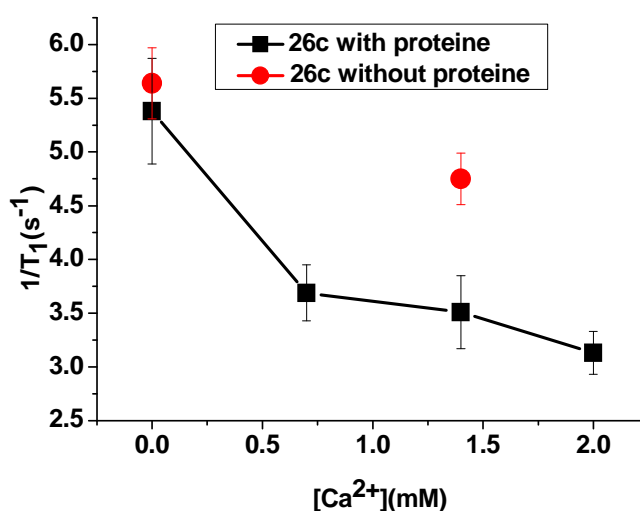
Figure 24.   Relaxation rates vs calcium concentrations in the presence and absence of protein mixture.

The relaxivity versus temperature were measured at 20 MHz (Figure 25). Decreases in relaxivity were observed for all measured compounds in the range of 5℃ to 45℃. These results indicate that a t low temperatures there are no limitations by the water residence time.
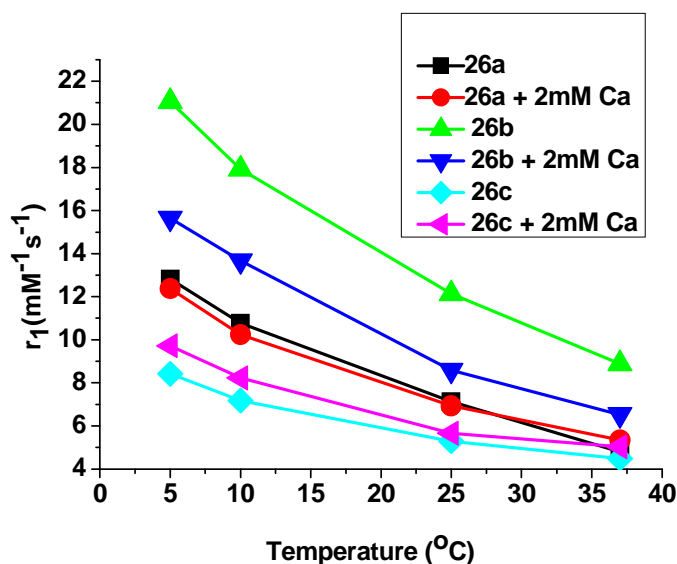
Figure 25. Relaxivity vs Temperature in the absence and presence of 2 mM Ca^{2+}.

^{31}P NMR studies of europium complexes

In the ^{31}P{^{1}H} NMR spectra of **27a** – **c** up to four signals are observed (Figure 26). They originate from the different coordination isomers which behave like diastereotopomers. The differences of the ^{31}P chemical shifts of the **27b** and **27c** complexes compared to their free ligands are rather small. This indicates that the phophonate groups are not coordinated to europium, while the chemical shift difference of 20 ppm in the case of **27a** points to an interaction between the metal center and the phosphonate functions.[181-183] Interestingly the ^{31}P resonances of **27a** are not affected by

the addition of Ca^{2+} ions to solutions of **27a** whereas the linewidths increased dramatically when the Ca^{2+} concentration is increased in the solutions of **27b** and **27c**, respectively. These results are in line with the relaxivity studies of the corresponding gadolinium complexes. Moreover after a addition of 2.5 eq of calcium to a solution of **27c** the hight field resonances are relaxed to the base line. This indicates the different diastereotopomers have a different inpact on the relaxivity.
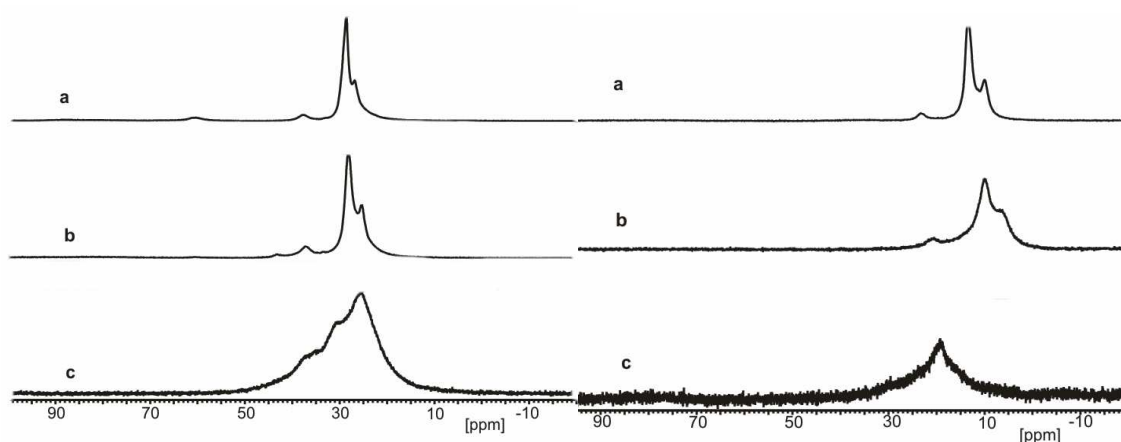
Figure 26. ^{31}P{^{1}H} NMR spectra of compounds **27a** (left) and **27c** (right) at 400 MHz, 0°C a) without calcium, b) 0.5 eq of calcium, c) 2.5 eq of calcium.

On the other hand in the amino(bismetylenephosphonate) side chains the two phosphonates provide negative charges. In conjunction with the appropriate length of the side chain this leads to the formation of the second sphere water of the gadolinium complexes which enforce the overall relaxivity of **26c** by endorsement of the water exchange rate[184]. As the Ca^{2+} cations neutralize the negative charge of the phosphonates, the water exchange rate is reduced which results in a decrease of the relaxivity.

2.3.4. In vivo studies

In vivo experiments in rats have been performed to characterize the distribution, half - live time and toxicity of the new contrast agent **26c** in the extracellular space of the brain. The feedback information that can be obtained from these experiments is essential to optimize the agents for *in vivo* situations adapting the chemical synthesis and MR contrast agent design/behavior.

The knowledge of the diffusion properties of the injected compounds in the *in vivo* experiments provides the information about their distribution in the tissue. The ideal compound should diffuse well from the ventricles and distribute all over the brain enhancing the overall contrast of the tissue. During the stimulations increase or decrease of the signal should be observed in the area of the brain responding to stimulation. Therefore, the first experiments of the direct injections into the ventricles have been performed in order to study the diffusion properties of complex **26c** (Figure 27).

| a | b | c | d |

Figure 27. Injection of the compound **26c** into the cerebroventricles. Pre injection (a), after 6 min (b), after 26 min (c) and after 1h (d).

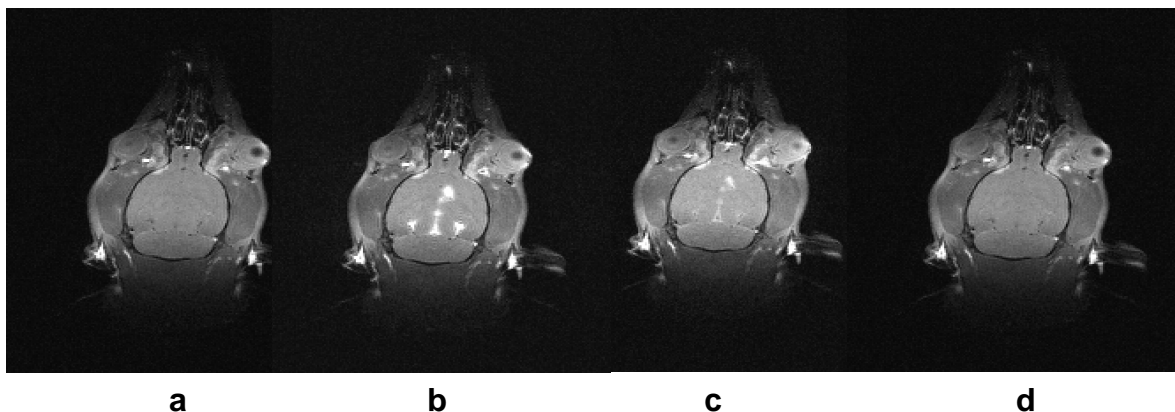The animals were prepared as described in the literature.[191] Injections were performed on animals which were placed inside the magnet in order

to provide a whole picture of the distribution of the contrast agent. The injections were done through a 4 m long sharpened fused silica capillary. 250 nL of the 20 mM solution of compound **26c** in ACSF (pH 7.4) was injected slowly over a period of 20 to 40 min. An increase of the contrast in the ventricular area directly after injection was observed (Figure 27b). Unfortunately the compound was washed out without the visible diffusion in the brain tissue. After 26 min of injection the signal was reduced (Figure 27c) and almost no contrast was detected after 1h (Figure 27d). The second series of the experiments were performed to study the diffusion of the compound in the brain by direct injection into the tissue. In these experiments injection was performed using the same method as it was described before. 120 nL of 20 mM solutions of **26c** in ACSF was slowly injected into the brain tissue of the animals. The results of the injection are presented in the Figure 28 and diagrams of the compound distribution in the tissue are shown in the Figure 29.

| **a** | **b** | **c** | **d** |
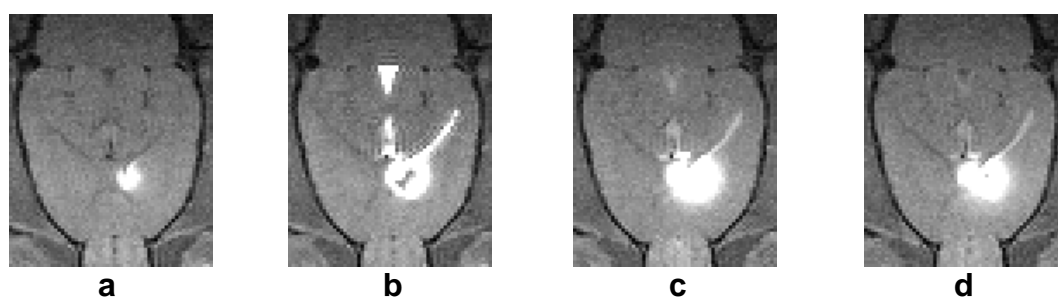
Figure 28. Direct injection of the compound **26c** into the brain tissue. a) reference; b) direct after injection; c) 1h after injection; d) 2h after injection.

Injection of the compound **26c** into the tissue, results in a local decrease of T1 values which can be seen as a white spot on the image (Figure 28b). The dark point inside the spot (Figure 28b), related to the injection place where the concentration of the contrast agent **26c** is very high. This dramatically reduced the T_1 relaxation time of the tissue and as a result the signal can not be detected. Moreover some amount of the compound

diffused into the ventricles and this results in the additional white spots in the Figure 28b. After 20 to 30 min the white spot becomes bigger (Figure 28c), but no further visible changes for the time of the whole experiment (~ 5 – 6h) were observed (Figure 28d). The diffusion of the compound can be followed by the distribution diagrams (Figure 29) according to the time course (top) and comparison of the signal intensity vs. the distance from the injection point (bottom).
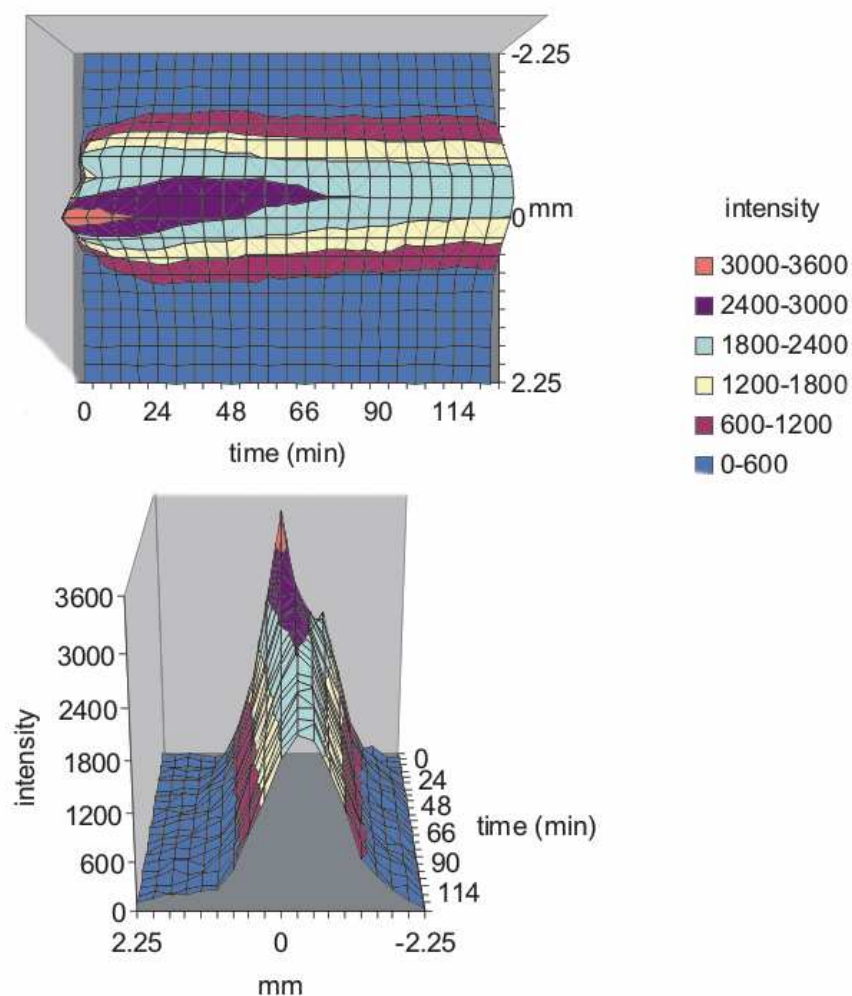
Figure 29.   Diffusion diagrams of the injected compound **26c** in tissue (different colors are the MR signal intensity related to the brain tissue without the contrast agent).

According to the diagram there is a very small diffusion and slow washout of compound during the whole time of the experiment. The maximal signal intensity is observed in the place of injection and it is almost constant in the time course. That can be a cause of the interaction of the negatively charged phosphonates with the cell membranes or with the proteins in the extracellular space.

The next step for *in vivo* experiments was performed in order to study the neuronal toxicity of the new compounds. Neuronal toxicity of the synthesized complex **26c** has been investigated by means of combined electrophysiological and fMRI experiments. Electrophysiological recordings and fMRI (BOLD) experiments were performed in Long Evans rats upon visual stimulations (1 and 4 Hz flickering), before and after the injection of the contrast agent **26c** into the visual cortex. After the local injection of 40nL of 20mM solution of compound **26c** in ACSF the tissue was allowed to recover for 15-20 min before the stimulation and recording was repeated. The recorded data were compared and results for the fMRI experiments are shown on the Figure 30.
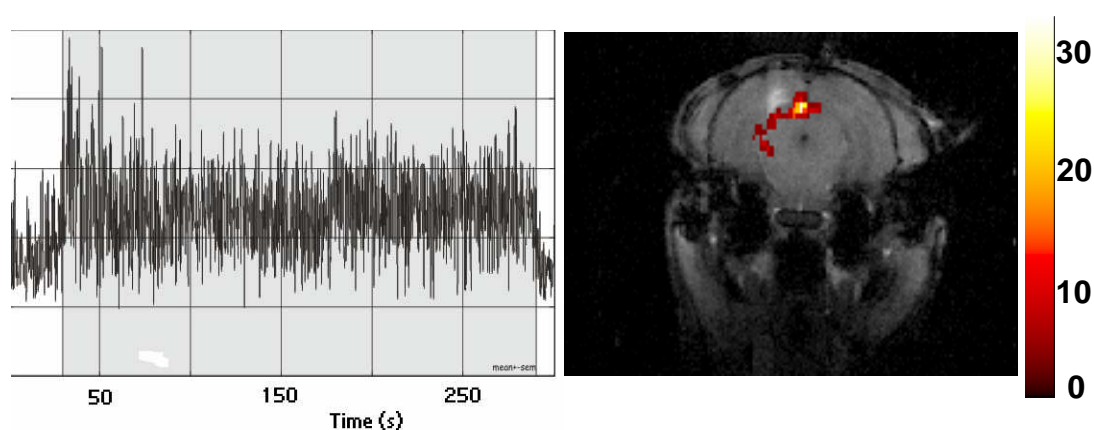
Figure 30.   Electrophysiological recording (left) and BOLD images (right) of post injection of the compound **26c.**

83

The fMRI experiment shows the normal neuronal activity after injection of compound **26c** (Figure 30, right). The same results were obtained from the electrophysiological data analysis (Figure 30, left), which shows the normal firing of the neurons after the injection. Moreover the complex is not toxic for the neurons and can be used for further *in vivo* studies. The most important series of the *in vivo* MRI experiments were performed to investigate contrast changes due to neural activations. For that purpose standard sensory stimuli (visual and somatosensory) were used. The injections were performed outside of the magnet. The compound **26c** (40nL of 20mM in ACSF) was injected in the right side of the visual or somatosensory cortex of the rat, while the left side was used as a control. Either visual (1 and 4 Hz flickering), whisker stimulations (air puffs) and hindpaw electrical stimulations were performed inside the magnet and T_1-weighted scans were acquired. Terminal depolarization was performed at the end of the each experiment to get a possible biggest change of the extracellular calcium concentrations *in vivo*. The analysis of the above experiments showed no changes in T_1 upon applied stimuli.

2.3.5. Conclusions

In conclusion, a series of lanthanide chelate complexes **26a – c** and **27a – c** with the variable length of the amino(bismethylen)phosphonate side chain have been synthetized and investigated. The dependence of the length of the side chain on the relaxivity and complexing properties of the complexes studied by the means of the potentiometric titration, NMR spectroscopy and relaxometry. According to the data of potentiometric titration the basisity of the ligands increased with increase of the length of the side chain, which can be explained by the interaction of the phosphonate moieties with the nitrogen atoms of the cyclen rim. T_1

relaxivity changes in the presence and absence of different concentrations of Ca^{2+} were observed for the complexes **25b** and **c**. For the compound **26c** these changes were observed for Ca^{2+} concentrations within physiological conditions in the extracellular space. To simulate *in vivo* conditions relaxivity measuerments were preformed in artificial CSF and in the presence of the mixture of proteins. The changes of the relaxivity were observed in both series of experiments. $^{31}P\{^1H\}$ NMR studies of the complexes **27a – c** pointed to the presence of diastereotopomers which have a different impact on the relaxivity. According to these results, **26c** has potential to act as calcium dependent MRI contrast agents and it was studied under *in vivo* conditions. *In vivo* injections in the rats show that the complex **26c** is not toxic for the neurons, but unfortunately it is not diffusing properly while injected in the tissue. Injections in the visual and somatosensory cortex of the rats did not show any changes of signal during the stimulation. This means that the compound does not works as 'smart' contrast agent *in vivo* conditions. It can be concluded, that the changes of the relaxivity obtained *in vitro* conditions, probably, are not strong enough to observe the signal changes *in vivo* and further modifications of complexes are needed to achieve a detectable changes in contrast during the neuronal activity.

3. EXPERIMENTAL PART

3.1.1. General remarks, material and instrumentation

All chemicals were purchased from commercial sources and were used without further purification. All dried solvents were stored under argon and distilled prior use.

The lanthanide metal ion solutions with the known concentrations were prepared by dissolving an accurately weighted amount of the chloride salt in the appropriate volume of doubly distilled water, and standardized with the complexometric titration with the disodium salt of EDTA.[192]

NMR

^1H *NMR,* $^{13}C\{^1H\}$ *NMR and* $^{31}P\{^1H\}$ *NMR spectra* were recorded on BRUKER DRX 250 MHz and DRX 400 MHz spectrometers at room temperature and the following frequencies: ^1H *NMR:* 250.13 MHz and 400.13 MHz respectively. The signals were referenced to the residual proton signals of the solvents relative to TMS. $^{13}C\{^1H\}$ *NMR:* 62.9 MHz. The signals were referenced to the ^{13}C signals of the deuterated solvents relative to TMS. $^{31}P\{^1H\}$ *NMR:* 101.26 MHz. The signals were referenced to external 85% H_3PO_4.

T_1 and T_2 measurements

Longitudinal and transverse relaxation times were measured on a Bruker Minispec pc120 and mq60 at 20 MHz (0.47 T) and 60 MHz (1.41 T) respectively. The concentration of each sample was determined by I.C.P.

(Jobin Yvon JY70, Lonjumeau, France) or at 300 MHz on a vertical 7 T/60 cm MRI Biospec system (Bruker Biospin, Germany). Up to 16 tubes could be measured simultaneously. The relaxation rate measurements of the samples were performed at room temperature (21 °C). For $R1$, a spin-echo saturation recovery sequence was used, varying the repetition time TR and keeping the echo time TE minimal and constant. Typical parameters were: field of view 17 _ 6.9 cm2, matrix 512 _ 256, slice thickness 4 mm, SW 70 kHz, TE 15 ms, TR 40-8000 ms (logarithmic time steps, 80 images). For $R2$, a multi-spin-echo sequence was used with a long TR between excitations. Similar parameters were used, but TR) 8 s and TE) 17-850 ms (linear echo time steps, 50 echoes). Proton nuclear magnetic relaxation dispersion (NMRD) profiles were recorded on a Field Cycling Relaxometer (Stelar, Mede, Italy). The accessible magnetic field range is 0.24 mT to 1.2 T, what corresponds to proton Larmor frequencies 0.01MHz to 20 MHz. Measurements are done on samples of 0.6 ml in 10 mm OD tubes.

Mass spectra

FAB spectra were recorded on a Finnigan MAT 711 A modified by AMD Company (10 kV, 323K), ESI spectra on an Agilent series 1100 MSD.
ESI-LRMS (in positive and negative ion mode) were performed on ion trap SL 1100 system (Agilent, Germany) and ESI-HRMS were performed on Bruker Daltonics Apex II FT-ICR-MS (Bruker,Germany).

Elemental analyses

Elemental analyses were obtained on a Vario EL made by Elemental Company.

Experimental Part

Column Chromatography

Column chromatography was performed on silica gel 60 (70-230 mesh ASTM).

Reversed Phase High-Performance Liquid Chromatography (HPLC)

HPLC was performed at room temperature on a Varian PrepStar Instrument, Australia, equipped with PrepStar SD-1 pump heads. UV absorbance was measured using a ProStar 335 photodiode array detector at 214 and 254 nm. This detector is equipped with a dual-path length flow cell which enables measurement of absorption of analytical and preparative samples without changing the flow cell. Reversed-phase analytical HPLC was performed in a stainless steel Chromsep (length 250 mm, internal diameter 4.6 mm, outside diameter 3/8 in. and particle size 8 *i*m) C18 column and preparative HPLC was performed in a stainless steel Chromsep (length 250 mm, internal diameter 41.4 mm, outside diameter 2 in. and particle size 8*i*m) C18 column (Varian, Advanced Chromatographic Solutions).

The pH-metric measurements

The pH metric titrations used in the determination of protonation and complexation constants were carried out on the Basic Titrino 794 from Metrom (Switzerland) with the combined glass electrode in a thermoregulated cell (25.0 ± 0.1 °C) with a nitroge n stream flowing over the solution to avoid the dissolution of carbon dioxide. The measured experimental data were transferred via RS 232C data interface into computer using Metrodata VESUV PC software and then the experimental data were treated by OPIUM software[190] in order to determine the equilibrium constants from titration curves. The combined electrode was calibrated using the following calibration function:

$$E = E_0 + S \log [H^+]$$

where E_0 is standard potential including mostly the contribution of reference electrode and S corresponds to the Nernstian slope, the value of which should be close to the theoretical one. The calibration parameters were estimated from titration of diluted solution of standard HCl with standard 0.1-M NaOH solution which concentration was checked against potassium hydrogenphthalate. The values of E_0 were in range 405-415 mV, while the slope S was about 58.5-59.8 mV.$(-\log [H^+])^{-1}$ which agree well with expected value for Nernstian slope of glass ion-selective electrode. The water ionic product $pK_w = 13.80 \pm 0.02$ was determined in order to check the correct work of our experimental instrumentation.

In vivo studies

Male Sprague–Dawley and Lang Evans rats (250–300 g) were used for in vivo studies. For surgery, animals were anesthetized with 2.0% isoflurane (Forene, Abbott, Wiesbaden, Germany) and placed in a stereotaxic frame (Kopf Instruments). Local anesthetic xylocain was used additionally for the surgery area. Bregma, the sagittal suture, and the surface of the brain were used as references for the anterior–posterior (AP), lateral (L), and ventral (V) coordinates, respectively. Guiding cannula (OD 360 ID 200) was implanted in the place of injection and fixed with dental cement (a small hole was drilled for cannula placement). The injections within the magnet were done through a 4m long sharpened fused silica capillary (ID 100μm, OD 160μm), connected with the guiding cannula, placed in the brain on the one side and 100 μL Hamilton syringe on the other side. The drive for the 50μl Hamilton Microliter Syringes was a modified Kopf Micropositioner (Model 650). During the scan, the isoflurane anesthesia was reduced to 1.5-1.7%. Rats were immobilized in a non-magnetic stereotaxic head holder. The rat body was placed on a heating pad to

maintain a body temperature of 37°C. Imaging was ca rried out on a vertical 7 T/60 cm MRI Biospec system (Bruker Biospin, Germany).

MR methods

The *in vivo* diffusion studies were performed on a 7T 300MHz NMR System, using a T1 wighted spin echo (SE) sequence with the parameters: TR 700ms, TE 20ms, FOV 13x17x0.4 cm, Matrix 256x512, Slices 20.

The *in vivo* experiments for detection of calcium concentration changes during the stimulations were done on a 4.7T 200MHz NMR System. One sequence used for a fast T1 measurement have been two segment gradient echo (GE), inversion recovery (IR) EPI with following parametrers: TR 750ms, TE 8ms, FOV 3.2x2.6x0.1 cm, Matrix 64x52, Slices 3, 16 variable inversion delays 15-3000ms, and a temporal resolution of ~2min.

Additionally conventional functional GE EPI as well T1 wighted GE IR EPI series with variable parameters have been performed for dedecting calcium concentration changes with the CAs.

3.2.2. Synthesis of acyclic bifunctional chelates and their lanthanide complexes

Compound **1** is commercially available and compound **2** was prepared according to the literature.[194]

N^1,N^3-bis(2-aminoethyl)-5-nitroisophthalamide (3). A suspension of **2** (5.0 g, 20.9 mmol) in dry methanol (15 mL) was added dropwise to ethylendiamine (50 mL) at r.t. with vigorous stirring. Stirring was continued for 18 h. Removal of the solvent left a brownish solid, which was dried at

50°C *in vacuo* for 6 h and left at r. t. *in vacuo* for another 24 h. Yield: 9.80 g (89 %). ^{13}C {^{1}H} NMR (D$_2$O): δ 39.9, 42.8 (CH$_2$), 124.6 131.7, 135.4, 147.6, (C$_6$H$_3$),166.3 (CO),. ^{1}H NMR (D$_2$O): δ 2.61 (t, ^{3}J$_{HH}$ = 6.3 Hz, 4H, CH$_2$), 3.19 (t, ^{3}J$_{HH}$ = 6.3 Hz, 4H, CH$_2$), 8.03 (s, 1H, C$_6$H$_3$),8.18 (s, 2H, C$_6$H$_3$), ES-MS: *m/z* 296.2 [M + H]$^+$, Calcd for C$_{12}$H$_{17}$N$_5$O$_4$ 295.3. EA Calcd: C 48.61%, H 5.80%, N 23.72%. Found: C 48.00%, H 5.37%, N 23.83%

5-Nitroisophtalamide-bis(ethylamine,N,N'bis-methylacetic acid t-butyl ester) (4). Compound **3** (2.95 g 10 mmol) was dissolved in 50 mL of acetonitrile. After addition of K$_2$CO$_3$ (5.52 g, 40 mmol) the solution was stirred for 30 min at r. t. To this mixture t-butyl bromomethylacetate (8.58 g, 44 mmol) in 50 mL of acetonitrile was added dropwise and stirred for 18 h at 70°C. The inorganic salts were filtered off a nd the solvent was removed under reduced pressure. The brown oil was purified by flash chromotogrophy using 5% of CH$_3$OH in DCM as an eluent. Yield: 6.53 g (86.9 %). ^{13}C {^{1}H} NMR (CDCl$_3$): δ 27.6 (CH$_3$), 47.7, 51.1 55.4, (CH$_2$), 81.5 (*C*(CH$_3$)$_3$), 123.6, 132.6, 136.2, 147.8, (C$_6$H$_3$), 164.1(COOtBu),171.1 (CONH); ^{1}H NMR (CDCl$_3$): δ 1.45 (s, 36H CH$_3$), 2.69 (t, ^{3}J$_{HH}$ = 5.3 Hz, 4H, CH$_2$NCO), 3.39 (s, 8H, CH$_2$COOtBu), 3.68 (m, 4H, CH$_2$), 8.64 (s, 1H, C$_6$H$_3$), 8.95 (s, 2H, C$_6$H$_3$), ES-MS: *m/z* 752.9 [M + H]$^+$, Calcd for C$_{12}$H$_{17}$N$_5$O$_4$ 751.9

5-Nitroisophtalamide- bis(ethylamine,N,N'bis-methylacetic acid) (5). Trifluoroacetic acid (20 mL) was added carefully to **4** (7.51 g, 10 mmol) dissolved in dichloromethane (20 mL). After the mixture had been stirred at r. t. for 24 h the solvents were removed under reduced pressure. To take out the excess of trifluoroacetic acid dichloromethane (40 mL) was added and evaporated off, twice. The same procedure was repeated twice with methanol as extracting agent. The viscous residues were taken up in a minimum amount of methanol and cold ether was added dropwise. The formed precipitate was recrystallized from hot methanol. The yellow to brown crystalline powder was filtered off, washed with methanol and dried

in *vacuo*. Yield: 3.66 g (69.5 %). ^{13}C $\{^1H\}$ NMR (D$_2$O): δ 30.2, 35.4, 56.1 (CH$_2$), 125.5, 132.1, 134.9, 147.9, (C$_6$H$_3$), 168.5 (CONH),169.3 (COOH),. ^{1}H NMR (D$_2$O): δ 3.51 (m, 4H, CH$_2$NCO), 3.73 (m, 4H, CH$_2$NCO), 4.01 (s, 8H, *CH$_2$*COOH), 8.41 (s, 1H, C$_6$H$_3$), 8.62 (s, 2H, C$_6$H$_3$), ES-MS: *m/z* 528.4 [M + H]$^+$, Calcd for C$_{12}$H$_{17}$N$_5$O$_4$ 527.4. EA Calcd: C 43.90%, H 4.52%, N 12.28%. Found: C 44.21%, H 4.30%, N 11.76%.

N1,N3-bis(2-aminoethyl)-5(phenethoxycarbonyloxyamino)isophthal - amide (8). Compound **7** (2.09 g, 10 mmol), was dissolved in a solution of DCM (20 mL) and water (40mL). The solution was treated with alternating addition of a solution of carbobenzoxy chloride (CBz) (1.9 g, 12 mmol) in DCM (20 mL), and of 3.5 M K$_2$CO$_3$ with vigorously stirring at room temperature. The pH was maintained at 6-7 by dropwise addition. After CBz was added over 0.5 h, it was stirred under pH 7-8 for 2 h. White precipitate was filtered and recrystallized from ethylacetate to give a white powder 3.0 g (88%) yield. ^{13}C $\{^1H\}$ NMR (DMSO): δ 52.4 (CH$_3$),. 66.1 (CH$_2$), 122.4, 123.3, 128.1, 128.4, 130.6, 136.3, 138.3, 140.1(C$_6$H$_3$),153.3,165.2 (CONH), ^{1}H NMR (DMSO): δ 3.80 (s, 6H, CH$_3$), 5.19 (s, 2H, CH$_2$), 7.32 – 7.46 (m, 5H, C$_6$H$_5$), 8.05 (s, 1H, C$_6$H$_3$), 8.32 (s, 2H, C$_6$H$_3$), 10.20 (s, 1H, NH); ES-MS: *m/z* 344.3 [M + H]$^+$, Calcd for C$_{18}$H$_{17}$NO$_6$ 343.3

Benzyl3,5-bis(2-aminoethylcarbamoyl)phenylcarbamate (9). Compound **9** was synthesized by the similar way as it was described for compound **3** starting from 3.0 g (8.75 mmol) of **8.** Finally it was recrystallized from ethylacetate to give 318 g (91%) of yield. ^{13}C $\{^1H\}$ NMR (CDCl$_3$): δ 40.1, 43.5 (CH$_2$), 67.1 (CH$_2$), 122.4 123.3, 128.1, 128.4, 130.6, 136.3 138.3, 140.1, (C$_6$H$_3$), 153.3,165.2 (CONH), ^{1}H NMR (CDCl$_3$): δ 3.80-4.60 (m, 8H, CH$_3$), 5.19 (s, 2H, CH$_2$), 7.32 – 7.46 (m, 5H, C$_6$H$_5$), 8.05 (s, 1H, C$_6$H$_3$), 8.32 (s, 2H, C$_6$H$_3$), 10.20 (s, 1H, NH); ES-MS: *m/z* 400.3 [M + H]$^+$, Calcd for C$_{20}$H$_{25}$N$_5$O$_4$ 399.4

5-Aminoisophtalamide-bis(ethylamine,N,N'bis-methylacetic acid t-butyl ester) (10). Compound **10** was synthesized similar to compound **4** starting with 3.5 g (8.8 mmol) of **9**. Light brown viscous oil was purified by column chromatography from DCM/ MeOH (5%) mixture as mobile phase. Yield: 6.53 g (86.9 %). ^{13}C {^1H} NMR (CDCl$_3$): δ 27.7 (CH$_3$), 38.6 52.5, 56.2, 66.9, (CH$_2$), 81.7 (C(CH$_3$)$_3$), 120.3, 120.5, 128.5, 128.8, 136.1, 136.7, 139.7, 153.9, (C$_6$H$_3$), 162.8, 167.3 (CONH),171.5 (COOtBu);
^1H NMR (CDCl$_3$): δ 1.80 (s, 36H, CH$_3$), 2.50 – 4.00 (m 16H, CH$_2$) 5.19 (s, 2H, CH$_2$), 7.32 – 7.46 (m, 5H, C$_6$H$_5$), 8.05 (s, 1H, C$_6$H$_3$), 8.32 (s, 2H, C$_6$H$_3$); ES-MS: m/z 857.1 [M + H]$^+$, Calcd for C$_{44}$H$_{65}$N$_5$O$_{12}$ 856.0

5-Aminoisophtalamide- bis(ethylamine,N,N'bis-methylacetic acid) (11). Compound **10** (2.13 g, 2.5 mmol) was taken in ethanol (50 mL) and hydrogenated at 30 psi in the presence of 200 mg of Pd/C (10%) for 24 h. The catalyst was removed by filtration through Celite and the filtrate was concentrated to dryness. A light brown powder (1.65 g) which was obtained dissolved in 5mL of DCM and10 mL of TFA was added to the solution. After mixture had been stirred at r.t. for 12 h the solvents were removed under reduced pressure. To take out the excess of trifluoroacetic acid dichloromethane (10 mL) was added and evaporated off, twice. The same procedure was repeated twice with methanol as extracting agent. The viscous residues were taken up in a minimum amount of methanol and cold ether was added dropwise. The formed precipitate was recrystallized from hot methanol. Yield: 0.931 g (73.5 %). ^{13}C {^1H} NMR (D$_2$O): δ35.7 (CH$_2$), 56.4 (CH_2COOH), 56.6 (CH$_2$), 125.1, 125.8, 133.2, 135.5(C$_6$H$_3$),169.9 (COOH), ^1H NMR (D$_2$O): δ 3.44 (m, 4H, CH$_2$NCO), 3.65 (m, 4H, CH$_2$NCO), 3.96 (s, 8H, CH_2COOH), 7.76 (s, 2H, C$_6$H$_3$), 8.00 (s, 1H, C$_6$H$_3$), ES-MS: m/z 498.5 [M + H]$^+$, Calcd for C$_{20}$H$_{27}$N$_5$O$_{10}$ 497.5.

Complexation with lantanides (6a – b and 12a – b). Compounds **5** and **11** (1.9 mmol) were dissolved in 30 mL of water, 1.0 eq. of the corresponding lanthanide chloride was added to the solution while the pH

was adjusted to 5.5 − 6.0. The reaction mixture was stirred at room temperature for 12 h. The solutions were filtered and an anion exchange resin (Chelex 100) was added to the stirring solution, the suspension was filtered after 1 h, syringed through 0.2 µm nylon filters and the solvent evaporated. The xylenol test showed the absence of the noncoordinated metal ions in the systems. ES-MS: compound **6a** − **b** m/z 681.5 [M + H]$^+$, Calcd for GdC$_{20}$H$_{21}$N$_5$O$_{12}$ 680.7; m/z 677.1 [M + H]$^+$, Calcd for EuC$_{20}$H$_{21}$N$_5$O$_{10}$ 675.4; compound **12a** − **b** m/z 651.5 [M + H]$^+$, Calcd for GdC$_{20}$H$_{23}$N$_5$O$_{10}$ 650.3; m/z 645.4 [M + H]$^+$, Calcd for EuC$_{20}$H$_{23}$N$_5$O$_{10}$ 645.2

3.1.3. Synthesis of the DO3A based mono(alkylphos- phonate) lanthanide complexes 17a – b and 19a - b

tri-tert-butyl 2,2',2''-(10-(3-(diethoxyphosphoryl)propyl)-1,4,7,10-tetraazacyclododecane-1,4,7-triyl)triacetate (15). To the solution of **7** (1 eq) and K$_2$CO$_3$ (1.5 eq) in 80 mL acetonitrile was added a solution of diethyl(3bromopropyl)phosphonate (1.2 eq) in 30 mL of acetonitrile. After the reaction mixture was stirred for 12 h at 70℃, the solution was allowed to cool to r. t., filtered and concentrated *in vacuo* to give yellow oil. The oil was purified by column chromatography (5% of MeOH in DCM) to give 78% of the final compound. ^{1}H NMR (CDCl$_3$, 400 MHz): δ (ppm) 0.8 (m, 6H), 1.02 − 1.08 (m, 27H), 1.21 (m, 4H), 1.26 -3.93 (m, 28H), ^{13}C {^{1}H} NMR (CDCl$_3$, 100 MHz): δ (ppm) 173.2, 172.6, 82.7, 82.4, 61.6, 58.2, 57.3, 56.5, 54,3, 52.2, 51.8, 49.1, 28.1, 27.8, 23.0, 22.1, 16.4. ^{31}P NMR (CDCl$_3$): δ (ppm) 33.6. HRMS (EI) for C$_{33}$H$_{65}$N$_4$O$_9$P: calc. 693.45619 [M + H]$^+$, found 693.45604.

2,2',2''-(10-(3-phosphonopropyl)-1,4,7,10-tetraazacyclododecane-1,4,7-triyl)triacetic acid (16).

To the solution of **15** (1eq) in dry dichloromethane bromtrimethylsilane was added slowly at 0℃ (10eq) and the mixture was stirred for 12 h at r. t. The solvent was removed by evaporation and the residue was dissolved in 20 mL of the trifluoroacetic acid. After the mixture had been stirred at r. t. for 24 h the solvent was removed under reduced pressure. The viscous residue was taken up in a minimum amount of methanol and was added dropwise into cold ether. The formed precipitates were filtered and resuspended in 3 mL of water. Then cold ethanol was added slowly under stirring. The solutions were cooled to -20 ℃ for 1 2 h. The solid product was separated by filtration and dried by prolonged standing *in vacuo* yielding 68% of a final product. ^{13}C {^{1}H} NMR (D$_2$O): δ 174.3, 169.6 (COOH), 57.3, 55.9, 53.1, 51.4, 49.6, 48.3, 48.1, 24.4 (^{1}J$_{PC}$ = 134.7 Hz), 17.3 (CH$_2$). ^{1}H NMR (D$_2$O): δ 3.8 (s, 3H, CH$_2$*COOH*), 2.9 – 3.5 (m, 24H,), 1.8 (br 2H, CH$_2$P), 1.5 (q, 2H,J$_{HH}$ = 8.6 Hz). ^{31}P {^{1}H} NMR (D$_2$O): δ 24.1. HRMS (EI) for C$_{17}$H$_{33}$N$_4$O$_9$P calc. 496.20563 [M + H]$^{+}$, found 469.20579.

2,2',2''-(10-(3-(diethoxyphosphoryl)propyl)-1,4,7,10-tetraazacyclododecane-1,4,7-triyl)triacetic acid (17).

Compound **15** (2 mmol) was dissolved in dichloromethane (10 mL) and to this solution trifluoroacetic acid (10 mL) was added carefully. After the mixture had been stirred at r. t. for 16 h the solvents were removed under reduced pressure. To take out the excess of trifluoracetic acid dichloromethane (40 mL) was added and evaporated off, twice. The same procedure was repeated twice with methanol as extracting agent. The viscous residues were taken up in a minimum amount of methanol and cold ether was added dropwise. The formed precipitates were filtered, washed with acetone and dried in *vacuo* yielding 72% of a final product.^{13}C {^{1}H} NMR (D$_2$O): δ 173.9, 168.9 (COOH), 63.4, 55.1, 53.6, 52.8, 51.5, 49.7, 48.3, 48.0, 20.9 (^{1}J$_{PC}$ = 141.1 Hz), 16.5 (CH$_2$), 15.6 (CH$_3$). ^{1}H NMR (D$_2$O): δ 3.7 – 3.9 (m, 7H, CH$_2$*COOH* and *CH$_2$*CH$_3$), 2.7 – 3.4 (m, 24H,), 1.5 – 1.7 (m, 4H, CH$_2$CH$_2$P), 1.1 (t, 6H, J$_{HH}$ = 7.1 Hz,

---

CH_2CH_3). ^{31}P {^1H} NMR (D$_2$O): δ 33.1. HRMS (EI) m/z 525.26909 [M + H]$^+$, Calcd for $C_{17}H_{34}N_4O_9P$ 525.26839.

General procedure for the synthesis of lanthanide complexes (17a –b and 19a - b). To the water solutions of 1 eq of the ligands **16** and **18,** 0.9 eq of GdCl$_3$ x H$_2$O or EuCl$_3$ x 6H$_2$O was added. The mixtures were heated to 60°C for 24 h. The pH was periodically checked a nd adjusted to 6.5 ~ 7.0 using a 1M solution of NaOH. The reaction mixtures were cooled, NaOH was added to bring the pH to 12 and the reaction mixture was syringed through 0.2 μm nylon filter to remove the excess of non coordinated metal. Anion exchange resin (Chelex 100) was added to the stirring solution, suspensions were filtered after 1 h and the solvents evaporated. The xylenol test showed the absence of the non-coordinated metals in the systems. ES-MS: for the compound **17a** m/z 645.2 [M + Na]$^+$, Calcd for GdC$_{17}H_{30}N_4O_9P$; for the compound **17b** 622.4; m/z 618.4 [M + H]$^+$, Calcd for EuC$_{17}H_{30}N_4O_9P$ 617.2; for the compound **19a** m/z 678.8 [M +H]$^+$, Calcd for GdC$_{21}H_{38}N_4O_9P$ 678.8; for the compound **19b** m/z 674.8 [M +H]$^+$, Calcd for EuC$_{21}H_{38}N_4O_9P$ 673.5;

3.1.4. Synthesis of the DO3A based amino(bismethylene)phosphonate lanthanide complexes

General procedure for N-Boc-3-aminoalkyl bromide (21a – c). A solution of NaOH (3 eq.) in 30 mL of water was added dropwise to a vigorously stirring biphasic mixture consisting of **20a – c** (1.5 eq.) in 50 mL of water and Boc$_2$O (1 eq.) in 100 mL of dichloromethane. After 3 h the organic phase was separated and washed with 50 mL of a 2N HCl and 50 mL of a saturated NaCl solution. The organic phase was dried over MgSO$_4$ and concentrated in *vacuo*. To the oil 20 mL of *n*-hexane was

added and the solution was stored at -20°C overnig ht. The products were separated from the solvent, washed with cold *n*-hexane and dried *in vacuo.*

***tert*-butyl 3-bromopropylcarbamate (21a):** Colorless crystals yield 68%. ^{13}C $\{^1$H$\}$ NMR (CDCl$_3$): δ 155.6 (CO), 79.8 (C(CH$_3$)$_3$), 38.6, 32.4, 30.4 (CH$_2$), 27.9 (CH$_3$). ^{1}H NMR (CDCl$_3$): δ 5.25 (s, 1H, NH), 3.38 (t, 2H, $^3J_{HH}$ = 6.5 Hz, BrCH$_2$), 3.25 (t, 2H, $^3J_{HH}$ = 6.5 Hz, NHCH_2), 1.95 (tt, 2H, $^3J_{HH}$ = 6.52, $^3J_{HH}$= 6.52, CH$_2$), 1.37 (s, 9H, CH$_3$). EA Calcd: C 40.35%, H 6.77%, N 5.88%. Found: C 40.29%, H 7.23%, N 5.88%

***tert*-butyl 5-bromopentylcarbamate (21b):** Yellow crystals, yield 65%. ^{13}C $\{^1$H$\}$ NMR (CDCl$_3$): δ 158.3 (CO), 79.8 (C(CH$_3$)$_3$), 40.5, 33.8, 32.6, 29.4 (CH$_2$), 28.7 (CH$_3$), 25.5 (CH$_2$). ^{1}H NMR (CDCl$_3$): δ 4.92 (s, 1H, NH), 3.52 (t, 2H, $^3J_{HH}$ = 6.74, BrCH$_2$), 3.25 (m, 2H, NHCH_2), 1.94 (tt, 2H, $^3J_{HH}$ = 6.7 Hz, $^3J_{HH}$ = 6.9 Hz, CH$_2$), 1.32 (s, 9H, CH$_3$), 1.25-1.40 (m, 4H, CH$_2$). EA Calcd: C 45.12%, H 7.57%, N 5.26%. Found: C 45.16%, H 7.20%, N 5.49%

***tert*-butyl 5-bromohexylcarbamate (21c):** Brown oil, yield 62%. ^{13}C $\{^1$H$\}$ NMR (CDCl$_3$): δ 158.6 (CO), 79.9 (C(CH$_3$)$_3$), 40.1, 33.9, 32.8, 30.0 (CH$_2$), 28.5 (CH$_3$), 27.9, 26.1 (CH$_2$). ^{1}H NMR (CDCl$_3$): δ 4.73 (s, 1H, NH), 3.19 (t, 2H, $^3J_{HH}$ = 6.8 Hz, BrCH$_2$), 2.94 (m, 2H, NHCH_2), 1.65 (tt, 2H, $^3J_{HH}$ = 6.8 Hz, $^3J_{HH}$ = 7.6 Hz, CH$_2$), 1.24 (s, 9H, CH$_3$), 1.22-1.40 (m, 6H, CH$_2$). EA Calcd: C 47.15%, H 7.91%, N 5.00%. Found: C 47.22%, H 7.22%, N 5.22%

General procedure for tri-tert-butyl 2,2',2''-(10-(3-(tert-butoxycarbonyl amino)alkyl)-1,4,7,10-tetraazacyclododecane-1,4,7-triyl)triacetate (22a - c). To the solution of 1,4,7-tri(t-butoxycarbonylmethyl)cyclen **8** (1 eq.) and K$_2$CO$_3$ (1.5 eq.) in 30 mL acetonitrile was added a solution of **21a – c** (1.1 eq.) in 20 mL of acetonitrile. After the reaction mixture had been stirred for 16 h at 70°C, the solution was allowed to cool to r. t., filtered and concentrated *in vacuo* to give a yellow to brown oil. The compounds were recrystallised from heptane.

---

tri-tert-butyl 2,2',2''-(10-(3-(tert-butoxycarbonylamino)propyl)-1,4,7,10-tetraazacyclododecane-1,4,7-triyl)triacetate (22a). Yellow oil, yield 85%. ^{13}C {^{1}H} NMR (CDCl$_3$): δ 173.6, 172.6 (COOt-Bu), 156.3 (COBoc), 82.7, 82.4, 81.7 (C(CH$_3$)$_3$), 57.4, 56.4, 55.7, 51.7, 50.2, 49.7, 38.7 (CH$_2$), 28.4, 28.0, 27.8 (C(CH$_3$)$_3$), 26.6, 18.3 (CH$_2$), ^{1}H NMR (CDCl$_3$): δ 5.90 (s,1H, NH), 3.60 – 2.03 (m, 26H, CH$_2$), 1.29 (m, 2H, CH$_2$NH), 1.11 – 1.05 (m, 36H, C(CH$_3$)$_3$). ES-MS m/z 672.4 [M + H]$^+$, Calcd for C$_{34}$H$_{65}$N$_5$O$_8$ 671.9.

tri-tert-butyl 2,2',2''-(10-(3-(tert-butoxycarbonylamino)pentyl)-1,4,7,10-tetraazacyclododecane-1,4,7-triyl)triacetate (22b). Yellow oil, yield 83%. ^{13}C {^{1}H} NMR (CDCl$_3$): δ171.6, 170.7 (COt-Bu), 155.7 (COBoc), 81.6, 80.2, 78.3 (C(CH$_3$)$_3$), 56.1, 55.9, 53.1, 51.9, 5.6, 51.3, 40.1, 33.3, 31.8 (CH$_2$) 28.0, 27.7, 27.5 (C(CH$_3$)$_3$), 24.3, 22.8 (CH$_2$). ^{1}H NMR (CDCl$_3$): δ 5.22 (s,1H, NH), 3.42 – 1.64 (m, 26H, CH$_2$), 1.36 – 1.32 (m, 36H, C(CH$_3$)$_3$), 1.14 – 1.30 (m, 6H CH$_2$). ES-MS m/z 700.6 [M + H]$^+$, Calcd for C$_{36}$H$_{69}$N$_5$O$_8$ 699.9.

tri-tert-butyl 2,2',2''-(10-(3-(tert-butoxycarbonylamino)hexyl)-1,4,7,10-tetraazacyclododecane-1,4,7-triyl)triacetate (22c). Brown oil, yield 82%. ^{13}C {^{1}H} NMR (CDCl$_3$): δ 172.4, 170.8(COOtBu), 155.8 (COBoc), 82.3, 82.0, 81.6, (C(CH$_3$)$_3$), 56.4, 56.1, 52.2, 51.8, 51.8, 51.6, 40.2, 33.7, 32.4, 29.8 (CH$_2$), 28.4, 28.0, 27.7(C(CH$_3$)$_3$), 27.6, 26.5(CH$_2$). ^{1}H NMR (CDCl$_3$): δ 4.83 (s,1H, NH), 2.93 – 1.26 (m, 26H, CH$_2$), 0.83 – 0.89 (m, 36H, C(CH$_3$)$_3$), 0.71 (m, 8H CH$_2$).
HR-FAB m/z 736.52186 [M + H]$^+$, Calcd for C$_{37}$H$_{71}$N$_5$O$_8$Na 736.519995.

General procedure for 2,2',2''-(10-(3-aminoalkyl)-1,4,7,10-tetraazacyclododecane-1,4,7-triyl)triacetic acid (23a – c). Compounds **22a – c** (2 mmol) were taken in dichloromethane (20 mL) and to these solutions trifluoroacetic acid (20 mL) was added carefully. After the mixture had been stirred at r. t. for 24 h the solvents were removed under reduced pressure. To take out the excess of trifluoracetic acid dichloromethane (40 mL) was added and evaporated off, twice. The same procedure was

repeated twice with methanol as extracting agent. The viscous residues were taken up in a minimum amount of methanol and cold ether was added dropwise. The formed precipitates were filtered and resuspended in 3 mL of water. A large excess of acetone (100mL) was added and the cloudy solutions were stored at -20 ℃ for 16 h. Co lorless crystalline powders were filtered off, washed with acetone and dried in *vacuo*.

2,2',2''-(10-(3-aminopropyl)-1,4,7,10-tetraazacyclododecane-1,4,7-triyl)triacetic acid (23a). Colorless crystalline powder, yield 54% ^{13}C {^{1}H} NMR (D$_2$O):174.2, 171.2 (COOH), 56.5, 53.8, 51.6, 50.6, 49.7, 48.7, 37.4, 24.9, 24.9 (CH$_2$). ^{1}H NMR (D$_2$O): δ 3.69 – 2.66 (m, 26H, CH$_2$), 1.73 (m, 2H, CH$_2$). HRMS (EI): for C$_{17}$H$_{33}$N$_5$O$_6$ Calcd: 408.32653 [M - H]$^-$; found: 408.326601

 2,2',2''-(10-(3-aminopentyl)-1,4,7,10-tetraazacyclododecane-1,4,7-triyl)triacetic acid (23b). Colorless crystalline powder, yield 50%. ^{13}C {^{1}H} NMR (D$_2$O): δ 174.4, 169.1 (COOH), 55.9, 54.1, 53.2, 51.6, 49.9, 48.5, 48.3, 39.2, 26.3, 22.9, 22.7 (CH$_2$). ^{1}H NMR (D$_2$O): δ 3.74 (m, 2H, *CH$_2$*NH$_2$), 3.50 – 2.64 (m, 24H, CH$_2$), 1.57 – 1.21 (m, 6H, CH$_2$); HRMS (EI): for C$_{19}$H$_{37}$N$_5$O$_6$ Calcd: 430.26711 [M - H]$^-$; found: 430.26642

2,2',2''-(10-(3-aminohexyl)-1,4,7,10-tetraazacyclododecane-1,4,7-triyl)triacetic acid (23c). Colorless crystalline powder, yield 58%. ^{13}C {^{1}H} NMR (D$_2$O): δ 174.4, 170.1 (COOH), 56.3, 54.3, 53.4, 51.5, 49.9, 48.5, 48.3, 39.4, 26.5, 25.4, 25.3, 22.9 (CH$_2$). ^{1}H NMR (D$_2$O): δ 3.69 (m, 2H, *CH$_2$*NH$_2$), 3.40 – 2.68 (m, 24H, CH$_2$N), 1.61 – 1.12 (m, 8H, CH$_2$). HRMS (EI): for C$_{20}$H$_{39}$N$_5$O$_6$ Calcd: 444.28276 [M - H]$^-$; found: 444.28282

2,2',2''-(10-(3-(bis(phosphonomethyl)amino)alky)-1,4,7,10-tetraazacyclododecane-1,4,7-triyl)triacetic acid (25a - c). Compounds **23a - c** (1 eq.) were dissolved in 10 mL of 6 M HCl. To these solutions phosphoric acid (2 eq.) in 5 mL of water was added and the mixtures were heated to reflux. Paraformaldehyde (4eq.) was added portionwise within 1 h and heating under reflux was continued for further 24 h. The reaction mixtures were concentrated under reduced pressure and cold ethanol was

added slowly under stirring. The solutions were cooled to -20 °C for 12 h. The solid product was separated by filtration and dried by prolonged standing in *vacuo*.

2,2',2''-(10-(3-(bis(phosphonomethyl)amino)propyl)-1,4,7,10-tetraazacyclododecane-1,4,7-triyl)triacetic acid (25a). Colorless powder, yield 54%. ^{13}C {^{1}H} NMR (D$_2$O): δ 173.7, 167.7 (COOH), 54.0 (d, $^{1}J_{PC}$ = 33.6 Hz), 52.9, 52.2, 51.5, 51.4, 50.9, 50.7, 50.1, 48.3, 19.4. ^{1}H NMR (D$_2$O): δ 2.20 − 3.35 (m, 30H), 1.29 − 1.39 (m, 2H). ^{31}P {^{1}H} NMR (D$_2$O): δ 10.02. HRMS (EI): for C$_{19}$H$_{39}$N$_5$O$_{12}$P$_2$ Calcd: 590.19977 [M - H]$^-$; found: 590.19852

2,2',2''-(10-(3-(bis(phosphonomethyl)amino)pentyl)-1,4,7,10-tetraazacyclododecane-1,4,7-triyl)triacetic acid (25b). Colorless powder, yield 52%. ^{13}C {^{1}H} NMR (D$_2$O): δ 174.3, 168.4 (COOH), 55.9, 54.1, 53.8, 52.8, 51.7, 50.5, 49.9, 48.7, 48.1(d, $^{1}J_{PC}$ = 33.8 Hz), 22.6, 22.5, 22.3. ^{1}H NMR (D$_2$O): δ 4.01 (m, 2H, C*H*$_2$N(CH$_2$PO$_3$H$_2$)$_2$), 2.85 − 3.60 (m, 28H), 1.25 − 1.66 (m, 6H). ^{31}P {^{1}H} NMR (D$_2$O): δ 7.44. HRMS (EI): for C$_{21}$H$_{43}$N$_5$O$_{12}$P$_2$ Calcd: 618.23107 [M - H]$^-$; found: 618.23101

2,2',2''-(10-(3-(bis(phosphonomethyl)amino)hexyl)-1,4,7,10-tetraazacyclododecane-1,4,7-triyl)triacetic acid (25c). Colorless powder, yield 56%. ^{13}C {^{1}H} NMR (D$_2$O): δ 174.3, 168.7 (COOH), 56.6, 54.9, 54.3, 53.0, 52.2, 51.9, 50.8, 50.2, 48.2 (d, $^{1}J_{PC}$ = 33.8 Hz), 25.3, 25.0, 23.2, 22.68. ^{1}H NMR (D$_2$O): δ 3.96 (m, 2H, C*H*$_2$N(CH$_2$PO$_3$H$_2$)$_2$), 2.75 − 3.31 (m, 28H), 1.53 (m, 4H), 1.18 (m, 4H). ^{31}P {^{1}H} NMR (D$_2$O): δ 10.23. HRMS (EI): for C$_{22}$H$_{45}$N$_5$O$_{12}$P$_2$ Calcd: 632.24672 [M - H]$^-$; found: 632.24670

General procedure for the synthesis of Ln- complexes (Gd 24a – c, 26a - c and Eu 27a – c). To the water solutions of 1 equivalent of the ligands **23a – c** and **25a – c** 0.9 to 1.0 equivalent of the corresponding LnCl$_3$ was added. The mixtures were heated to 90°C for 24 h. The pH was periodically checked and adjusted to 6.5 ∼ 7.5 using a 1M solution of

NaOH. After 24 h the reaction mixture had been cooled, NaOH was added to bring the pH to 12. The reaction was syringed through 0.2 µm nylon filters to remove the excess of Ln^{3+}. An anion exchange resin (Chelex 100) was added to the stirring solution, the suspensions were filtered after 1 h and the solvent evaporated. The xylenol test showed the absence of the non-coordinated metal ions in the systems. ES-MS: for the compound **26a** m/z 746.7 $[M + H]^+$, Calcd for $GdC_{19}H_{36}N_5O_{12}P_2$ 745.6; for the compound **26b** m/z 773.9 $[M - H]^+$, Calcd for $GdC_{21}H_{40}N_5O_{12}P_2$ 773.8; for the compound **26c** m/z 789.1 $[M +H]^+$, Calcd for $GdC_{22}H_{42}N_5O_{12}P_2$ 787.9; for the compound **27a** m/z 741.6 $[M +H]^+$, Calcd for $EuC_{19}H_{36}N_5O_{12}P_2$ 740.4; **27b** m/z 769.7 $[M +H]^+$, Calcd for $EuC_{21}H_{40}N_5O_{12}P_2$ 768.5; for the compound **27c** m/z 783.4 $[M +H]^+$, Calcd for $EuC_{22}H_{42}N_5O_{12}P_2$ 782.5;

REFERENCES

1) A. E. Merbach and E. Toth (eds.), *The Chemistry of Contrast Agents in Medical Magnetic Resonance Imaging*; John Wiley & Sons, Ltd., New York, **2001**.

2) W. Krause *Top.Curr.Chem.* Springer-Verlag Berlin Heidelberg, **2002**.

3) W.G. Bradley *Noninv.Med.Imaging,* **1984**, 1, 93-204.

4) M.H. Mendonca-Dias; E. Gaggelli; P.C. Lauterbur *Semin. Nucl. Med.* **1983**.

5) V.M. Runge; J.A. Clanton; C.M. Lukehart et al. *Am.J.Radiochem.***1983**, 141, 1209.

6) K.M. Donahue; R.M.Weisskoff; D. Burstein *J. Magn.Res.Imaging*, **1997**, 7(1), 102-10.

7) G.L. Wolf and T.H. Juha *MRI Clinics of North America*, **1996**, 4(1), 1-10.

8) M.T. Vlaardingerbroek; J.A. Boer *J.Magn.Res.Imaging. Theory and Practice.* Springer Verlag, Germany, **1996**, pp 242-243.

9) M.A. Mendonca-Dias; E. Gaggelli; P. Lauterbur *Semin. Nucl. Med.* **1983,** 12, 364-376.

10) P. Caravan; J.J. Ellison; T.J. McMurry and R.B. Lauffer *Chem. Rev.* **1999**, 99, 2293-352.

11) W.Cacheris; S.Quay; S. Rocklage *Magn. Res. Imag.* **1990**, 8, 467-481

12) I.V. Kuriashkin and J.M. Losnsky *Vet. Radiol. Ultrasound*, **2000**, 41(1), 4-7.

13) R.B. Lauffer. *Chem.Rev.* **1987**, 87, 901-927.

14) G.N. La Mar; W.D. Horrocks; and R.G. Holm; (eds.) NMR of Paramagnetic Molecules. New York: Academic, **1973**.

15) S.H. Koenig; and R.D. Brown; 3rd. *Magn. Reson. Annu.* **1987**, 263-86.

16) A. Borel; Yerly; Helm and A.E. Merbach *J. Am. Chem. Soc.* **2002**, 124(9), 2042-8.

17) A.D. Sherry *J. Less-Comm. Metals*, **1989**, 149:133.

18) R.C. Brasch J *Comput.Assist.Tomog.* **1993**, 17:S14-8.

19) D.W. Paty and D.K. Li *Ann. Neurol.***1996**, 40(6), 951-3.

20) M.F. Tweedle; S.M. Eaton; W.C. Eckelman; G.T. Gaughan; J.J. Hagan; P.W. Wedeking and F.J. Yost *Invest. Radiol.* **1988,** 23, S236-9.

21) É. Tóth; L. Helm; A.E. Merbach *Topics in Current Chemistry*, **2002**, 221, 61- 101.

22) A. Borel; F. Yerly; L. Helm; A.E. Merbach *CHIMIA*, **2004**, 58, 200-203

23) A. Sigel; H. Sigel Metal ions in biological system; Marsel Dekker AG, Basel, 40, **2003**

24) D. M. J. Doble, M. Melchior, B. O'Sullivan, C. Siering, J. Xu, V. C. Pierre, andK. N. Raymond, *Inorg.Chem.* **2003**, *42*, 4930-4937.

25) S. Webb, *The Physics of Medical Imaging*; Institute of Physics Publishing, Bristol; Philadelphia, 1993.

26) R. Weissleder; A. Bogdanov; E. Neuwelt and Papisov M. *Adv.Drug.Deliv. Rev.*, **1995**, 16, 321-334.

27) S.H. Koenig and K.E. Kellar *Acad. Radiol.* **1996**, 3, S273-S276.

28) W.W. Mayo-Smith; S. Saini; G. Slater; J.A. Kaufman; P. Sharma and P.F. Hahn *AJR Am. J. Roentgenol.* **1996**, 166(1), 73-77.

29) W.S. Enochs; G. Harsh; F. Hochberg and Weissleder R. *J. Magn. Reson. Imaging*, **1999**, 9, 228-32.

30) K. Turetschek; T.P. Roberts; E. Floyd; A. Preda; V. Novikov; D.M. Shames; W.O. Carter and R.C. Brasch *J. Magn. Reson. Imaging*, **2001**, 13(6), 882-8.

31) Y. Anzai, M.R. Prince, T.L. Chenevert, J.H. Maki, F. Londy, M. London and S.J. McLachlan MR *J. Magn. Reson. Imaging*, **1997**, 7, 209-14.

References

32) A.E. Stillman; N. Wilke; D. Li. Haacke and S. McLachlan J. *Comput. Assist. Tomogr.* **1996**, 20(1), 51-5.

33) K.E. Kellar; D.K. Fujii; W.H. Gunther; K. Briley-Saebo; A. Bjornerud; M. Spiller and S. H. Koenig *J. Magn. Reson. Imaging*, **2001**, 14(1), 94-6.

34) P. Wunderbaldinger; L. Josephson and R. Weissleder *Acad. Radiol.* **2002**, 9, S304-6.

35) C.W. Chen; J.S. Cohen; C.E. Myers and M. Sohn *FEBS Lett.* **1984**, 168(1), 70-4.

36) Y.J. Lin and A.P. Koretsky *Magn. Reson. Med.* **1997**, 38, 378‑88.

37) R.G. Pautler; A.C. Silva; A.P. Koretsky *Magn. Reson. Med.* **1998**, 40(5), 740-8.

38) U. P. Schmiedl; J. A. Nelson; D. H. Robinson; A. Michalson; F. Starr; T. Frenzel; W. Ebert and G. Schuhmann-Giampieri *Invest. Radiol.* **1993**, 28(10), 925-32.

39) S. Aime; M. Botta; E. Gianolio and E. Terreno *Angew. Chem. Int. Ed. Engl.* **2000**, 39(4), 747-50.

40) S. E. Matthews; C. W. Pouton; and M. D. Threadgill; *Adv. Drug Deliv. Rev.* **1996**,*18*, 219-267.

41) D. Sahani; R. Prasad Srinivasa; M. Maher; L. Warshaw Andrew; F. Hahn Peter; and S. Saini; *J. Comput. Assist. Tomogr.* **2002**, *26*, 126-128.

42) J.T. Halavaara and A. E. Lamminen *J. Comput. Assist. Tomogr.* **1997**, *21*, 94-99.

43) Y.Ni; G. Marchal; X. Zhang; P. Van Hecke; J. Michiels; J. Yu; E. Rummeny; K. P. Lodemann; and A. L. Baert; *Invest. Radiol.* **1993**, *28*, 520-528.

44) G. N. Mann; H. F. Marx; L. L. Lai; and L. D. Wagman; *Ann. Surg. Oncol.* **2001**, *8*, 573-579.

45) M. Kobayashi; H. Tajiri; T. Hayashi; M. Kuroki; and I. Sakata; *Can. Lett.* **1999**, *137*, 83-89.

46) Y. Takehara; H. Sakahara; H. Masunaga; S. Isogai; N. Kodaira; M. Sugiyama; H.Takeda; T. Saga; S. Nakajima; and I. Sakata; *J. Magn Reson. Imaging* **2002**, *47*, 549-553.

47) P. Wedeking; K. Kumar and M. F. Tweedle *J. Magn. Reson. Imaging,* **1992**,10(4), 641-8.

48) D.G. Mitchell *J. Magn. Reson. Imaging*, **1997**, 7(1),1-4

49) Tweedle; S.M. Eaton; W.C. Eckelman; G.T. Gaughan; J.J. Hagan, P.W. Wedeking; and F.J. Yost *Invest. Radiol.* **1988**, 23, S236-9.

50) A.N. Oksendal and P.A. Hals *J. Magn. Reson. Imaging*, **1993**, 3(1), 157-65.

51) S.M. Rocklage and SH. Worah Dand Kim *J. Magn. Reson. Med.*, **1991**, 22(2), 216-21; discussion 229-32.

52) W.P. Cacheris; S.C. Quay and S.M. Rocklage *J.Magn.Reson. Imaging*, **1990**, 8(4), 467-81.

53) S.M. Rocklage and A.D. Watson *J. Magn. Reson. Imaging*, **1993**, 3(1), 167-78.

54) H.J. Weinmann; R. C. Brasch; W. R. Press and G. E. Wesbey *AJR Am.J. Roentgenol.* **1984**, 142(3), 619-24.

55) V. M. Runge *Int J Rad Appl Instrum B*, **1988**, 15(1), 37-44.

56) M. Van Wagoner and D. Worah *Invest Radiol*, **1993**, 28, S44-8.

57) J.J. Brown; R. M. Kristy; G.R. Stevens; and J. A. Pierro *J. Magn. Reson. Imaging*, **2002**, 15(4), 446-55.

58) T.J. Vogl; W. Pegios; C. McMahon; J. Balzer; J. Waitzinger; G. Pirovano and J. Lissner *AJR Am. J. Roentgenol.* **1992**, 158(4), 887-92.

59) C. Haen; M. Cabrini; L. Akhnana; D. Ratti; L. Calabi and L. Gozzini *J Comput. Assist. Tomogr.* **1999**, 23, S161-8

60) C. Bartolozzi and A. Spinazzi *J. Comput. Assist. Tomogr*, **1999**, 23, S151-9.

61) F. Fellner; R. Janka; C. Fellner; M. Dobritz; M. Lenz; W. Lang and W. Bautz *Röntgenpraxis*, **1999**, 52(2), 51-8.

References

62) H. Schmitt-Willich; M. Brehm; C. L. Ewers; G. Michl; A. Müller-Fahrnow; O. Petrov; J. Platzek; B. Raduchel and D. Sulzle *Inorg Chem*, **1999**, 38(6), 1134-44.

63) R.C. Carlos; H. K. Hussain; J. H. Song and I. R. Francis *AJR Am.J. Roentgenol. 2002*, 179(1), 87-92.

64) R.B. Lauffer; D. J. Parmelee; S. U. Dunham; H. S. Ouellet; R. P. Dolan; S. Witte; T. J. McMurry and R. C. Walovitch *Radiology*, **1998**, 207(2), 529-38.

65) S.G. Ruehm; T. Schroeder and J. F. Debatin *Radiology*, **2001**, 220(3), 816-21.

66) G. Dorta; A. Uske and A. L. Blum *Digestion*,**1997**, 58(3), 289-92.

67) P. Wedeking, C. H. Sotak, J. Telser, K. Kumar, C. A. Changh and M. F. Tweedle *Magn. Reson. Imaging*, **1992**, 10(1), 97-108.

68) M. Oudkerk, P. E. Sijens, E. J. Van Beek and T. J. Kuijpers *Invest.Radiol.* **1995**, 30(2), 75-8

69) H. Vogler, J .Platzek, G. Schuhmann-Giampieri, T. Frenzel, H. J. Weinmann, *Eur. J. Radiol.* **1995**, 21(1), 1-10.

70) M. F. Tweedle Physicochemical *Invest. Radiol*, **1992**, 27, S2-6.

71) M.F. Tweedle *Eur.Radiol*, **1997**, 7, 225-30.

72) R. Moats, S. Fraser and T. Meade *Angew. Chem. Int. Ed.* **1997**, 36, 725-728.

73) T. Meade Seeing is believing. *Acad.Radiol.* **2001**, 8(1), 1-3.

74) R. E. Jacobs; E. T. Ahrens; T. J. Meade and S. E. Fraser *Trends Cell Biol.* **1999**, 9(2), 73-6.

75) S. M. Rocklage; A. D Watson and M. J. Carvalin *Magn. Reson. Imaging,* St. Louis:Mosby, **1992**.

76) P. L. Anelli; I. Bertini; M. Fragai; L. Lattuada; C. Luchinat and G. Parigi *Eur. J. Inorg. Chem.* **2000**, 625-630.

77) A. L. Nivorozhkin; A. F. Kolodziej; P. Caravan; M. T. Greenfield; R. B. Lauffer; and T. J. McMurry; *Angew. Chem. Int. Ed.* **2001**, *40*, 2903-2906.

78) A. Bogdanov; Jr. L. Matuszewski; C. Bremer; A. Petrovsky and R. Weissleder *Molec. Imag* **2002**, *1*, 16-23.

79) J. M. Perez; T. O'Loughin; F. J. Simeone; R. Weissleder and L. Josephson *J. Am. Chem. Soc.* **2002**, *124*, 2856-2857.

80) M. Zhao; L. Josephson; Y. Tang; and R. Weissleder *Angew. Chem. Int. Ed.* **2003**, *42*, 1375-1378.

81) W.-h. Li, S. E. Fraser, and T. J. Meade, *J. Am. Chem. Soc.* **1999**, *121*, 1413-1414.

82) S. Aime; A. Barge; D. D. Castelli; F. Fedeli; A. Mortillaro; F. U. Nielsen; and E. Terreno *Magn. Reson. Med.* **2002**, *47*, 639-648.

83) S. Zhang; K. Wu; and A. D. Sherry; *Angew. Chem. Int. Ed.* **1999**, *38*, 3192-3194.

84) M. Mikawa; N. Miwa; M. Brautigam; T. Akaike and A. Maruyama *Chem.Lett.* **1998**, 693-694.

85) M. Mikawa; N. Miwa; T. Akaike and A. Maruyama *Proceedings of the International Symposium on Controlled Release of Bioactive Materials* **1999**,*26th*, 1158-1159.

86) R. Hovland; C. Glogard; A. J. Aasen and J. Klaveness *J. Chem. Soc., Perkin Trans. 2* **2001**, 929-933.

87) M. Kresse, S. Wagner, D. Pfefferer, R. Lawaczeck, V. Elste, and W. Semmler,*Magn. Reson. Med.* **1998**, *40*, 236-242.

88) V. Comblin, D. Gilsoul, M. Hermann, V. Humblet, V. Jacques, M. Mesbahi, C. Sauvage, and J. F. Desreux, *Coord. Chem. Rev.* **1999**, *185-186*, 451-470.

89) K. Hanaoka, K. Kikuchi, Y. Urano, and T. Nagano, *J. Chem. Soc., Perkin Trans.2* **2001**, 1840-1843.

90) K. Hanaoka, K. Kikuchi, Y. Urano, M. Narazaki, T. Yokawa, S. Sakamoto, K.Yamaguchi, and T. Nagano, *Chem. Biol.* **2002**, *9*, 1027-1032.

91) W.H. Li, S. E. Fraser, and T. J. Meade, *J. Am. Chem. Soc.* **1999**, *121*, 1413-1414.

92) W.H. Li, G. Parigi, M. Fragai, C. Luchinat, and T. J. Meade, *Inorg. Chem.* **2002**, *41*, 4018-4024.

References

93)   Aime S, D'Amelio N, Fragai M, Lee YM, Luchinat C, Terreno E and
        Valensin G. *J. Biol. Inorg. Chem.* **2002**, 7(6), 617-22.

94)   Moseley ME, deCrespigny A, Spielman DM. *Surg. Neur.* **1996**, 45,
        385-391.

95)   Thulborn KR, Waterton JC, Matthews PM, Radda GK. *Biochem.
        Biophys. Acta* **1982**, 714, 265-270.

96)   L. Mastronardi, P. Lunardi, F. Puzzilli, G. Schettini, F. Lo Blanco, A.
        Ruggeri Zentralbl. Neurochir. **1999**, 60(3), 141-145

97)   R.T. Higashida et al *Stroke.* **2003**, 34(8), 109-37

98)   S. Laughlin; W. Montanera *Postgraduate medicine*, **1998**, 204(5)

99)   N.K. Logothetis, J.M. Paul, M. Augath, T.Trinath, A. Oeltermann,
        Nature, **2001,** 412, 150-157.

100)   R. Turner; D. Le Bihan; C.T. Moonen; D. Despres; J. Frank *Magn
        Reson Med* **1991**, 22, 159-166.

101)   A. David; A. Blamire, H. Breiter *Brit. J. Psychiatry* **1994**, 164, 2-7.

102)   M.S. George; T. A. Ketter; T. A. Kimbrell; A. M. Speer; J.
        Lorberbaum; C. C. Liberatos; al. *The Neuropsychology of Emotion*.
        New York: Oxford University Press, **1999**.

103)   R.S. Menon; S. Ogawa; X. Hu; J. P. Strupp; P. Anderson; K. Ugurbil
        Magn. Res. Med. **1995,** 33, 453-459.

104)   H. C. Breiter; S. L. Rauch; K. K. Kwong; J. R. Baker; R. M.
        Weisskoff; D. N. Kennedy et al. *Arch. Gen. Psychiatry* **1996**, 53,
        595-606.

105)   M.J. SCHLOSSER; N. Aoyagi; R. K. Fulbright, J. C. Gore and
         G. McCarty *Human Brain Mapp*, **1998**, 6,1-13

106)   R.B. Tootel; A. M. Dale; M. I. Sereno and R. Malach *Trends
        Neurosci.* **1996;** 19,481-489

107)   R. Kurth; K. Villringer; B.M. Mackert; J. Schwiemann; J. Braun; G.
        Gurio; A. Villringer; K. J. Wolf; *Neuroreport*, **1998**;9,207-212

108)   S.G. Kim; J. Asche; A. P. Georgpoulos; H. Merkle; J. M. Ellermann;
        R.S. Menon; S. Ogawa; K. Ugurbil *J. Neurophysiol.*, **1993**, 69, 297-
        302

109) N.K. Logothetis; H. Guggenberger; S. Peled and J. Paul *Nat. Neurosci.* **1999,** Jun, 2(6), 555-62.

110) N.K. Logothetis *Philos. Trans. R. Soc. London B. Bio. Sci.* **2002;** 29, 357(1424), 1003-37.

111) S.Ogawa; T.M. Lee; R. Stepnoski; W. Chen; X. H. Zhu and K. Ugurbil *Proc. Natl. Acad.Sci.USA*, **2000**, 97, 11026-31.

112) S. Ogawa; R.S. Menon; D. W. Tank; S. G. Kim; H. A. Merkle; J. M. Ellermann and K. Ugurbil *Biophysics J,* **1993**, 64, 803-812.

113) G. Rainer; M. Augath; T. Trinath and N. K. Logothetis *Neuroimage*, **2002**, 6(3 Pt 1), 607-16.

114) G. Rainer; M. Augath; T. Trinath and N. K. Logothetis, *Current Biology* **2001,** 11, 846-854..

115) M. Marval; Z. F. Mainen; B. Sabatini; K. Svoboda *Biophys. Jorn.* **2000**, 78, 2655-2667

116) M.W. Sundberg; C.F. Meares; D.A. Goodwin;C.I. Diamanti *J. Med. Chem.* **1974,** 17(12),1304-1307**.**

117) G. Li, A. Slansky, M.P. Dobhal, L.N. Goswami, A. Graham *Biocon.Chem.* 2005, 16(1), 32-42

118) M. Rousset, T. Cens, N. Van Mau, P. Charnet *FEBS Lett.* ,**2004**, 41-45

119) I. Spigelman, M. Tumanski, C.M. Wallage, P.L. Carlen, .A.A. Velumiani *Neurosci.* **1996,** 2, 559-572.

120) R.J. Tsien *Ann. Rev. Neurosci.* **1989**, 12, 227-253

121) S.R.Adams ; R.J. Tsien *Ann. Rev. Neurosci.* **1993**, 55, 755-784

122) S. Mirzadeh, R.W. Ather, O.A. Gansow *Bioconj. Chem.* **1990***, 59-65*

123) L.A. Levy, E.Murphy, B. Raju, and R.E. London *Biochem.* **1988,** 27, 4041-4048

124) S.M. Cohen, X. Jide, E. Radkov, and K. N. Raymond *Inorg. Chem.* **2000**, 39, 5746-5756

125) D.T. Puerta, M. Botta, C. J. Jocher, E. J. Werner, S. Avedano, K. N. Raymond, S. M. Cohen *JACS Comm.* **2006**, 128, 2222-2223

References

126) S. Aime, M. Botta, M. Fasano, E. Terreno, P. Kinchesh, L. Paleari *Mag. Res. Med.* **1996**,35, 648-651

127) R.D. Peters, R.M.Henkelmann *Mag. Res. Med.* 2000, 43, 62-66

128) S. Aime, E. Gianolio, D. Corpillo, C. Cavallotti, G. Palmisano, M. Sisti, G.B. Giovenzana, R. Pagliarin *Helv. Chim. Acta.* **2003**, 86, 615-632.

129) S. Aime, A. Barge, M. Botta, A.K. Howard,M.P. Lowe, D. Parker, A.S. Suoussa *Chem. Comm.* 1999, 1047-1049

130) S. Zhang, K. Wu, A.D. Sherry *Angew. Chem. Int. Ed.* 1999; **38**, 3192-3194.

131) M.L. Garcia-Martin, G.V. Martinez, A.D. Sherry, S. Zhang and R. Gillies *Mag. Res. Med.* **2006**, 55, 309-315.

132) J. Rudovský, P. Cígler, J. Kotek, P. Hermann, P. Vojtíšek, I. Lukeš, J.A. Peters, L.V. Elst, R.N. Muller *Eur. J. Chem.* **2005**; 11, 2373-2383.

133) P. Vojtíšek, P. Cígler, J. Kotek, J. Rudovský, P. Hermann, I. Lukeš *Inorg. Chem.* **2005**; 44, 5591-5599.

134) A. Dadabhoy, S. Faulkner, P.G. Sammes *J. Chem. Soc. Perkin Tranc.* **2002**, 2, 348-357.

135) B. Paull, P. R. Haddad. Chelation ion chromatography of trace metal ions using metallochromic ligands. *Trac-Trends in Anal. Chem.* 1999; **18**, 107-114.

136) P. Táborský, P. Lubal, J. Havel, J. Kotek, P. Hermann, I. Lukeš, Collect. *Czech. Chem. Commun.* **2005**, 70, 1909

137) J. Moreau, E. Guillon, J.-C. Pierrard, J. Rimbault, M. Port, M. Aplincourt, *Chem. Eur. J.* **2004**, 10, 5218

138) G. Anderegg, F. Arnaud-Neu, R. Delgado, J. Felcman, K. Popov, *Pure Appl. Chem.* **2005**, 77, 1445.

139) Bianchi, L. Calabi, C. Giorgi, P. Losi, P. Mariani, P. Paoli, P. Rossi, B. Valtancoli, M. Virtuani, *J. Chem. Soc., Dalton Trans.* **2000**, 697

140) A.E.Martell, R.M.Smith, R.J.Motekaitis, NIST database of Critically Selected Stability Constants v. 7.

141) K. Popov, H. Rönkkömäki, L.H. Lajunen *Pure Appl. Chem.* **73**, 1641 (2001).

142) J. Huskens, D.A. Torres, Z. Kovacs, J.P. André, C.F.G.C. Geraldes, A.D. Sherry *Inorg. Chem.* **1997**, 36, 1495

143) L. Burai, R. Király, I. Lázár, E. Brűcher, *Eur. J. Inorg. Chem.*, **2001**, 813

144) A. Lázár, D. Sherry, R. Ramasamy, E. Brücher, R. Király, *Inorg. Chem.* **1991**, 30, 516

145) J.Kotek, J.Rudovský, P.Hermann, I.Lukeš, *Inorg. Chem.* **45**, 3097 (2006).

146) P. Vojtíšek, J. Kotek, V. Kubíček, J. Rudovský, P. Hermann, I. Lukeš, *5th International Conference on f-elements (ICFE)*, COST, Geneva (Switzerland) **2003**.

147) K. Kumar, C.A. Chang, L.C. Francesconi, D.D. Dischino, M.F. Malley, J.Z. Gougoutas, M.F. Tweedle, *Inorg. Chem.* **1994**, 33, 3567

148) K. Kumar, M.F. Tweedle, M.F. Malley, J.Z. Gougoutas *Inorg. Chem.* **1995**, 34, 6472

149) C.A. Chang, *J. Chem. Soc., Dalton Trans.* **1996**, 2347

150) H.Z. Cai, T.A. Kaden, *Helv. Chim. Acta* **1994**, 77, 383

151) S.H. Koenig, K.E.Kellar *Magn. Reson. Med.* **1995,**34(2):227-33

152) J. Sarapuk; D. Bonarska,; H. Kleszczynska *Journ. of Appl. Biomed.* **2003**, 1(3), 169-173.

153) N. Linhong; S. Baoan; Z. Guoping; X. Ruiqing; Zh. Sumei; G. Xingwen; Hu. Deyu; Y. Song. *Bioorg. & Med. Chem. Let.* **2006**,16(6), 1537-1543.

154) D. Bonarska; J. Sarapuk; H. Kleszczynska *Polish Journal of Food and Nutrition Sciences* **2003**, 12(SI 2), 17-19.

155) S. W. Bligh; C. T. Harding; A. B. McEwen; P. J. Sadler; K. J. Duncan; J. A. Marriott *Polyhedron* **1994**, 13(12), 1937-43.

References

156) T. Kiss; I. Lazar; P. Kafarski, *Metal-Based Drugs* **1994**, 1(2-3), 247-64.

157) T. Kiss; I. Lazar. *Aminophosphonic and Aminophosphinic Acids* **2000**, 285-325. CODEN: 69ABMI CAN 133:355826 AN 2000:435911 CAPLUS

158) E. Matczak-Jon, B. Kurzak, A. Kamecka, et al. *Polyhedron* **1999**, 21 (3), 321-332

159) Kamecka; B. Kurzak *Wiadomosci Chemiczne* **2003**, 57(9-10), 797-825.

160) F. Budsky; P.Kopecky; J. Prokop *Czech Rep.Chem. Comm.* **1998**, 345-348

161) O. G. Arkhipova; M. R. Zel'tser; A. A. Petushkov *Radiobiologiya* **1966**, 6(5), 754-5.

162) K. Adzamli, M. Blau, M.A. Pfeffer, M. A. Davis *Invest. Radiol.* **1991,** 26, 242-7.

163) K. Adzamli; D.Johnson; M. Blau *Invest. Radiol.* **1991**, *26*, 143-148.

164) K. Adzamli; M. Blau; M. A. Pfeffer; M. A. Davis, *Magn. Reson. Med.* **1993**, *29*, 505-511.

165) V. Kubicek, J. Rudovsky, J. Kotek, et al. *J. Am. Chem. Soc.* **2005**, 127 (47), 16477-16485.

166) G. Schwarzenbach, H. Ackerman and P. Ruchstuhl, *Helv.Chim. Acta.* **1949**, 32, 1175.

167) G. Schwarzenbach and J. Zurc *Moizatsh. Chern.,* **1950,** 81, 202.

168) G. Schwarzenbach, P. Ruckstuhl, and J Zurc, *Helv. Chim. Acta,* **1951,** 34, 485.

169) R.J. Motekaitis, I. Murase and A. E. Martell, *J. Inorg. Nucl. Chem.,* **1971**, 33, 3353.

170) S. Westerback, K. S. Rajan and A. E. Martell, *J. Am. Chem. Soc.,* **1965**, 87, 2567.

171) R.J. Motekaitis, I. Murase and A. E. Martell, *Inorg. Chem.*, 1976, **15**, 2303.

172) R. R. Irani and K. Moedritzer *J. Phys. Chem* , 66, **1969** (1062).

173) M. M. Crutchfield and R. R. Irani *J .Am. Chem. Soc.,* **1965,** 87, 2816.

174) R. P. Carter; M. M. Crutchfield; R. R. Irani *Inorg. Chem.*, **1967**, 5, 943-946.

175) R. P. Carter; M. M. Crutchfield; R. R. Irani *Inorg.* Chem., **1967**, 6, 939-942.

176) R. Samokayev, N.M. Dyatlova, R. Gurevich *J.Obsh. Khim.* **1984**, 1720-1726.

177) E. Matczak-Jon, B. Kurzak, A. Kamecka, P. Kafarski *J.Chem. Soc., Dalton Trans.* **1999**, 3627-3637.

178) L. Helm, A. Merbach, *Chem. Rev.*, **2005**, 105, 1923-1959.

179) L. Helm, G. L. Nicole, A. Merbach, Adv.*Inorg. Chem.*, **2005**, 57, 327-379.

180) P. A. Joäo, H. R. Maecke, E. Töth, A. Merbach, *J. Bio.I norg. Chem.*, **1999**, 4, 341-347.

181) S. Aime, M. Botta, M. Fasano, E. Terreno, *Acc. Chem. Res.,* **1999**, 32, 941-949.

182) X. Li, Sh. Zhang, P. Zhao,Z. Kovacs, and A. D. Sherry, *Inorg. Chem.,* **2001**, 40, 6572-6579.

183) K. Sawada, T. Araki, T. Suzuki, *Inorg. Chem.* **1987**, 26, 1199-1204.

184) T.G. Appleton, J. R. Hall, I. J. McMahon, *Inorg. Chem.* **1986**, 25, 726-734.

185) S.Dadabhoy, Faulkner and P. G. Sammes *J. Chem. Soc., Perkin Trans. 2*, **2002**, 348–357.

186) K. Moedritzek, R.R. Irani, *Inorg.Chem.* **1966**, (31), 1603-1607.

187) E. Matczak-Jon, B. Kurzak, P. Kafarski, A. Wozna *J. Inorg. Biochem.* **2006,** 100, 1155-1166

188) E. Matczak-Jon, B. Kurzak, A. Kamecka, P. Kurzak, J. Jezierska, P. Kafarski *Polyhedron* **2000**, 19, 2083-2093

189) E. Matczak-Jon, B. Kurzak, A. Kamecka, W. Sawka-Dobrowska, P. Kafarski*, Polyhedron* **2002,** 321-332

190) Preparation of ACSF http://www.alzet.com/products/cfs_prep

References

191) L.F. Callado, J.A. Stamford *J. Neurochem.* **2000**, 74(6), 2350-2359.

192) Schwarzenbach, G. *Standardization of Lanthanides with EDTA in Complexometric Titrations*; Interscience: New York, USA, 1957; pp 77-82.

193) M. Kývala, I. Lukeš, *Intern. Conf. Chemometrics '95*,. Pardubice, Czech Republic, **1995**, 63

194) G.M. Blackburn, P. Wentworth *Eur. Pat. Appl.* 1996, 141pp.

ABSTRACT

Magnetic Resonance Imaging (MRI) is a diagnostic scanning technique based on the principles of nuclear magnetic resonance. It is a method of obtaining images of the body in thin slices. Functional magnetic resonance imaging (fMRI) is based on Blood-Oxygen-Level-Dependent (BOLD) contrast. It is currently the mainstay of neuroimaging, whose ever growing applications provide a wealth of information regarding the processes in the brain. The chief disadvantages of BOLD-fMRI are its limited temporal and spatial resolution. In fact, BOLD imaging as well as other fMRI methods alone is insufficient for a detailed study of the neural networks that underlie human or animal cognition.

In general MRI measures the signal from the hydrogen nuclei of water which can be modified by the chemical environment. This signal intensity and therefore, contrast of the image depends essentially on three factors: the density of proton spins in a given volume and the longitudinal and transverse relaxation times T_1 and T_2 of these spins. The relaxation times may be shortened considerably in the presence of paramagnetic species which are called contrast agents. While both organic and inorganic radicals can be MRI contrast agents, this work is restricted to gadolinium(III) containing agents. The lanthanide ion gadolinium(III) is generally chosen, because it has a high magnetic moment, and the most unpaired electrons of any stable ion. But because of the high toxicity of gadolinium, it must be chelated with organic molecules to form a strong seven to eight coordinated complex which will be less toxic, while having one or two coordination sites free for interaction with water molecules. The aim of the present work is to develop contrast agents which are 'smart' biochemical functional markers that detect neuronal activity in real time and translate it into changes in MR contrast. That can be temperature, pH, pO_2, presence of aminoacids and proteins or changes in the concentration of any cations and anions involved in the process of

neuronal activity. Since calcium plays an important role in neuronal processes in present work pH and calcium sensitive contrast agents have been developed. Therefore, a series of gadolinium based complexes have been designed, synthesized and characterized. Finally *in vivo* investigations of the compounds have been preformed by combined electrophysiological and fMRI methods.

Acyclic bifunctional chelating agents **1** and **2** were synthesized by two different ways starting from the dimethylester of nitro- or aminoisophtalic acid.
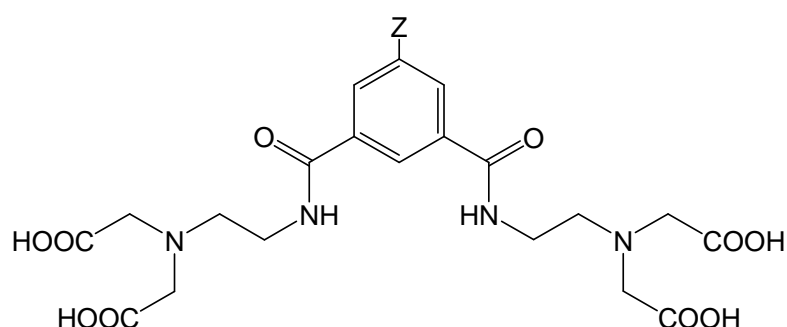
.

Chart 1. Bifunctional chelating agent. Z = -NO$_2$(1), -NH$_2$(2)

Complexes with gadolinium and europium were obtained and relaxivities were measured at 300 MHz and 25°C. The very poor solubility of the complexes in water and most organic solvents indicate the formation of di- or polymer chains upon the complexation. This makes the complexes useless for further investigations as MRI contrast agents. Although the amino derivative can be modified and used as a building blocks in the syntheses of the specific chelators.

The second set of compounds was designed to be sensitive to changes of pH. The DO3A molecule which is known to form stable complexes with lanthanides was used as a base for the synthesis of macrocyclic monophosphonates (Chart 2). The choice of phosphonate groups was due to their protonation constants which are in slightly acidic/neutral range

(pK = 6-7) and the ability to form strong hydrogen bonds with water molecules, which are sensitive to changes of pH. That could lead to possible changes in the number of inner/secondary/outer sphere water molecules of the lanthanide complex, and therefore its relaxivity properties. Protected and unprotected phosphonates **3** and **4** were used to study the effect of the charge and acidity of the complexes on the relaxivity.
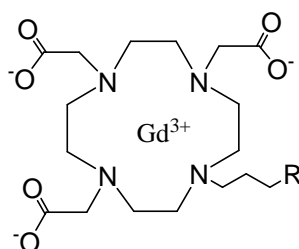

Chart 2.   Macrocyclic phosphonate containing compounds.
3, R = PO_3H_2; **4,** R = PO_3Et_2.

Thermodynamic investigations of the ligands have been performed using glass-electrode potentiometric titrations and protonation constants of the phosphonates as well as stability constants of the ligand-calcium(II) complexes (as model for the stability of gadolinium(III) complexes) have been determined. pK values of the phosphonic functional groups increase with increase of the chain length of the pendant arm. The reverse behavior was observed for the second protonation constant of the nitrogen atom of the cyclen rim. Relaxometric measurements of the gadolinium(III) complexes have been performed at various magnetic fields (20, 60 and 300 MHz) and different pH of the water solutions (pH 4-10). The most interesting result was obtained at acidic pH where relaxivity of the complexes **3** and **4** increased by 23% and 60% respectively, when the pH of the medium has changed from neutral to pH 4 (20 MHz). The ^{31}P NMR studies of the europium complexes supported by the data of potentiometric titration demonstrated that the compounds **3** and **4** are

Abstract

stable in the range of pH 4 to 10. Slow decomplexation of complexes is observed at pH < 3. This means that the changes of the relaxivity are not due to the decomplexation of the compounds.

Amino(bismethylene)phosphonates are well known for there affinity toward calcium. In order to design complexes which will be sensitiv to changes of extracellular calcium concentrations a series of macrocyclic compounds with variable length of the amino(bismethylene) phosphonates containing side chain were synthesized and characterized (Chart 3).
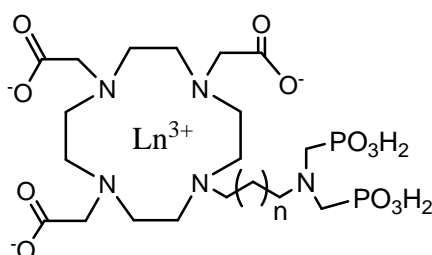

Chart 3. Macrocyclic compounds with the variable length of the side chain **5a – b**, n = 1; **6a – b**, n = 3: **7a – b**, n = 4 (Ln^{3+} = Gd^{3+}(**a**), Eu^{3+} (**b**))

The compounds were synthesized by the alkylation of the *tert*-butyl ester of DO3A with the corresponding Boc protected bromoalkylamines. After the cleavage of the protection groups, phosphonates were introduced by Mannich reaction with phosphorous acid and formaldehyde at $100^{\circ}C$. The relaxivity studies of the compounds were preformed at high field (300 MHz). The T_1 relaxation time of water was measured for the contrast agents **5a – 7a** while varying the concentrations of Ca^{2+} ions. No significant changes of the water relaxivity of **5a** were found over the whole span of Ca^{2+} concentration. Interestingly, the water relaxivity of **6a** solutions which remained constant in Ca^{2+} concentrations from 0 to 1.0 mM dropped from 3.49 to 2.56 $mM^{-1} s^{-1}$ when the Ca^{2+} concentration was increased to 10 mM. More importantly in solutions of the **7a** major effect of the change in relaxivity was shifted to Ca^{2+} concentration range which is covering the physiologically relevant area. A maximum decrease in r_1 of 36% within the

118

physiological range was observed, which was only slightly reduced in artificial cerebrospinal fluids (CSF).

The differences of the ^{31}P chemical shifts of the **6b** and **7b** complexes compared to their free ligands indicates that the phosphonate groups were not coordinated to europium, while the chemical shift difference of 20 ppm in the case of **3b** points to an interaction between the metal center and the phosphonate functions. Interestingly, the ^{31}P resonances of **5b** are not affected by the addition of Ca^{2+} ions whereas the line widths increased dramatically when the Ca^{2+} concentration was increased in the solutions of **6b** and **7b**, respectively. These results are in line with the relaxivity studies of the corresponding gadolinium complexes.

In vivo experiments show that the compounds are not toxic and could be used for in rat investigations. Unfortunately the analysis of the *in vivo* in the rat experiments showed that no changes in T_1 upon stimuli did occur.